Quantum Computation by Transport: Development and Potential Implementations

Nicholas Chancellor

University of Southern California

Table of Contents

Personal Acknowledgements

I would like to thank my parents, Dan and Paula for raising me and instilling an interest in science in me at an early age. I would also like to thank my fiancé Shanelle for her love and support since I met her. In addition I would like to than my brother Graham and his wife Ashley for believing in me and for their support during college and graduate school. As well I would like to thank Bob, Lida, Sarah and Laura Wachel for taking me into there home for a large portion of my graduate studies. I would also like to thank my extended family, my grandmothers Bonnie and Tess, my aunt Theresa, my cousin Ryan, my uncle Bill and aunt Nazerina, my uncle Mike and my aunt Nancy, and my cousin Corrine for there support. In addition I would like to acknowledge the positive impact on my life from the brothers of the Gamma Kappa chapter of Phi Gamma Delta, pergé brothers.

I would also like to thank many people who have helped academically throughout my academic career, in particular my advisor Stephan Haas, who has been an excellent advisor and a good friend. Acknowledgements of academic contributions are done on a chapter by chapter basis and can be found near the end of the chapter. All of the chapters are based on published or submitted papers, and the references to these papers can be also found in the chapters.

Introduction

This thesis deals with effects on antiferromagnetic Heisenberg spin chains and clusters which can be used for universal holonomic quantum computing. I will discuss in detail an architecture for a Holonomic quantum computer, and how to it may be implemented with superconducting flux qubits (see [1](ch. 4)). In addition to demonstrating this architecture, this thesis will also shed light on the behavior of these chains and the effects which make such an architecture possible. These effects include entanglement which allows disturbances that are excited by a quench to travel an unlimited distance, even in a gapped system. I will also examine anomalous equilibration behavior which can be seen in these systems.

Holonomic quantum computation (HQC) was conceived and shown to be universal by Zanardi and Rasetti [5](ch. 4) who formulated it in terms of a non-abelian Berry phase. HQC is considered to be an appealing method for achieving fault tolerant quantum computing because of its geometrical nature and because it can be implemented adiabatically. Therefore it has all of the advantages of adiabatic quantum computation [6](ch. 4). Although many implementations of holonomic and geometric quantum computation are adiabatic, there are examples which are not [7, 8](ch. 4).

Unlike most other implementations of HQC, the one which we propose in this thesis does not require us to explicitly consider curvature of a degenerate ground state manifold within a complex projective space. Although such methods could in principle be applied to the designs given here, they are not necessary. The architecture proposed in this thesis relies on real space twists performed on a Hamiltonian which initially performs transport with a trivial (non-abelian) Berry phase. Because these twists have a real space physical interpretation, the effects they will have on transported qubits can be inferred without considering the geometry of the underlying Hilbert space.

I focus on an adiabatic transport protocol which involves the slow attachment and removal of spins from an antiferromagnetic Heisenberg spin chain or cluster. There are other transport protocols which could also be used, most notably the non-adiabatic protocol discussed in [8–11](ch. 4). The reason that this thesis focuses on adiabatic transport protocols is that the architecture proposed in this thesis could potentially be implemented with a superconducting flux qubit circuit which only faithfully reproduces the low energy degrees of freedom of a spin Hamiltonian, and therefore is not appropriate for non-adiabatic computation.

Superconducting flux qubits are a popular architecture for implementing scalable adiabatic quantum computing [2–6](ch. 4), and therefore are a natural choice for designing a scalable holonomic quantum computer. An additional advantage of the use of superconducting flux qubits is that the designs tend to have spatially extended qubits and a high degree of connectivity[17](ch. 4). The large spatial extent of the qubits means that a design could be implemented in which a qubit would only need to be transferred across a small number of spins to be moved from one location in a computer to any other arbitrary location.

There has been recent experimental work involving quantum annealing to degenerate ground state manifolds using currently available superconducting flux qubit hardware[18](ch. 4). It was demonstrated experimentally that signatures of quantum behaviors can be observed in the final state within a degenerate ground state manifold. This provides an indication that a ground state manifold can be produced accurately enough on the D-wave 1 quantum annealing processor that quantum effects dominate over classical effects and design inaccuracies. Although the architecture proposed here cannot be implemented on the hardware used in [18](ch. 4), this experiment does provide proof of principle for the use of degenerate manifolds in superconducting flux qubit systems.

The adiabatic transport protocol which I propose is discussed extensively in chapter 3 of this thesis which is based on a separately published work [1](ch. 3). This protocol relies only on the tendency of antiferromagnetic systems to repel excess polarization, and is therefore quite versatile. This protocol does fail for certain highly frustrated regimes of parameter space, but works well in other regimes. This thesis examines several variations of this transport protocol including sequential versus simultaneous uncoupling as well as methods which involve simultaneous variations of the J2 coupling parameter so that the easily prepared nature of the ground state at the so called Majumdar-Ghosh point [15](ch. 3) can be exploited. I also discuss the effect of making the coupling anisotropic, by using a XYZ or XXZ Heisenberg model instead.

This protocol was motivated by a phenomenology in which transport can be achieved over long distances in a system which is gapped but has a degenerate ground state. It is shown in chapter 2 of this thesis which is based on separately published work [1](ch. 2) that a ground state degeneracy arising from either topological effects or from particle hole symmetry can be used to send disturbances which carry information and can lead to equilibration throughout a spin chain system. This investigation makes heavy use of quantum information related quantities to elucidate the dynamics of a many body system, as has also been done successfully in many other works [4–9](ch. 2). Also the interest in this phenomenology may extend beyond the quantum computer design proposed in chapter 4 of this thesis, for example a J_1-J_2 Heisenberg spin chain can be realized with cold trapped atoms [10, 11](ch. 2). An extension of this system has also been identified as being important for other applications in quantum computing [15].

Thesis Structure

This thesis primarily examines a method of achieving universal holonomic quantum computation by using transport protocols to transport qubits down spin chains with unitary twists. This thesis however is not intended to simply summarize these results, which have been published elsewhere [1] (ch. 4). I will also also summarize the transport protocol which is used, as well as to illuminate many ideas related to the development of this architecture as well as examining the potential of implementation using superconducting qubits.

The first chapter of this thesis summarizes the phenomenology of J_1-J_2 Heisenberg spin chains which are locally quenched, with a strong focus on equilibration. The subject of equilibration of closed quantum systems, which is a primary focus of the first chapter is an interesting topic in its own right. This chapter is included because it gives insights into the rich world physics of local manipulations of spin chains on which the design given in this thesis is based. This first chapter provides groundwork for the proceeding chapters which discuss transport of information by exploiting a degenerate ground state.

The second chapter continues the study of J_1-J_2 Heisenberg spin chains under local quenches. This chapter, however, shifts its focus away from equilibration and instead focuses on the transfer of information and polarization using a degenerate ground state manifold. In this paper studies of quenched systems lay the groundwork for the next chapter which discusses a kind of transport which can be achieved adiabatically.

The third chapter lays out an adiabatic transport protocol for transporting a qubit of information through an antiferomagnetically coupled Heisenberg spin chain. In this chapter I explore the effect of frustration by examining the protocol on a J_1-J_2 spin chain. I also discuss the effect of making the coupling anisotropic, by using a XYZ or XXZ Heisenberg model instead.

The fourth chapter is divided into 3 sections. The first section discusses how the spin chains used in the third chapter can be twisted to produce arbitrary single qubit gates. This section gives a list of the twists necessary for a universal set of single qubit gates, as well as laying out the method for calculating the twist necessary for an arbitrary gate. The second section demonstrates how a controlled not gate can be implemented with a cluster of 8 spins. The third section suggests a method of implementing the necessary Heisenberg systems with superconducting flux qubits.

A summary of the design itself, and the related data are all contained in the third and fourth chapters. The first two chapters provide context for how this design came about.

Chapter 1: Local Quenches on Heisenberg Spin Systems

This chapter is based on the paper [1]. In this chapter, We study the long-time equilibration behavior following a local quench using a frustrated quantum spin chain as an example of a fully interacting closed quantum system. Specifically we examine the statistics of time series of the Loschmidt echo, the trace distance of the time evolved local density matrix to its average state and the local magnetization. Depending on the quench parameters, the equilibration statistics of these quantities show features of good or poor equilibration, indicated by Gaussian and exponential or bistable distribution functions of the linear quantities. This provides insight into the universalities and the richness of equilibration of complex closed quantum systems.

I. INTRODUCTION

Equilibration behavior of closed quantum systems is a topic of recently growing interest. As opposed to equilibration in an open quantum system, for example coupled to a bath at a certain temperature, a closed quantum system does not only not encounter dissipation and conserve energy - like even a classical system would. But its time evolution is unitary, initially being in a pure state it therefore remains pure for all time. Equilibration under these constraints is much less straight forward and in some cases, especially for finite systems, might even fail completely.

Recent numerical and theoretical studies have taken approaches to study equilibration compatible with the unitary evolution of closed quantum systems. Some approaches include bounds related to the Levi lemma [2, 3], through typicality arguments based on treating wave functions as random states [4, 5] as well as analytical and numerical approaches to time series statics [6–8]. Motivated by our interest in the equilibration properties of isolated quantum systems following a quench - more specifically the evolution statistics of quantum information quantities such as the Loschmidt echo and the local trace distance - we perform numerical studies of finite-size systems. As a representative example, we examine J_1-J_2-quantum-spin-chains with N spin-1/2 degrees of freedom, periodic boundary conditions and a local magnetic field term,

$$\begin{aligned} H\left(J_1, J_2, h\right) \; = \; & J_1 \sum_{j=1}^{N} \vec{S}_j \cdot \vec{S}_{j+1} + J_2 \sum_{j=1}^{N} \vec{S}_j \cdot \vec{S}_{j+2} \\ & -h \sum_{j=1}^{N'} S_j^z . \end{aligned} \tag{1}$$

Here J_1 and J_2 denote nearest-neighbor and next-nearest-neighbor Heisenberg couplings. $\vec{S}_j$ and S_j^z are the spin operators of the corresponding spin j. For simplicity J_1 is chosen to be one. J_2 varies from quench to quench, but remains constant within a given quench. Instead, the magnetic field term in the Hamiltonian is used to perform local quenches on a subset of N' adjacent spins of the form $H(h) \to H'(h')$. Starting in the ground state $|\Psi_0\rangle$ of $H(h)$ at $t = 0$, after the quench the system evolves according to $H'(h')$. In this set up the local magnetic field term introduces a perturbation, which does not commute with the first two terms of equation (1). Moreover it breaks translational symmetry, thus it allows one to generate more complex excitations. [10] [11]

Even for finite h the Hamiltonian given by equation (1) preserves the total magnetization $M = 1/N \sum_{j=1}^{N} S_j^z$, since M commutes with H. H therefore splits in to $2N+1$ independent sectors. This reduces the actual system size from 2^N eigenstates to only $\binom{N}{N_{up}}$ eigenstates, where $N_{up} = N(M + 1/2)$ is the number of spins pointing up. The largest of these sectors is the sector, where $M = 0$ or $N_{up} = N/2$, which is also the sector of the ground state of H for zero or small h.

To address the quench numerically we thus calculate the ground state energy in each of the total magnetization sectors of the initial Hamiltonian $H(h)$ using Lanczos diagonalization. We then only keep the ground state of the sector with the lowest ground energy and diagonalize the evolution Hamiltonian $H'(h')$ in this sector. This is done through iterative Lanczos diagonlization, calculating the first 500 hundred lowest energy eigenstates. [12] To simplify the notation when talking about eigenstates or eigenstate expansions in the following we always refer to only this sector.

Unitary evolution after a quench A sudden change of a system parameter pulls the system, originally in the ground state of the Hamiltonian $H(h)$ into an out of equilibrium state of the new Hamiltonian $H'(h')$. The state of the system then evolves according to H'. The time evolved density matrix is given by $\rho(t) = U_t^{\dagger} \rho_0 U_t$, where $\rho_0 = |\Psi_0\rangle \langle\Psi_0|$ denotes its initial state and $U_t = \exp(-\mathrm{i}H't)$ the time evolution operator. Note that since the evolution

is unitary this state is always pure, i. e. its purity $P[\rho(t)] = \mathrm{Tr}[\rho(t)^2] = 1$.
Equilibration in the long time behavior of some observable O can then be studied, by looking at the time series of its expectation value $O(t) = \mathrm{Tr}[\rho(t)O]$. One can expand this expectation value in the energy basis of the Hamiltonian H'

$$O(t) = \sum_{n',m'} c_{n'} c^*_{m'} \exp\left[-\mathrm{i}\left(E_{n'} - E_{m'}\right) t\right] O_{n'm'}, \tag{2}$$

where $c_{n'} = \langle n'|\Psi_0\rangle$. As one can see from equation (2) in a finite system all expectation values are rapidly oscillating functions over time, namely they are trigonometric polynomials in the energy differences. The long time behavior of an observable O is given by its probability distribution function $P(o) \equiv \overline{\delta(o - O(t))}^t$. Equilibration of such an observable can then be defined in terms of concentration of its probability distribution function. A simple recipe for a concentration result is the signal to noise ratio $\overline{O}^t/\sqrt{\mathrm{Var}(O)}$, where

$$\overline{O}^t \equiv \lim_{T\to\infty} \frac{1}{T}\int_0^T O(t)\mathrm{d}t \tag{3}$$

denotes the time average of the expectation value $O(t)$ and $\mathrm{Var}(O)$ its variance. Since the trace in the expectation value commutes with the time average, one obtains $\overline{O}^t = \mathrm{Tr}[\overline{\rho(t)}^t O]$. If we assume the system to be non-degenerate, the time average on the density matrix simply leads to a dephasing of the oscillating off-diagonal terms in its expansion in the eigenstate basis $\rho(t) = \sum_{n',m'} c_{n'} c^*_{m'} \exp[-\mathrm{i}(E_{n'} - E_{m'})t] \left|m'\right\rangle \left\langle n'\right|$. The average of the off-diagonal terms vanishes, what remains unchanged are the diagonal terms $\overline{\rho} = \sum_{n'} p_{n'} \left|n'\right\rangle \left\langle n'\right|$, where $p_{n'} = c^*_{n'} c_{n'}$.

This state is not any more pure, but describes an ensemble, which is often called the dephased state. If the variance of an observable O is very small, $P(o)$ is peaked around its mean, O is equilibrated and $\overline{\rho}$ provides a useful ensemble.
This is generically the case for systems in the large size limit. However if the system is finite the distributions of generic observables are less narrow. In this regime it becomes interesting to study probability distribution functions. As shown in the following numerical calculations, in some cases one encounters simple distribution functions such as Gaussian or exponential distributions. The former is completely defined by its first two commulants, i. e. its mean and its variance. The later is already defined by its first commulant. Because of their simple structure and their generality - Gaussian distribution functions are obtained, where ever the central limit theorem applies - they indicate a straight forward way of equilibration

behavior in a finite system. In other cases one obtains more complex, specifically bistable distribution functions. Usually accompanied by larger spreads they indicate the lack of a smooth equilibration.

Introduction of the studied quantities To study the equilibration behavior following a quench we focus on four quantities. We look at global as well as local quantities. The first two are global: the energy probability distribution of the initial state

$$p_{n'} \equiv |\langle\Psi_0|n'\rangle|^2 \tag{4}$$

describes the relative weight of the elementary excitations caused by the quench, and the Loschmidt echo

$$L(t) \equiv |\langle\Psi_0\,|\exp\left(-\mathrm{i}H'\left(h'\right)t\right)|\,\Psi_0\rangle|^2 \tag{5}$$

is the probability of finding the system in its initial state $|\Psi_0\rangle$ at a given time t after the quench. It can be seen as some sort of memory of the initial state left in the system after the quench. In recent publications ([6] and [7]) the Loschmidt echo has been identified as a useful quantity to study the equilibration of generic closed quantum systems after a quench. It only depends on the initial ground state and its energy probability distribution in the eigenbasis of the evolving Hamiltonian

$$\begin{aligned} L(t) &= \sum_{n',m'} p_{n'}p_{m'}\exp\left[-\mathrm{i}\left(E_{n'}-E_{m'}\right)t\right] && (6)\\ &= \sum_{n'} p_{n'}^2 + 2\sum_{n'<m'} p_{n'}p_{m'}\cos[(E_{n'}-E_{m'})t] && (7)\end{aligned}$$

Its mean is equal to the purity of the dephased state, which defines its effective dimension, as introduced in [3]:

$$\overline{L}^t = \sum_n p_n^2 = \mathrm{Tr}\left[\left(\overline{\rho}^t\right)^2\right] = P\left[\overline{\rho}^t\right] \equiv \frac{1}{d_{eff}} \tag{8}$$

The two other quantities we examine, are localized in the subsystem S of the spins 1 to N', which are (initially) exposed to the magnetic field. The remaining spins $N'+1$ to N are called the environment E. The first local quantity follows the quantum informational context of the Loschmidt echo: the local trace distance of the time-evolved density matrix $\rho_S\left(t\right) = \mathrm{Tr}_E\,|\Psi(t)\rangle\,\langle\Psi(t)|$ to its time average

$$d_S(t) \equiv \left\|\rho_S(t) - \overline{\rho_S}^t\right\|_1, \tag{9}$$

where norm 1 is the trace norm given by

$$\|O\|_1 \equiv \frac{1}{2}\mathrm{Tr}\sqrt{O^\dagger O} \tag{10}$$

for an observable O. It describes the experimental distinguishability of the time-evolved local state and the average local state. More precisely equation (9) provides a bound for the expectation values of any local observable O given its range of eigenvalues $\lambda_{min}, \ldots, \lambda_{max}$, which is proved in [3] for the generic case of a system with non-degenerate energy gaps: [13]

$$\left|\mathrm{Tr}[\rho(t)O] - \mathrm{Tr}[\overline{\rho}^t O]\right| \leq |\lambda_{max} - \lambda_{min}|\, d_S(t). \tag{11}$$

Moreover this bound holds for the time average on both sides of equation (11) and therefore provides a bound to the fluctuations of the expectation values of any local observable.[14] Locally, this trace distance defines equilibration in a strong sense. If it were almost vanishingly small for all time, this would imply that the local system is in perfect equilibrium. Namely the system would always be practically indistinguishable from its time average. Globally, equilibration can not be achieved in the same strong sense because the trace distance is invariant under unitary evolution, and therefore globally cannot get smaller than its initial value.

Through the use of the earlier introduced effective dimension one can a looser but even simpler bound of equation (11) using [3]

$$d_S(t) \leq \frac{1}{2}\sqrt{\frac{d_S'^2}{d_{eff}}} = \frac{d_S'}{2}\sqrt{\overline{L}^t}, \tag{12}$$

where d_S' is the dimension of the subsystem S in our case $d_S' = 2^{N'}$ and N' is the number of spins in the subsystem. However if the system size is finite and the quench comparably small, as in the cases discussed here, this bound becomes trivial, e.g. for $N' = 4$ and $\overline{L}^t = 0.9$ one obtains $d_S(t) \leq 7.59$, but the normalized trace distance between any two density matrices is always less or equal to 1.

As the most natural observable of a spin chain we also look at the normalized local magnetization

$$m_S(t) \equiv \frac{1}{N'}\langle\Psi(t)|\sum_{j=1}^{N'} S_j^z|\Psi(t)\rangle. \tag{13}$$

Because of the finite size of the system - the numerical calculations presented here have been performed on 16 spins in a chain - all of the quantities are rapidly oscillating functions over

time. As in equation (7) the Loschmidt echo and in equation (2) the local magnetization are trigonometric polynomials over time, the quantity d_S is a more complicated nonlinear functional involving square roots of a trigonometric polynomial. To study the long-time behavior, instead of looking at the actual time series, we therefore examine their distribution functions $P(x) \equiv \overline{\delta\left(x - O(t)\right)}^{t}$, as well as their time-averaged mean, and their variance.
Numerically this is done by diagonalizing the evolution Hamiltonian in the corresponding sector, as described earlier and expanding the evolution in the eigenstate basis. Though this restricts the analysis to relatively small system sizes, it allows one to calculate quantities at any given time. Using 400.000 random samples within a time range more than two orders of magnitude larger as the smallest gap in the system, we obtain good statistics of these rapidly oscillating time series. For the calculation of d_S this is done by expansion of the local density matrix at each sampling time in the basis of spin correlates $S_1^{\alpha_1} \otimes \cdots \otimes S_{N'}^{\alpha_{N'}}$, where $\alpha_i = 0, x, y, z$ and $S_i^0 = \mathbb{1}$.
It is important to note that both the magnetization and distance from the average density matrix have interesting features only when observed locally and would give a trivial Dirac delta distribution if observed globally. For the magnetization this is due to the conservation of angular momentum. For the trace distance this comes from the fact that unitarily evolving the state in the trace distance from the average is equivalent to evolving both states, because the dephased state is stationary under unitary evolution. Since the trace distance is invariant under unitary transformations, the distance globally remains unchanged.

II. FIELD-ENERGY-DEPENDENCE AND QUENCHES IN DIFFERENT REGIMES

The Hamiltonian of the model given in equation (1) represents a fully interacting system. Nevertheless, one can find approximations for some regions and even exact solutions for some particular points. We numerically calculated the five lowest energy levels of the model as a function of the field h on the four adjacent spins in a chain of 16 spins and different ratios of the nearest and next-nearest neighbor coupling (see Fig. 1).

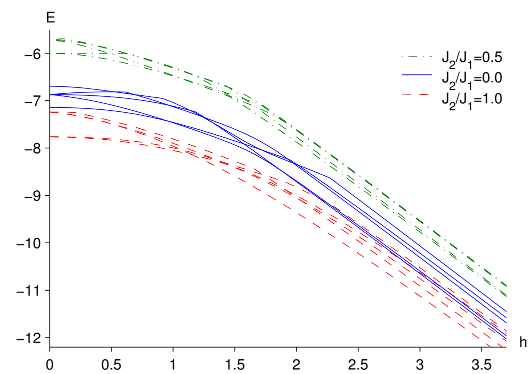

Figure 1: Lowest five energy levels of the model Hamiltonian $H\left(J_1 J_2, h\right) = J_1 \sum_{j=1}^{16} \vec{S}_j \cdot \vec{S}_{j+1} + J_2 \sum_{j=1}^{16} \vec{S}_j \cdot \vec{S}_{j+2} - h \sum_{j=1}^{4} S_j^z$ as a function of the field on four adjacent spins for different ratios of J_2/J_1 ($J_1 = 1$).

Phase diagram for $h = 0$ The phase diagram for the model in zero field and in the large N limit is well known and has been studied for example in [9]. At zero field and $J_2/J_1 = 0$ the model is exactly solvable. In this case we have a Heisenberg spin chain with only nearest-neighbor coupling, which is solvable using the well known Bethe ansatz. For both positive J_1 and J_2 the system is frustrated. For small values of J_2 a gapless antiferromagnetic phase is present. At $J_2/J_1 = 0.241$ a gap opens up and the system remains gaped for all finite J_2 but the gap closes in the limit of $J_2 << J_1$, where the model is approximately described by two weakly coupled chains. At zero field and $J_2/J_1 = 0.5$ is the so-called Majumdar-Ghosh point of the J_1-J_2-model. At this specific coupling, the ground state of the system can be determined analytically. Namely, the system has a two-fold degeneracy at its minimum energy, consisting of the symmetric and the antisymmetric superpositions of the two product states of nearest-neighbor singlets.

The model in finite field For small but finite fields - roughly $h < 0.3$ - we encounter a regime, in which the inter spin coupling still dominates, but the local field acts as a perturbation. The energy-field dependence here is relatively flat. Degeneracies which occur for zero field are lifted.

For intermediate fields - $0.5 < h < 2$ - the Heisenberg coupling and the local magnetic field compete. In this regime we observe numerous level crossings.

For large fields - $h > 2.5$ - the energy levels are dominated by the applied magnetic field, and thus simply decrease linearly with its amplitude. This is caused by the alignment of the

affected spins along the field direction, i. e. $m_S \to 1/2$, thus maximizing the contribution of the Zeeman energy term, $E_{Zeeman} = -h \cdot N'/2$. In this regime one can effectively treat the Heisenberg interaction as a perturbation on the field Hamiltonian for the spins with an applied field. In fact for large fields the slope of all the energy levels in Fig. 1 approach what one would expect from a dominating Zeeman term $\frac{\partial E}{\partial h} \to N'/2 = 2$.
Having these regimes of the model in mind, one could think of various quench scenarios: Small quenches within each of the regimes or large quenches across different regimes.
The simplest are small quenches within the regime of large dominating local fields, where the energy levels in good approximation simply vary linearly with the field amplitude h. As an example of this case, we quenched from an initial field $h = 3.5$ to an evolution field $h' = 3$ for the three different couplings $J_2/J_1 = 0, 0.5, 1$. In all of these cases the Loschmidt echo as well as the local magnetization show Gaussian distributions with very small variances, indicating a good, straightforward equilibration. This is exactly the behavior expected for small quenches in regular regimes.[6] The distribution of the quantity d_s in these cases also resembles a Gaussian, only experiencing a slight asymmetry due to the nonlinearity of the norm. So in regular regimes our example system shows good equilibration, both locally and globally.
Another set of relatively simple quenches are those from large fields to zero field. As the system in this case is strongly perturbed, one would expect numerous excitations across a wide range of energy. According to $\overline{L}^t = 1/d_{eff}$ (equation (8)) a large number of excitations causes a small Loschmidt echo. More specifically such quenches lead to an exponential distribution of the Loschmidt echo with an average very close to zero.[6] In fact we numerically observe such a behavior when quenching from $h = 5$ to $h' = 0$ for all three couplings. Figure 2 shows a good example of a quench from $h = 3$ to $h' = 0$ using only nearest neighbor coupling. In this quench we also obtain single peaked and relatively narrow distributions of the local magnetization and the quantity d_S. Results for different couplings are not shown here, but very similar. This indicates a measure concentration and exactly the kind of strong local equilibration that is possible even for closed quantum systems which has been discussed in [3].

For small quenches in the regime of dominating coupling, we observe different types of equilibration and a strong dependence on the inter-spin coupling. This is discussed in the

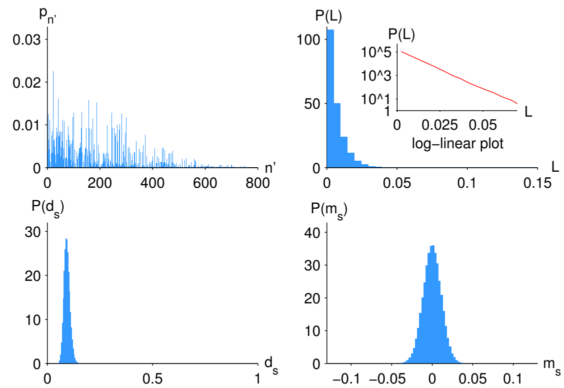

Figure 2: Equilibration statistics of a system of 16 spins in a chain with only nearest neighbor Heisenberg couplings ($J_1 = 1, J_2 = 0$), quenched from an initial configuration with a field $h = 3$ in the z-direction applied to four adjacent spins (denoted by the sublabel S) to zero field on all spins. a) shows the energy probability distribution $p_{n'} \equiv |\langle \Psi_0 | n' \rangle|^2$, b) the corresponding probability distribution of the Loschmidt echo $P(L) = \overline{\delta(L - |\langle \Psi_0 | \Psi(t) \rangle|^2)}^t$, c) the distribution of d_S $\overline{\delta(d_S - \| \rho_S(t) - \overline{\rho_S}^t \|_1)}^t$ and d) the distribution of the normalized local magnetization $\overline{\delta(m_S - 1/2 \mathrm{Tr}[\rho_S(t) \sum_{j=1}^4 S_j^z])}^t$.

following section.

Because of the numerous level crossings between different levels at different amplitudes of the local field, it is very difficult to obtain the phenomenology of quenches within the intermediate regime. Furthermore since different energy level crossings occur at close field amplitudes, we can not separate them numerically.

III. NUMERICAL RESULTS FOR NON-TRIVIAL QUENCHES

We investigate quenches of the form $H(h) \rightarrow H'(h')$ on systems of sizes N=12, N=14 and N=16. We have also performed simulations with different subsystem sizes (N'=3,4). The results we present here are six representative examples of chains with N=16 and a subsystem of four (Quenches 1-3, $N' = 4$) or three adjacent spins (Quenches 4-6, $N' = 3$). For all of them, as numerically calculated, the starting ground state is located in the $M = 0$ sector of vanishing total magnetization.

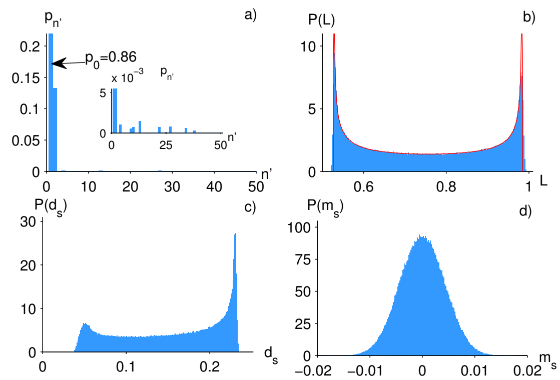

Figure 3: Equilibration statistics of a system of 16 spins in a chain with equal nearest and next-nearest neighbor Heisenberg couplings ($J_2 = J_1 = 1$), quenched from an initial configuration with a field $h = 0.2$ in the z-direction applied to four adjacent spins (denoted by the sublabel S) to zero field on all spins. The quantities shown are the same as in Fig. 2a) to 2d).

A. Quenches on four adjacent spins

Quench 1: The first example is a quench on a system of equal next and next-nearest neighbor couplings ($J_1 = J_2 = 1$). The system is quenched from $H(h = 0.2)$ to $H'(h' = 0)$. The resulting equilibration statistics are shown in Fig. 3. As one would expect for a small quench, the energy probability distribution p_n in Fig. 3a) is dominated by the ground state ($p_0 = 0.86$). A more interesting feature is an additional sizeable contribution of only the first excited state (the population of the first excited state is about two orders of magnitude larger than the population of all the others ($p_1 \ll p_i, i > 1$)).

The existence of two dominating modes leads to a double-peaked distribution function of the Loschmidt echo $P(L)$, which is clearly observed in Fig. 3b). In fact one can completely neglect all the other states $|i\rangle$ for $i > 1$, treat the model as an effective two state system and get a good approximation for the Loschmidt echo using only a constant and a cosine from equation (7):

$$L(t) \approx \underbrace{p_0^2 + p_1^2}_{\approx \overline{L}^t} + 2p_0p_1 \cos[(E_0 - E_1)t]. \tag{14}$$

The corresponding probability distribution function can be calculated analytically:

$$P(l) = \overline{L}^t + \frac{1 - \overline{L}^t \, (l_2 - l_1)}{\pi\sqrt{(l - l_1)(l_2 - l)}}, \tag{15}$$

where $l_1 = \overline{L}^t - 2p_0p_1$, $l_2 = \overline{L}^t + 2p_0p_1$ give the lower and upper edges of the distribution. The result using p_0 and p_1 as numerically obtained for this quench is shown as a red line in Fig 3b). It shows how the system after the quench oscillates between to "states", one of which is close two its initial state, the other relatively far away. This indicates a lack of equilibration, that can also be observed in the variance, which is an order of magnitude higher than in the following quenches (see Table I).

Note, that although double peaked, this distribution should not be confused with the universal double peaked distribution of the Loschmidt echo obtained, if there are exactly three non vanishing p_ns mentioned in [6]. A behavior describing generic quenches from a critical point. The model studied here is far from the large N limit and moreover at $J_2 = J_1 = 1$ and $N \to \infty$ the $J_1 - J_2$ model is gapped.

Especially since the evolution Hamiltonian is translationally invariant, one would also expect to see this non-equilibrium behavior locally. Accordingly, the statistics of d_s in Fig. 3c) shows lack of equilibration. Its distribution function also has a large spread and two maxima, one of which shows a similar divergence as the Loschmidt echo. The asymmetry and the lack of a second peak are not numerical artifacts but arise due to the high nonlinearity of the trace distance, namely its absolute value. A simplified example of this behavior is given in the Appendix.

It is interesting to notice that the distribution of the local magnetization is a Gaussian and is not sensitive to the effects which caused the distributions of the other two observables to display clear signatures of lack of equilibration. This can be explained by the simple fact that the operator for the local magnetization of four adjacent spins has zero weights on the two energy states and their cross terms, which dominate the energy probability distribution. The fact that this observable shows a Gaussian distribution function with a small variance, while others show double-peaked distributions and large variances provides a warning to anyone who may try to use universal distributions of some particular observable to study equilibration. Even though maybe very natural, some observables are simply not well suited to detect the effects which cause such double peaked distributions, namely those observables with very small or zero weights in the low energy states. [15]

Quench 2: The second quench we show is the same quench from a field of $h = 0.2$ on four adjacent spins to zero field, but using only nearest-neighbor coupling ($J_2 = 0$). The energy probability distribution of this quench is shown in Fig. 4a). In this distribution the

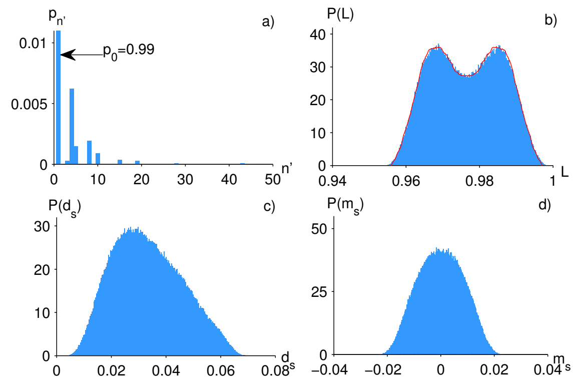

Figure 4: Equilibration statistics of a system of 16 spins in a chain with only nearest-neighbor Heisenberg couplings ($J_1 = 1, J_2 = 0$), quenched from an initial configuration with a field $h = 0.2$ in the z-direction applied to four adjacent spins (denoted by the sublabel S) to zero field on all spins. The quantities shown are the same as in Fig. 3a) to 3d).

ground state is by far dominating ($p_0 = 0.99$), the probability of the next highest populated state is two orders of magnitudes smaller. Overall, there still is a concentration of excitations in the low frequencies ($n < 20$).

As indicated by the distribution of $p_{n'}$, the Loschmidt echo mean of this quench is much closer to one and its variance is about an order of magnitude smaller than with $J_2/J_1 = 1$ (Fig. 4b)). Its distribution still shows two maxima, but they are less pronounced and more Gaussian shaped.

A more general approximation of the Loschmidt Echo distribution function as in the previous quench, that has only two non negligible terms, can be obtained by ordering the cosine terms in equation (7) by the magnitude of their amplitudes $p_{n'}p_{m'}$, keeping only the N_{max} largest terms:

$$\begin{aligned} L(t) &= \overline{L}^t + 2 \sum_{n'<m'} p_{n'}p_{m'} \cos[(E_{n'} - E_{m'})t] \\ &= \overline{L}^t + 2 \sum_{j=1}^{N^2/2-N} A_j \cos(\omega_j t) \\ &\approx \overline{L}^t + 2 \sum_{j=1}^{N_{max}} A_j \cos(\omega_j t), \end{aligned} \tag{16}$$

where $A_j = p_{n'_j}p_{m'_j}$, $\omega_j = E_{n'_j} - E_{m'_j}$ and $A_i < A_j$ for $i < j$. This approximation can then be used to calculate the corresponding distribution function for some particular N_{max}, obtaining an approximation for the Loschmidt echo distribution function. This is done for all of the following quenches. For the quench discussed here, we use $N_{max} = 5$. The resulting approximate distribution is shown as a red line in Fig 4b).

Taking the purity of the original ground state $|\Psi_0\rangle$ in the eigenstate basis of the evolution Hamiltonian H' as a measure, even though h and h' are the same, the effective quench strength is much smaller than in the strongly coupled system with $J_2/J_1 = 1$.

The distribution of d_S in Fig. 4c) looks also very different from the one of the previous quench. Its variance is more than five times smaller, and its relatively flat maximum is at a value about ten times smaller than the peak in the case $J_2/J_1 = 1$. Its asymmetric shape should again be explainable with the high non-linearity of the norm, though we can not think of a simple calculation as in case of the previous shape.

Both quantities, the Loschmidt echo and d_S indicate a much better equilibration. This is somewhat contrary to the behavior of the local magnetization in Fig. 3d), which is again Gaussian, but shows larger rather than a smaller variance.

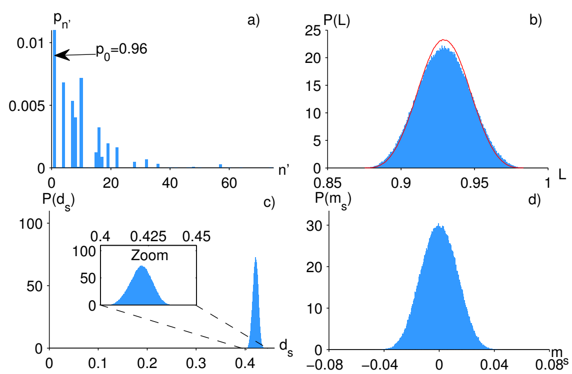

Figure 5: Equilibration statistics of a system of 16 spins in a chain with next-nearest neighbor couplings half as strong as the nearest neighbor couplings ($J_1 = 1, J_2 = 0.5$), quenched from an initial configuration with a field $h = 0.2$ in the z-direction applied to four adjacent spins (denoted by the sublabel S) to zero field on all spins. The quantities shown are the same as in Fig. 3a) to 3d).

Quench 3: The last quench we want to discuss in detail is the special case of $J_2/J_1 = 1/2$. The evolution system in zero field is at the earlier mentioned Majumdar-Ghosh point of the $J_1 - J_2$ model. The system has a two-fold degeneracy at its minimum energy, consisting of two states, each of them being a product state of nearest-neighbor singlets. This degeneracy is lifted in the prequench system of a field $h = 0.2$ on again four adjacent spins.

As a consequence the system can not be treated as non-degenerate as it is done in the introduction, where we discuss the time evolution of observables after a quench in a generic system. To take such degeneracies into account the corresponding formulas have to be modified, e. g. $\overline{\rho}$ includes off-diagonal terms, where $E_{n'} = E_{m'}$ for $n' \neq m'$. Furthermore the prove for inequality (11) given by [3] no more holds, since degenerate systems also break the no degenerate gap condition. Never the less numerically the bound still holds for the local magnetization (see section IV).

Looking at $p_{n'}$ in Fig. 5a), as in the case of $J_2 = 0$ the ground state population is by far dominating. $p_0 = 0.96$, which is a little less than in the previous quench. We also observe many more excitations, non of which is considerably larger than the others. The eigenstate probabilities are still concentrated at low frequencies, but even for $n' > 100$ there are some weak excitations.[16] Notice that quite a few of the lowest energy states, like the first excited state, are not populated at all, but protected by symmetry.

Since the $p_{n'}$ are relatively widely distributed, and other than the ground state there is no special state, we expect and numerically obtain a Gaussian distributed Loschmidt echo, as shown in Fig. 5. As in the previous quench we approximate the Loschmidt echo using the expansion given in equation 16. Only here to obtain a Gaussian shaped distribution of the right width we have to include the 20 largest terms, i.e. $N_{max} = 20$. The corresponding probability distribution is the line shown in Fig. 5b). Compared to the quench at zero next-nearest neighbor coupling the Loschmidt mean is smaller and shows a higher variance. Compared to the quench at $J_2 = J_1$ the effective quench strength still is relatively small. So far this indicates relatively straightforward equilibration.

Therefore the distribution of the quantity d_S shown in Fig. 5c) is quite surprising. It shows the lowest variance of all the quenches discussed and a relatively smooth slightly asymmetric shape, still similar to a Gaussian, but its distribution is separated from zero by a large gap and concentrated around a mean $\overline{d_S} = 0.4195$. This behavior is very different from what we observed so far. Since a similar behavior is shown for small system sizes of 12 and 14 spins in a chain, this appears to be a property of the special point $J_2/J_1 = 1/2$. Even though the evolution is obviously not unitary, since this would lead to a $P(d_s)$ delta-peaked at some fixed value, the subsystem system circles around its average state in a relatively small shell at a large minimum distance. This indicates that it is relatively weakly coupled to the environment, which can be explained by a factorizing dimer phase present even for small local fields $h \neq 0$.

In fact, the ground state of the initial Hamiltonian with a finite local field shows a large overlap with one of the two earlier mentioned product states of nearest-neighbor dimers, whereas the overlap with the other one is effectively zero. Namely it largely overlaps with the state, where the two inner spins of the four adjacent spins affected by the local field form a singlet and the two outer spins each form a singlet with the neighboring spin in the environment. This can be intuitively understood by the field slightly breaking the outer singlets such that the net magnetization on the single spin of the new dimer, which is affected by the field, becomes nonzero, while the singlet in the center is left almost completely undisturbed. This is confirmed by considering a subsystem S' consisting of only the two spins in the center of the field and checking that their evolution is close to unitary. This is in fact the case: both $d_{S'} = 0.3449$ as well as the local von Neumann entropy $S_{S'} = -\mathrm{Tr}(\rho_{S'} \log_2 \rho_{S'}) = 2.0620 \cdot 10^{-4}$ remain constant over time. The evolution of the original subsystem S consisting of all the four spins initially affected by the field, can be understood by combining the evolution of the two outer and the two inner spins. The two dimers crossing the edge of the subsystem are entangled with the environment, which gives $P(d_S)$ a finite width, but then the intact singlet in the center of the subsystem evolves unitarily, and so the subsystem remains far form its time average.

A large d_s does not mean bad equilibration for any local observable, but indicates that there is at least one local observable, which equilibrates badly. As in the other quenches, the distribution function of the local magnetization is a Gaussian centered around zero. Here, in agreement with the Loschmidt echo, its variance is larger than in the case $J_2 = J_1$.

B. Quenches on three adjacent spins

We also show the equilibration statics of the same three quenches just discussed, but with an initial magnetic field of $h = 0.2$ on three instead of four adjacent spins and also referring to these three spins as the subsystem S, i. e. $N = 16$ and $N' = 3$ (Fig. 6-8). As before the system is quenched to an evolution according to the Hamiltonian in zero field $H'(h' = 0)$. These quenches do not need to be discussed in the same detail, but indicate that some of the

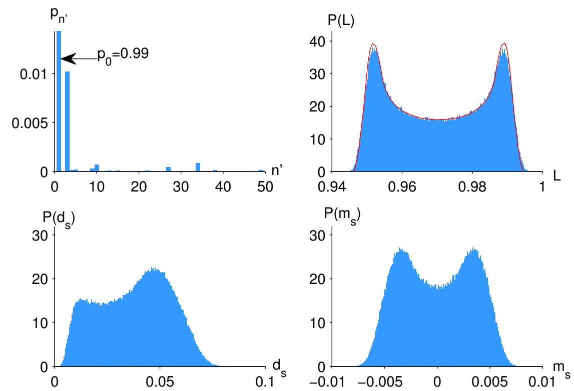

Figure 6: Equilibration statistics of a system of 16 spins in a chain with equal nearest and next-nearest neighbor Heisenberg couplings ($J_1 = J_2 = 1$), quenched from an initial configuration with a field $h = 0.2$ in the z-direction applied to three adjacent spins (denoted by the sublabel S) to zero field on all spins. The quantities shown are the same as in Fig. 3a) to 3d).

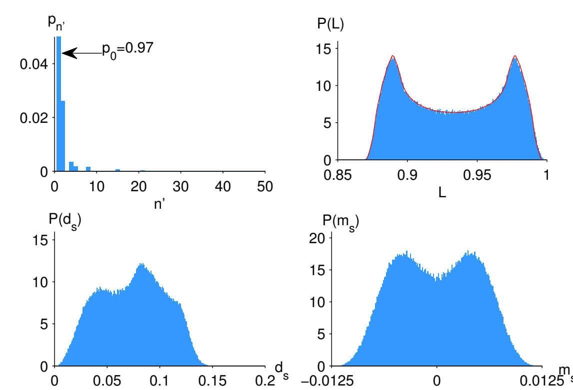

Figure 7: Equilibration statistics of a system of 16 spins in a chain with only nearest-neighbor Heisenberg couplings half ($J_1 = 1, J_2 = 0$), quenched from an initial configuration with a field $h = 0.2$ in the z-direction applied to three adjacent spins (denoted by the sublabel S) to zero field on all spins. The quantities shown are the same as in Fig. 3a) to 3d).

observed patterns are not restricted to $N' = 4$ and provide a few interesting other features. Also notice that the corresponding variances of the considered quantities L, d_S and m_S in the case of $N' = 3$ are much smaller than for $N' = 4$. One reason, why we do not consider quenches on only 1 or 2 spins (see Tables I and II).

Quench 4: In the case of $J_2 = J_1 = 1$ (Fig. 6) one obtains a similar dominance of two modes as in the case of $J_2 = J_1 = 1$ and $N' = 4$, but with a few contributions of other

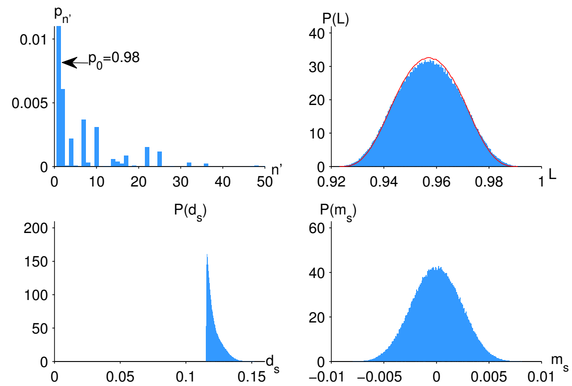

Figure 8: Equilibration statistics of a system of 16 spins in a chain with next-nearest neighbor Heisenberg couplings half as strong as the nearest neighbor couplings ($J_1 = 1, J_2 = 0.5$), quenched from an initial configuration with a field $h = 0.2$ in the z-direction applied to three adjacent spins (denoted by the sublabel S) to zero field on all spins. The quantities shown are the same as in Fig. 3a) to 3d).

states, that are only one order of magnitude smaller than the smaller of the two dominating modes. The Loschmidt echo distribution accordingly is similarly double peaked but more smooth and with a spread, that is about an order of magnitude smaller. To obtain a good result using the approximation given by equation (16), we use $N_{max} = 5$. The contribution of these few other states is even more visible in the distribution of d_S, which again shows two maxima, but is much less spiked. Note that the local magnetization as opposed to the quench on four spins is in fact double peaked, following a distribution function similar to the one of the Loschmidt echo. This can simply be explained by the fact that the two dominating modes, namely the ground state and the second excited state in this case have a finite crossterm in the local magnetization.

Quench 5: The quench using only nearest neighbor coupling in Fig. 7 shows a distribution of the $p_{n'}$, which is very similar to case of $J_2 = J_1 = 1$ and $N' = 3$, but the additional non-negligible modes are concentrated in the low lying energy eigenstates as in the case of $J_2 = 0, J_1 = 1$ and $N' = 4$. The Loschmidt echo is again double peaked and approximated nicely using $N_{max} = 5$ in equation (16), but opposed to the case of $J_2 = J_1 = 1$ and $N' = 3$ there is a small additional kink in the to outer "flanks" of the distribution. This leads to an additional kink on the right end of distribution function of d_S, which due to the nonlinearity of the trace distance is in fact much more visible. As in the case of $J_2 = J_1 = 1$ and $N' = 3$ the magnetization also shows two maxima, but they are less sharp.

Quench 6: The last quench shown in Fig. 8 is in the case of $J_1 = 1, J_2 = 0.5$, where the evolution Hamiltonian in zero field is at the Majumdar-Gosh point. As in the case of $N' = 4$ one observes a relatively large number of non-vanishing modes and a Gaussian distribution of both the Loschmidt echo and the local magnetization. To obtain the approximation shown in Fig. 8b) one has to keep only the ten largest terms of equation (16), i. e. $N_{max} = 10$. The distribution of d_s shows a similar gap at small distances as in the case of $N' = 4$, but its mean is smaller and the distribution is highly non symmetric and peaked at its minimum distance.

J_2/J_1	$\overline{L}$	$\overline{d_S}$	$\overline{m_S} \cdot 10^{-5}$
1	0.7506	0.1540	0.6466
0.5	0.9256	0.4195	0.0467
0	0.9727	0.0332	-2.8494
J_2/J_1	Var(L)	Var(d_S)	Var(m_S)
1	0.0282	0.0040	0.000075
0.5	0.0037	0.0007	0.00065
0	0.0039	0.0002	0.00028

Table I: Means and Variances of the Loschmidt echo $L = |\langle\Psi_0|\Psi(t)\rangle|^2$, the quantity $d_S = \|\rho_S(t) - \overline{\rho_S}^t\|_1$ and the normalized local magnetization $m_S = 1/2\text{Tr}\left[\rho_S(t)\sum_{j=1}^4 S_j^z\right]$ for quenches form a field of $h = 0.2$ on a Subsystem S consisting of 4 adjacent spins to zero field on all 16 spins for different coupling ratios J_2/J_1.

IV. DISCUSSION OF THE BOUND INDUCED BY THE QUANTITY d_S WITH RESPECT TO THE LOCAL MAGNETIZATION

The interpretation of d_S as an upper bound for the distinguishability from equation (11) can be applied to the magnetization in several ways, first off one can look at the closest the magnitude of the local magnetization can be to d_S at any time. [17] If the maximum ratio between the magnitude of the local magnetization and the quantity d_S is 1 it would

J_2/J_1	$\overline{L}$	$\overline{d_S}$	$\overline{m_S} \cdot 10^{-5}$
1	0.9704	0.0376	-1.5295
0.5	0.9571	0.1214	0.4531
0	0.9334	0.0740	-3.9441
J_2/J_1	Var(L)	Var(d_S)	Var(m_S)
1	0.00021	0.00028	0.00043
0.5	0.00013	0.000028	0.00019
0	0.0013	0.00094	0.00082

Table II: Means and Variances of the Loschmidt echo $L = |\langle\Psi_0|\Psi(t)\rangle|^2$, the quantity $d_S = \|\rho_S(t) - \overline{\rho_S}^t\|_1$ and the normalized local magnetization $m_{S'} = 1/2\mathrm{Tr}\left[\rho_S(t)\sum_{j=1}^4 S_j^z\right]$ for quenches form a field of $h = 0.2$ on a Subsystem S consisting of 3 adjacent spins to zero field on all 16 spins for different coupling ratios J_2/J_1.

indicate that, at some time, the local magnetization is among the best local operators for distinguishing a local state from the time average, this would correspond to the fluctuations in the subsystem being describable as a superposition of classical states all with the same non zero magnetization, at least this instant. If this ratio is very small it says that the magnetization is always a relatively poor operator for distinguishing a local state from the time average, meaning that the fluctuations have a very small net magnetization for all time. For the four local spins after a quench from a small local magnetic field applied to these four spins to an evolution Hamiltonian at the Majumdar-Ghosh point (Quench 3, Section III), the maximum ratio is 0.049, meaning that the net magnetization is never a very good operator for detecting fluctuations in the subsystem and the bound easily holds even though the system is degenerate. This is not surprising because the subsystem wave-function is known to contain a singlet, which by construction has a zero magnetization. If most of the deviation from the time average in this system is caused by this singlet than the magnetization will never be a good observable to distinguish a state from the time average.

For a quench on three local spins again from a small local magnetic field applied to these three spins to again zero field in the evolution Hamiltonian using $J_2 = 1$, the ratio of the local magnetization to d_S is 0.4859, at some time, roughly an order of magnitude higher than in the previous quench at the Majumdar-Ghosh point.

The maximum ratio for the other quenches lies somewhere between these two extremes. Instead of looking at the maximum ratio of magnetization to d_S one could look at the time average ratio, on average the local magnetization appears to be a very poor operator for distinguishing from the time average state for all quenches we look at. The ratio is of order $10^{-7} - 10^{-8}$ in all cases. Surprisingly the average of this ratio for the quenches to the Majumdar-Ghosh point is not always smaller than for other quenches, this can be explained by the fact that for most times the local magnetization seems to be such a poor operator for distinguishing from the time average that the effect of the singlet in the Majumdar-Ghosh system is not immediately obvious.

V. CONCLUSIONS

Using a numerical approach to study local quenches on a fully interacting system, we show that quantum informational quantities such as the Loschmidt echo and the trace distance of the time evolved local density matrix to its time average provide a useful tool to study equilibration in closed quantum systems. Even in a relatively small but complex system we observe some of the universal behavior of the Loschmidt echo as discussed in [6] and [7], namely Gaussian and exponential shaped distribution functions. We also gain some insight in how these relate to distributions of the quantity d_S and the local magnetization. We thereby show that this natural observable of spin chains can be a bad choice to study equilibration. Namely, in some cases it indicates smooth equilibration, whereas the first two quantities show clear non-equilibrium features.

We also observe that simple quantities such as the mean and the variance of the Loschmidt echo or the quantity d_s provide bounds, but insight in the quenches shown is only given by their distribution functions.

Global and local equilibration In fact, the long-time behavior of the system after a quench can depend on the details of the parameters used. In most cases we find agreement between the indications of the global quantity Loschmidt echo and the quantity d_S. For quenches within the regime, which is dominated by the local magnetic field, or for quenches from a large local magnetic field to zero magnetic field (section II) both quantities show a smooth equilibration. In the case of a quench from a small local field to zero field using equal nearest and next-nearest neighbor Heisenberg couplings (quench 1, section III) both show strong non-equilibrium features. However in some cases the relation between the first one providing a measure for global weak equilibration and the second one measuring local strong equilibration, can be more complicated. In the special case given by a quench form a small local field to zero field using $J_2/J_1 = 0.5$ (quench 3 and quench 6,section III), even though the Loschmidt echo indicates a global equilibration in the weaker sense, the system locally stays very far from its average state for all time.

These observations demonstrate that even though some natural quantities might show a Gaussian distribution and might therefore even be well described by some statistical ensemble, this does not imply that the system itself and therefore any reasonable quantity is close to equilibrium. We showed that in some cases the Loschmidt echo and the local trace distance indicate different equilibration behaviors globally and locally and in such a way cannot be thought of as containing the same information, but as providing complimentary insights.

Different shapes of equilibration For the Loschmidt echo we show a simple way of almost perfect approximation using only the largest contributions in the eigenstate expansion given by equation (16). Not only does this provide a nice tool for a fast and easy calculation, it is also helpful in understanding the phenomenology observed.

The quench from a small field on four adjacent spins to zero field shown in Fig. 3 using $J_2 = J_1 = 1$ provides the extreme example of only two dominating modes giving rise to a distribution function with two square root divergences and a large spread. As in Fig. 6, a quench starting from a small field on three adjacent spins using again $J_2 = J_1 = 1$, an increased number of non-negligible excitations can lead to a distribution that is still double peaked but less divergent. The example provided in Fig. 4, a quench from a small field on four adjacent spins using only nearest neighbor Heisenberg coupling $J_2 = 0, J_1 = 1$, shows a transient example of a smooth transition, to a Gaussian distribution of the Loschmidt echo as it is seen in quenches using $J_2 = 0.5, J_1 = 1$ from a small field on three or four adjacent spins (Fig. 8 and 5), nicely approximated using 10 or 20 non-negligible terms of $p_n p_m$.

Furthermore the quenches studied here, a large spread of the time series of the Loshmidt echo is accompanied with the arise of two rather then only a single peak in its distribution function. Although we only show this for some examples on a specific system and do not provide any further arguments, we do not see a reason, why this behavior should not be encountered in other systems of similar size, especially in one dimensional spin chains.

Appendix

Let us assume that we have a system divided in a subsystem S and an environment E. The two corresponding basis shall be given by $\{|a\rangle, |b\rangle, \cdots\}$ and $\{|\alpha\rangle, |\beta\rangle, \cdots\}$. To model quench 1 and to simplify the calculation we further assume that only two eigenstates of the closed system $S \otimes E$ contribute to the full density matrix. (A reasonable simplification of the p_n distribution in Fig. 3a).) To model the strongly coupled system and to obtain a non-unitary evolution of the subsystem, we have to introduce entanglement. This can be done by taking the to following states:

$$|1\rangle \equiv \left(|a, \alpha\rangle + |b, \beta\rangle\right)/\sqrt{2} \tag{17}$$

$$|2\rangle \equiv \left(|a, \alpha\rangle - |b, \beta\rangle\right)/\sqrt{2}. \tag{18}$$

Note that this is an assumption, which makes the further calculation very simple, but here is not physically motivated. Using the initial state $|\Psi_0\rangle \equiv c_1 |1\rangle + c_2 |2\rangle$ we compute $d_s(t)$ and its distribution. Given the energy difference $\omega = E_2 - E_1$ of the two eigenstates we obtain

$$\rho - \overline{\rho} = c_1 c_2^* |1\rangle \langle 2| e^{-i\omega t} + h.c. \tag{19}$$

Tracing out the degrees of freedom of the bath this simplifies to

$$\rho_S - \overline{\rho_S} = \mathrm{Tr}_B \left(\rho - \overline{\rho}\right) \tag{20}$$

$$= c_1 c_2^* \left(|a\rangle \langle a| - |b\rangle \langle b|\right) e^{i\omega t} + h.c.. \tag{21}$$

Calling $c_1 c_2^* = \sqrt{p_1 p_2} e^{i\varphi}$ and using a matrix representation we get

$$\rho_S - \overline{\rho_S} = \sqrt{p_1 p_2} \cos\left(\omega t + \varphi\right) \begin{pmatrix} 1 & 0 \\ 0 & -1 \end{pmatrix} \tag{22}$$

We finally get

$$d_S(t) = \sqrt{p_1 p_2} \left|\cos\left(\omega t + \varphi\right)\right| \tag{23}$$

Its distribution function can be calculated analytically, giving a simple description of a divergence similar to what we have seen numerically:

$$
\begin{aligned}
P\left(d_S\right) &= \lim_{T\to\infty}\frac{1}{T}\int_0^T \delta\left(d_S\left(t\right)-d_S\right)dt && (24)\\
&= \frac{1}{\pi/\omega}\int_0^{\pi/\omega}\delta\left(\sqrt{p_1p_2}\left|\cos\left(\omega t\right)\right|-d_S\right)dt && (25)\\
&= \frac{2/\pi}{\sqrt{p_1p_2-d_S^2}} && (26)
\end{aligned}
$$

Note that in this case d_S takes values in $d_S \in \left[0,\sqrt{p_1p_2}\right]$, so such a $P\left(d_S\right)$ has only one square root singularity at the upper edge. If we simply take the two largest amplitude contributions of Fig. 3a), we can estimate the peak in Fig. 3c) to be around $\sqrt{0.86\cdot 0.13}=0.33$. Given the great simplification this estimate is quite useful.

Chapter 1 References

[1] N. Chancellor and S. Haas, Phys. Rev. B 84, 035130 (2011)

[2] S. Popescu, A. J. Short and A. Winter, Nature 444, 754-758 (2006)

[3] N. Linden, S. Popescu, A. J. Short and A. Winter, Phys. Rev. E 79, 061103 (2009)

[4] S. Goldstein, J. L. Lebowitz, R. Tumulka and N Zanghi, Phys. Rev. Lett. 96, 050403 (2006)

[5] P. Reimann, Phys. Rev. Lett. 99, 160404 (2007)

[6] L. Campos Venuti and P. Zanardi, Phys. Rev. A 81, 022113 (2010)

[7] L. Campos Venuti and P. Zanardi, Phys. Rev. A 81, 032113 (2010)

[8] D. Rossini, T. Calarco, V. Giovannetti, S. Montangero and R. Fazio, Phys. Rev. A 75, 032333 (2007)

[9] L.C. Kwek, Y. Takahasi and K.W. Choo, Journal of Physics: Conference Series 143, 012014 (2009).

[10] A global field of the form $h\sum_{j=1}^{N} S_j^z$ commutes with Heisenberg couplings. Corresponding quenches would be trivial.

[11] Using a local field of the form $h\sum_{j=1}^{N'} S_j^z$, there is an interesting symmetry. Performing a quench by applying an initial field on N' adjacent spins is effectively the same as applying the same field on $N - N'$ adjacent spins.

[12] To obtain a good approximation of the full sector we checked for the normalization condition $\sum_{n'=1}^{500} |\langle\Psi_0|n'\rangle|^2 > 0.9999$.

[13] i. e. given any four energy eigenvalues $E_n - E_m = E_l - E_k$ implies that ether $n = m$ and $k = l$ or $n = l$ and $m = k$. As described in [3], this assumption is very generic, since it can always be achieved by introducing an arbitrarily small perturbation.

[14] Note as a positive quantity fluctuations can be bound against the mean using Markov's inequality.

[15] For a quench using a field on only three adjacent spins, we observed a similar p_n distribution. Only here not the first, but the second excited state got a large contribution. This state has a cross term with the ground state in the local magnetization of three adjacent spins, and hence a double-peaked distribution function was observed not only in the Loschmidt echo, but also

in the local magnetization. (see Quench 4)

[16] For visibility reasons these are not shown in the graph. But for all the examples given here, we calculated the first 500 eigenstates of H' and their overlap with the ground state of H.

[17] In the quenches discussed here the average of the local magnetization is so close to zero that the offset from the time average is basically already given by the magnetization

Chapter 2: Transport by Degenerate Groundstates

This Chapter is based on Propagation of Disturbances in Degenerate Quantum Systems by N. Chancellor and S. Haas [1].

Disturbances in gapless quantum many-body models are known to travel an unlimited distance throughout the system. Here, we explore this phenomenon in finite clusters with degenerate ground states. The specific model studied here is the one-dimensional J1-J2 Heisenberg Hamiltonian at and close to the Majumdar-Ghosh point. Both open and periodic boundary conditions are considered. Quenches are performed using a local magnetic field. The degenerate Majumdar-Ghosh ground state allows disturbances which carry quantum entanglement to propagate throughout the system, and thus dephase the entire system within the degenerate subspace. These disturbances can also carry polarization, but not energy, as all energy is stored locally. The local evolution of the part of the system where energy is stored drives the rest of the system through long-range entanglement. We also examine approximations for the ground state of this Hamiltonian in the strong field limit, and study how couplings away from the Majumdar-Ghosh point affect the propagation of disturbances. We find that even in the case of approximate degeneracy, a disturbance can be propagated throughout a finite system.

VI. INTRODUCTION

This paper uses quantum information measures, such as entanglement, and trace distance to study quantum many body systems. Unlike physical observables, such quantities usually cannot be directly measured [2], but can give an important insight into the properties of the system. Abstract concepts such as quantum entanglement have been important for almost as long as quantum mechanics has existed [3]. The power of these information theoretical quantities is that they represent general ideas that can be applied to any system which can be considered quantum. By studying such abstract quantities one can more easily generalize a result for a specific system to more universal behavior. Examples of successful application of quantum information measures to the study of quantum many body systems are many, a few examples are [4–9]. The specific uses of these quantities can be diverse, for example in [5] the authors use the concept of trace distance from an averaged density matrix to define a type of quantum equilibration which would be analogous to equilibration in classical thermodynamics. Similar questions are examined, but with different methods, in [6, 7], where the concept of equilibration is used to detect criticality in a system. In [4] a quantity related to fidelity is used to detect quantum chaos. This chapter will make broad use of such quantum informational quantities, but will deal with relatively few direct observables. This is because our intention is to provide a study which can be easily related to other quantum systems, and to quantum many body theory in general.

The central result of this paper involves a type of local quench which can propagate disturbances an unlimited distance in a J1-J2 Heisenberg spin chain. The unitary dynamics of spin chains which can be studied through quenches can be realized experimentally with trapped cold atoms [10, 11]. Certain superconducting qubit arrays can also provide promising physical realizations of spin chain Hamiltonians [12, 13]. Quenches are also important from a theoretical perspective. For example, quantum equilibration can be induced and studied in spin chains using various quenches [5–7, 14]. Certain local quenches have also been proposed as a way to physically measure entanglement entropy [2]. Furthermore local magnetic field quenches similar to those studied in this paper have been used to study entanglement specifically in Heisenberg spin chains[8], as well as other quantum systems [9]. A generalization of the specific system which is studied in this paper has also been proposed as being possibly useful in quantum computation [15].

The frustrated spin-1/2 anti-ferromagnetic Heisenberg chain has one of the most prototypical matrix product ground states, featuring a two-fold degeneracy at the so-called Majumdar-Ghosh point [16], when the nearest-neighbor and next-nearest-neighbor exchange integrals are the same. The Hamiltonian of this system is given by

$$H_{MG} = \sum_{j=1}^{N} \left(\vec{S}_j \cdot \vec{S}_{j+1} + \frac{1}{2} \vec{S}_j \cdot \vec{S}_{j+2} \right), \tag{27}$$

where the sum extends over N lattice sites, and the two terms represent anti-ferromagnetic nearest-neighbor and next-nearest neighbor Heisenberg interactions respectively. The ground state of this model is exactly known [16],

$$|\psi_{1,MG}\rangle = \bigotimes_{l=1}^{\frac{N}{2}} \frac{(|\uparrow_{2l-1}\downarrow_{2l}\rangle - |\downarrow_{2l-1}\uparrow_{2l}\rangle)}{\sqrt{2}}, \tag{28}$$

i.e. the product of nearest-neighbor spin singlets, assuming an even number of lattice sites. For the case of open boundary conditions, this state is unique, whereas for periodic boundary conditions it is two-fold degenerate, as the underlying lattice can be decorated by the singlet product state in another unique way,

$$|\psi_{2,MG}\rangle = \bigotimes_{l=1}^{\frac{N}{2}} \frac{1}{\sqrt{2}}(|\uparrow_{mod_N 2l}\downarrow_{mod_N(2l+1)}\rangle - |\downarrow_{mod_{\frac{N}{2}} 2l}\uparrow_{mod_{\frac{N}{2}}(2l+1)}\rangle).$$

The resulting ground state for the periodic system is a superposition,

$$|\psi_{PB,MG}\rangle = a|\psi_{1,MG}\rangle + b|\psi_{2,MG}\rangle, \tag{29}$$

where the two terms are not automatically orthogonal.[17] Hence, changing the boundary conditions of the Hamiltonian from open to periodic one goes from a unique to a two-fold degenerate ground state, thus allowing us to study the effects of a ground state degeneracy.

Local disturbances of this ground state can be introduced by applying a local magnetic field h to a subset of N' adjacent spins,

$$H(h, N') = H_{MG} - h\sum_{j=1}^{N'} S_j^z, \tag{30}$$

where without loss of generality we consider the direction of the applied field to be along the z-direction.

One can take advantage of the fact that spin polarization is conserved in this system, allowing one to reduce the complexity of the problem by dividing the Hamiltonian into independent spin sectors, which may each be diagonalized independently. These sectors correspond to the total polarization of the system in the z direction, and may be diagonalized independently. The polarization sector which contains the global ground state of the system changes with field strength, therefore figures 11, 11,13,17, 18, and 19 all show curves for three different polarization sectors. Each sector is labeled with the total z polarization of the entire spin chain in that sector, which is conserved under the action of all Hamiltonians considered in this paper. For example in the basis where S_j^z is diagonal, all of the basis

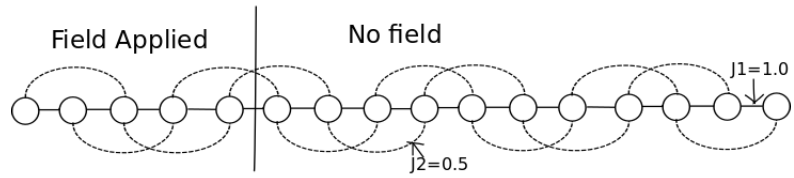

Figure 9: Example of a local field applied to the Majumdar-Ghosh Hamiltonian.

states in the L=0 sector will have the same number of spins pointing in +z as -z, in the L=-1 state, 2 more spins will be facing in -z than +z, etc.

In this study, we identify several effects induced by the application of a local magnetic field, as depicted in Fig. VI. Here we briefly summarize our findings.

Firstly, for sufficiently small field amplitudes polarization induced by the local magnetic field is stored in the vicinity of the region to which the field is applied, instead of spreading throughout the entire system. Only beyond a certain threshold field, i.e. once some of the polarization in this boundary region has saturated, can it spread throughout the entire system. We argue that this is to be expected because at the Majumdar-Ghosh point the energy spectrum of the J1-J2 Heisenberg Hamiltonian is gapped. Provided that the energy gained from the locally applied magnetic field is small compared to the coupling energy of the spins, any state which keeps the majority of spins in a matrix product configuration similar to the zero field ground state will have a lower energy. For an even number of spins in the non-field region, the system can only accomplish this if the total polarization of a given subsystem far from the field region is zero. The spins in the field region align in the direction of the applied field, thus in turn leading to an excess opposite polarization of the spins not directly subjected to the field. This induced polarization is typically localized near the edge of the field region. We will show, however, that this effect does not occur if the two degenerate ground states lie in different polarization sectors, because in this case the polarization can spread through the degenerate subspace at no energy penalty.

We will also show that, for a sufficiently small fraction of the spins subjected to the field, there exists at least one state in one of the polarization sectors which looks locally like the zero field (MPS) ground state far from the field (Fig. 10). For the systems studied in this paper one of these states is always the ground state.[18]

For the case of periodic boundary conditions, any state which lies locally in the degenerate

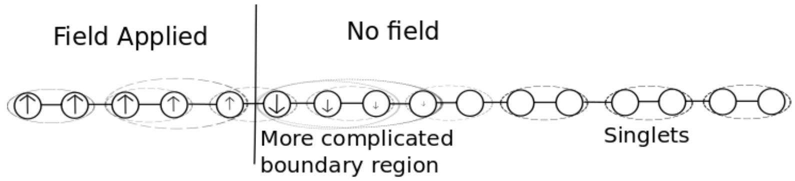

Figure 10: Sketch of a typical state of the spins when exposed to a field. For all field strengths studied here, the ground state of at least one total spin sector behaves like this, and one of these states always is the global ground state of the system. Ovals represent entanglement, arrows indicate spin polarization.

subspace far from the local magnetic field region will have the minimum local contribution to the energy. This means that even for a system with many more spins outside of the field than within it, a disturbance can easily propagate throughout the entire zero field region.

This paper is organized as follows. In the following section VII, we introduce the observables on which we focus on understanding the effects of a local applied magnetic field on this many-body system. The cases of open and periodic boundary conditions need to be treated separately. In section VII, we then discuss the physics of open chains, and in section 4 the phenomena observed in periodic systems. In section IX, we consider how these results are affected when one departs from the Majumdar-Ghosh point in the underlying Hamiltonian. This is followed by conclusions in section X.

VII. PHYSICAL OBSERVABLES

A. Open boundary conditions

For open boundary conditions the field is applied to N' spins on one end of the chain. Unless otherwise stated, we consider finite chains with a total number of spins, N, performing full numerical diagonalizations of the frustrated Majumdar-Ghosh Heisenberg Hamiltonian. Several observables are studied. The first is the total polarization outside of the region subjected to the applied field. While the total spin polarization of the chain is conserved, local polarization is not. This quantity is defined as

$$L_{\neg N'} = \left\langle \psi \mid \textstyle\sum_{j=N'+1}^{N} S_j^z \mid \psi \right\rangle \tag{31}$$

Furthermore, we study the trace distance from a singlet state of the two spins at the end of the chain opposite to the region of the applied magnetic field, i.e. the spins located at sites $N-1$ and N. This observable is defined as

$$d_s = \frac{1}{2}\|\rho_s - \frac{1}{2}(|\uparrow\downarrow\rangle - |\downarrow\uparrow\rangle)(\langle\uparrow\downarrow| + \langle\downarrow\uparrow|)\|_1, \tag{32}$$

where

$$\rho_s = \mathrm{Tr}_{\neg s}(|\psi\rangle\langle\psi|), \tag{33}$$

$$\|O\|_1 \equiv \mathrm{Tr}\sqrt{O^\dagger O}. \tag{34}$$

Finally, we focus on the polarization of the spins at sites $N-1$ and N, defined the same as in Eq. 31, but with the sum running from N-1 to N. In this paper the subsystem of the 2 furthest spins will be labeled f. This observable tells about whether the polarization has been allowed to spread to the furthest 2 spins from the field.

Two different sizes of field regions are considered, N'=5 and N'=4. The reason that both are considered separately is that there are significant even-odd effects.

In this paper, no actual quenches are performed in the system with open boundary conditions, and all observables are given for the ground state of a given sector.

B. Periodic boundary conditions

For periodic boundary conditions, the field is applied to a region of N' adjacent spins. In this case, we are considering chains with an even number of sites. While the observables studied in the periodic case are defined in analogy to those studied in the open case, some extra care is necessary. In particular, a complication arises for the trace distance from a singlet for the two spins furthest from the field region. For periodic boundary conditions, there is no unique choice of singlet covering for the system. Two different approaches to this problem are examined. Firstly, one can consider the distance from the closest of the two singlet coverings for a subsystem,

$$\begin{aligned} d_{s,cover} = min(&\|\rho_s - \mathrm{Tr}_{\neg s}(|\psi_{1,NF}\rangle\langle\psi_{1,NF}|)\|_1, \\ &\|\rho_s - \mathrm{Tr}_{\neg s}(|\psi_{2,NF}\rangle\langle\psi_{2,NF}|)\|_1). \end{aligned} \tag{35}$$

However, this quantity has a drawback, i.e. all but a zero measure set of states in the degenerate subspace will have a finite distance to either of these coverings. An alternative approach is to look at the distance from the closest point in the subspace to the reduced density matrix,

$$d_{s,subspace} = min_{a,b}(\|\rho_s - (\|a|\psi_{1,NF}\rangle + b|\psi_{2,NF}\rangle\|_2)^{-2} \times (\mathrm{Tr}[(a|\psi_{1,NF}\rangle + b|\psi_{2,NF}\rangle)(a^\dagger\langle\psi_{1,NF}| + b^\dagger\langle\psi_{2,NF}|)]\|_1). \tag{36}$$

This equation appears as though it can be further simplified in an obvious way, but remember that the two wave functions are not orthogonal. The norm in the denominator is the usual L2 norm for a vector. Also in this case the minimization is actually simpler than it looks, by realizing that it can be reduced to: $d_{sing,subspace} = min_{0\leq\alpha\leq 1}\|\rho_s - ((1-\alpha) \times \frac{1}{2}(|\uparrow\downarrow\rangle - |\downarrow\uparrow\rangle)(\langle\uparrow\downarrow| + \langle\downarrow\uparrow|) + \alpha \times 1_4)\|_1$ where $1_4$is the 4-dimensional identity operator.

While the observables presented in this section could be considered as time dependent variables, in this paper they are always studied for the ground state of a given polarization sector.

C. Small magnetic field quenches

Because of the degeneracy caused by the periodic boundaries there is another quantity which is interesting to look at, relating to a field quench performed by changing the magnetic field instantaneously and subsequently monitoring the time evolution of the system, especially in regions far from where the local field is applied. Unitary evolution gives the time evolution of a system following a quench at time $t = 0$, in terms of energies E_n,

$$\rho_{m,n}(t) = c_m^* c_n \exp[-\imath(E_n - E_m)t] \quad , \tag{37}$$

where $c_m = \langle m \mid \psi\rangle$, where $|\psi\rangle$is the pre-quench ground state of the system. This leads to a definition of the time averaged state,

$$\bar{\rho}_{m,n} = c_m^* c_n \delta(E_n - E_m) \quad . \tag{38}$$

The field quench is performed by taking $|\psi(t=0)\rangle = |\psi_0\rangle$ to be the ground state of a Hamiltonian with a slightly stronger field, $H_0 = H - \epsilon\sum_{j=1}^{N'} S_j^z$. At $t = 0$, ϵ is instantaneously turned off. In our analysis of the time evolution, we will focus on the trace distance from the time averaged (or dephased) state of the density matrix of the two spins furthest away from the field region

$$d_{av}(t) = \|\mathrm{Tr}_{\neg s}(|\psi(t)\rangle\langle\psi(t)|) - \bar{\rho}_s\|_1. \tag{39}$$

D. Large magnetic field quenches

We also examine the time evolution due to large local field quenches. Several statistical distributions are studied to understand the ensuing equilibration behavior. These quenches are performed in a regime where quenches are shown to disturb the entire system, even regions far away from the field region. A global quantity which is studied is the Loschmidt echo, a measure of the overlap of the time evolved system with the initial state,

$$LE(t) = |\,\langle \psi \mid exp(-\imath\, H\, t) \mid \psi \rangle\,|^2. \tag{40}$$

Two local linear quantities are examined as well. In the region subjected to the local external field, the local polarization is studied. This is simply the expectation value of the magnetization operator with respect to the local density matrix,

$$L_{N'}(t) = \mathrm{Tr}(\rho_{N'}(t) M). \tag{41}$$

In the region far from the spins where the local magnetic field is applied, all of the states are expected to be locally within the degenerate ground state subspace and therefore have zero magnetization. Therefore, a more appropriate observable to use is the overlap with a singlet state,

$$O_s(t) = \mathrm{Tr}(\rho_s(t)\mathrm{Tr}_{\neg s}(|\psi_{1,NF}\rangle\langle\psi_{1,NF}|)). \tag{42}$$

Finally an important non-linear local quantity is studied far from the local magnetic field, the time evolving distance to the average state, defined by

$$d_s(t) = \|\rho_s(t) - \bar{\rho}_s\|_1. \tag{43}$$

This quantity is important, as it provides a direct measure of equilibration locally, and can thus be used to show that the quench not only disturbs the system far from the field, but also that these disturbances can cause equilibration.

E. Entanglement maps

A tool which is used in this paper for visualizing quantum states is a map of two point entanglement. In these graphics, colors are used to indicate entanglement strength between single spins using von Neumann entropy,

$$S_{VN}(\rho) \equiv \mathrm{Tr}(\rho \log(\rho)), \tag{44}$$

as a measure of entanglement.

These graphics consist of arrays of colored squares where, for off-diagonal elements, the color corresponds to the entanglement between the two spins. The diagonal elements correspond to the difference between the maximum possible entropy on a spin and the actual entropy. This represents the the amount of information left about a spin after the rest of the system is measured. These maps are created using

$$\begin{aligned} entMap(i,j) \;=\; & (1-\delta_{ij}) * ((S_{VN}(\rho_i) + (S_{VN}(\rho_j) - S_{VN}(\rho_{ij})) + \\ & \delta_{ij} * (S_{VN}(\frac{1}{2} * 1_2) - S_{VN}(\rho_i)) \end{aligned} \tag{45}$$

The color scale with the maximum entanglement normalized to 1 appears in Fig. 12. It is important to note that while these figures can give a good general impression of entanglement behavior of the system, they do not tell the whole story, i.e. they only give information about two-point entanglement. Just because one of these figures shows no two point entanglement for a pair of spins, this does not mean that they are not entangled in a more complicated way.[19]

Although in principle there is nothing preventing one from obtaining entanglement maps for time averaged states, in this paper we only use this technique to study eigenstates.

VIII. LOCAL MAGNETIC FIELD APPLIED TO MAJUMDAR-GHOSH CHAINS WITH OPEN BOUNDARIES

Subjecting a local region of a Majumdar-Ghosh spin chain to an external magnetic field forces the exposed spins to align with the field. Because of polarization conservation, excess polarization opposite to the direction of the field is generated in the field-free region of the system. In the sector of zero total spin polarization ($L = 0$), and for sufficiently large magnetic field strengths, this can cause spins far from the field region to switch to non-trivial polarized configurations, whereas for smaller applied fields they remain in a spin singlet product state. In contrast, in polarization sectors with $L \neq 0$ excess polarization is trapped close to the region where the field is applied, and singlets are pushed far away from this field region. This is demonstrated graphically in Fig. 11 where parts (a) and (b) show the trace distance of two spins far from the locally applied magnetic field from a singlet for fields on an even and odd number of spins respectively. Parts (c) and (d) show the polarization stored in the region with no applied magnetic field versus field strength, again for fields on an even and odd number of spins respectively. As Figs. 11(a) and (b) show, for local fields applied to regions with both an even and odd number of spins, there is always at least one polarization sector for which singlets are located far away from the field region. Even for relatively small finite systems, such as the ones studied here, the ground state always lies in one of these sectors.

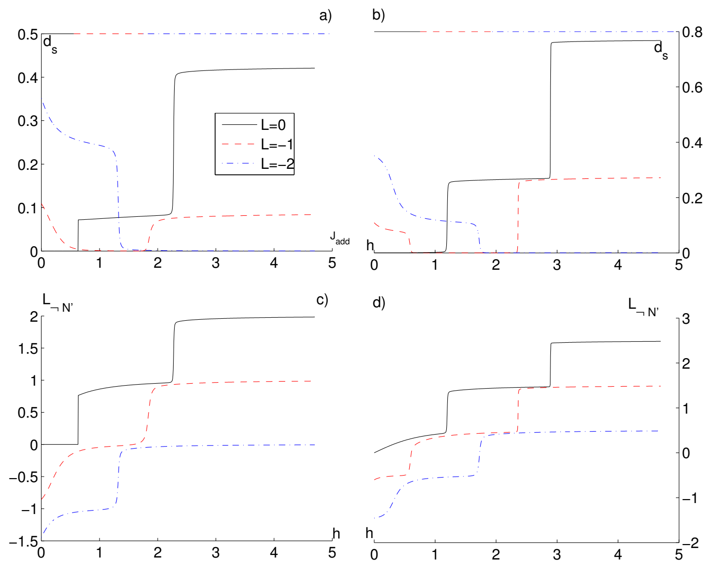

Figure 11: (a) and (b): Trace distance from a singlet state of the two spins at the end of the chain opposite to the region subjected to the local magnetic field. (c) and (d): Total spin polarization outside of the region subjected to the local field. (a) and (c) are for local fields applied to 4 spins, and (b) and (d) are for local fields applied to 3 spins. On all figures, the solid line is the L=0 sector, dashed lines indicate the L=-1 sector and the dot dashed lines indicate the L=-2 sector. Note that for sufficiently small local fields, the global ground state lies in the L=0 sector, whereas for larger local field strengths it lies in higher polarization sectors. In both cases the global ground state is locally close to the singlet state on spins far from the field. These plots are all properties relating to the ground states of given sectors.

It is also interesting to note from Figs. 11(c) and (d) that for a small field in the L=0 sector, the spins in the field-free area behaves differently, depending on whether the local field is applied to an odd or to an even number of spins. This can be explained by the fact that for a field on an odd number of spins, the boundary between the field and the region with no field cuts through a singlet, in the original ground state. E.g. the field gradient makes one component of the singlet more energetically favorable than the other. By rotating these two spins between the singlet and the classical $|\downarrow\uparrow\rangle$ state, the ground state can be adjusted locally. When, however the field boundary is between two singlets, a critical local field strength must be reached for any polarization to be transferred from the field region to the field-free region as Fig. 11(c) demonstrates. This is because the matrix product state of singlets is still an eigenstate of the Hamiltonian for any field strength in this case, and a level crossing must occur before the ground state can change. [20]

Fig. 12 shows the entanglement map of a system in the L=-1 global spin sector, with a magnetic field of h=5J applied on 4 of 16 spins. Fig. 12 suggests that for a range of field values, the distance from a singlet is caused by frustration from having an effectively odd number of spins available in the Majumdar-Gosh Hamiltonian. In this case, however, the frustration is alleviated by an intermediate transition region between the field behavior and far from field behavior changing its length (at the cost of some energy). [21]

A. Polarization effects

The way the system distributes polarization depends strongly on even-odd effects. To study the effects of polarization we examine Fig. 13 which shows the dependence of trace distance from a singlet for spins far from the locally applied magnetic field on the polarization in the non-field region in parts (a) and (b) for fields on an even and odd number of spins respectively. Parts (c) and (d) show the polarization of the last 2 spins rather than trace distance from a singlet. From Figs. 13(c) and (d) one can tell that if the field is placed on an even number of spins, any polarization that is in the non-field region will be immediately spread, even to the furthest spins. In the case where the field is placed on an odd number of spins, however, a finite amount of polarization can be sequestered near the boundary. Figs. 13(a) and (b) show that this trend is mirrored in distance from a singlet for far-away spins.

The differences between the even-spin and odd-spin ground state for the zero-field spin chain can be used to explain why polarization sequestration can occur in one case and not the other. Any spin $\frac{1}{2}$ spin chain with an odd number of spins and no applied local field must have a degenerate ground state because the particle-hole duality. The degenerate ground states also have different polarization and, therefore, 2 degenerate ground states with a

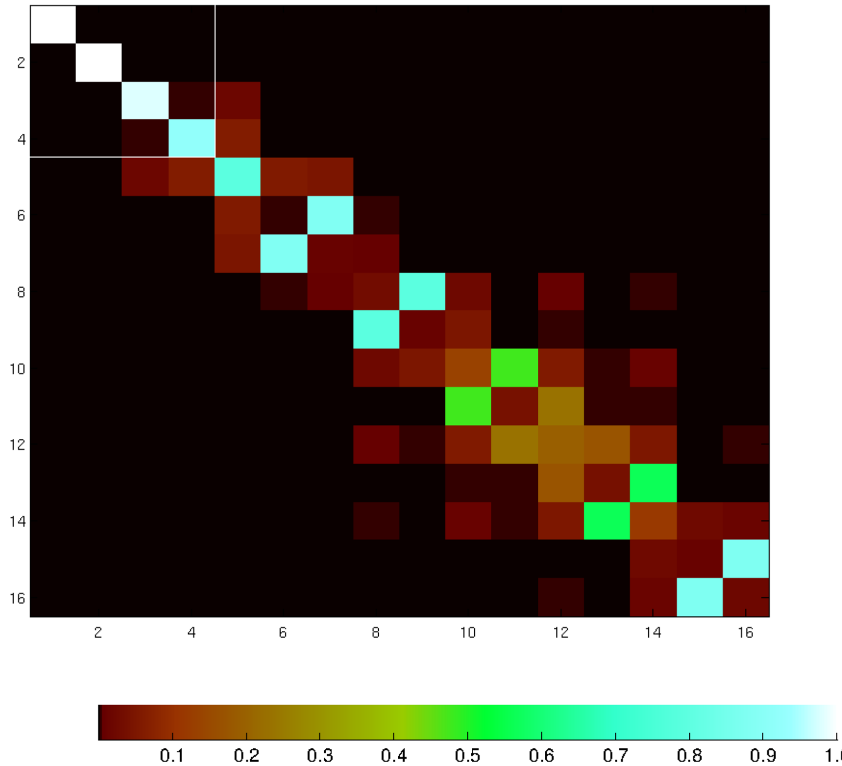

Figure 12: Entanglement map for the L=-1 sector ground state (note that this is not the global ground state) for a Majumdar-Ghosh chain of 16 spins with 4 adjacent spins, whose position is indicated by the white square, subjected to a local magnetic field of strength h=5J . The color scale is normalized to 1 as shown.

continuum of polarization between $L = -\frac{1}{2}$ and $L = \frac{1}{2}$ are possible. This means that for a chain which is effectively "odd", there is no energy penalty for being anywhere in this range. This effect allows polarization to be spread throughout the no-field region without increasing the energy in that region. Polarization can effectively be moved through this locally degenerate subspace, therefore polarization sequestration does not occur. Conversely, for a spin chain which is effectively "even", the ground state is unique, and polarization will tend to be localized in the ground state to avoid raising the energy of all of the no-field spins. As Fig. 12 suggests, for certain field ranges in a given sector, the length of the non-field region of the chain is effectively "odd". When this happens polarization can be spread freely throughout the non-field region, and sequestration does not occur, see Fig. 14.

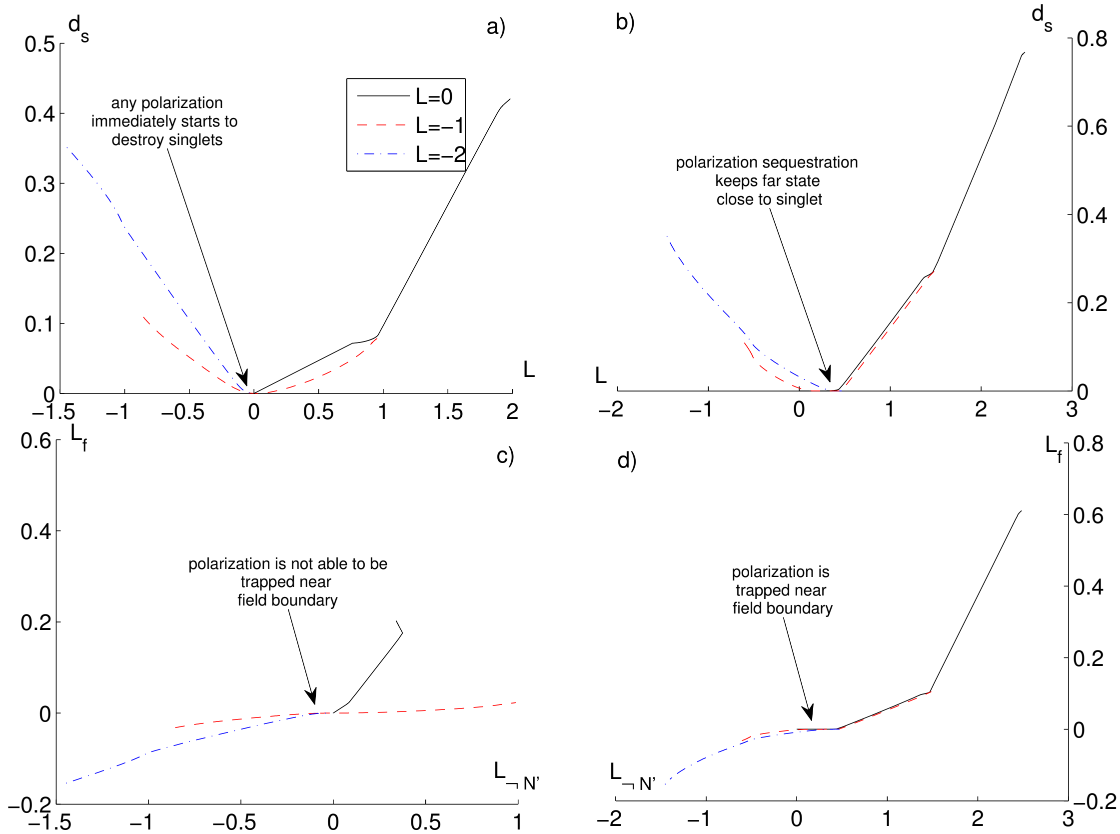

Figure 13: (a) and (b): Trace distance from a singlet state of the two spins at the end of the chain opposite to the region subjected to the local magnetic field versus polarization of the entire field free region. (c) and (d): Spin polarization of the 2 furthest spins versus polarization of the entire field free region. Local field on 4 of 16 spins with periodic boundary conditions (left column). Local field on 5 of 16 spins with periodic boundary conditions (right column). In all parts, the solid line is the L=0 sector, dashed lines indicate the L=-1 sector and the dot dashed lines indicate the L=-2 sector. These plots are all properties relating to the ground states of given sectors.

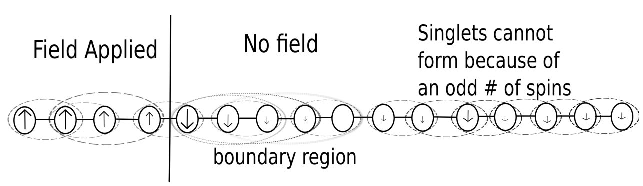

Figure 14: Cartoon representation of the effect which prevents polarization sequestration for a field on an even number of spins.

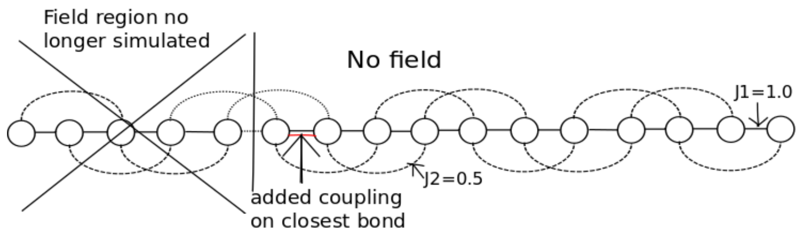

Figure 15: The approximation used to simulate behavior with a strong field.

	$\langle\psi_0 \mid \psi_0^{app}\rangle$	J_{add}
N'=1	0.9976	-0.3323
N'=3	0.9980	-0.3786
N'=5	0.9983	-0.3756
N'=7	0.9987	-0.3706

Table III: Statistics considering a field of h=100 placed on N' spins, comparing the approximate to the actual Hamiltonian. The coupling listed here is the additional coupling added to the 2 closest spins to the field

B. Field Induced Effects

For very strong fields, the spins within the field should have no entanglement with the rest of the system, in low energy states. This is because the spins subjected to the field will align with the field. Therefore an effective Hamiltonian which acts only on the spins outside of the field should be able to describe the system in low energy states. A simple model for this Hamiltonian would be to alter the coupling between the two spins closest to the field, with the supposition that the coupling with the field spins acts to mediate the interaction between the two spins coupled to them (see Fig. 15). The overlap between the known ground state, and the ground state calculated using the approximation shown in Fig. 15 for different added coupling strengths and different spins in the field region appear in Fig. VIII B. Fig. VIII B supports the claim that this approximation works fairly well in the ground state for a field on an odd number of spins. For numerical results see table III.

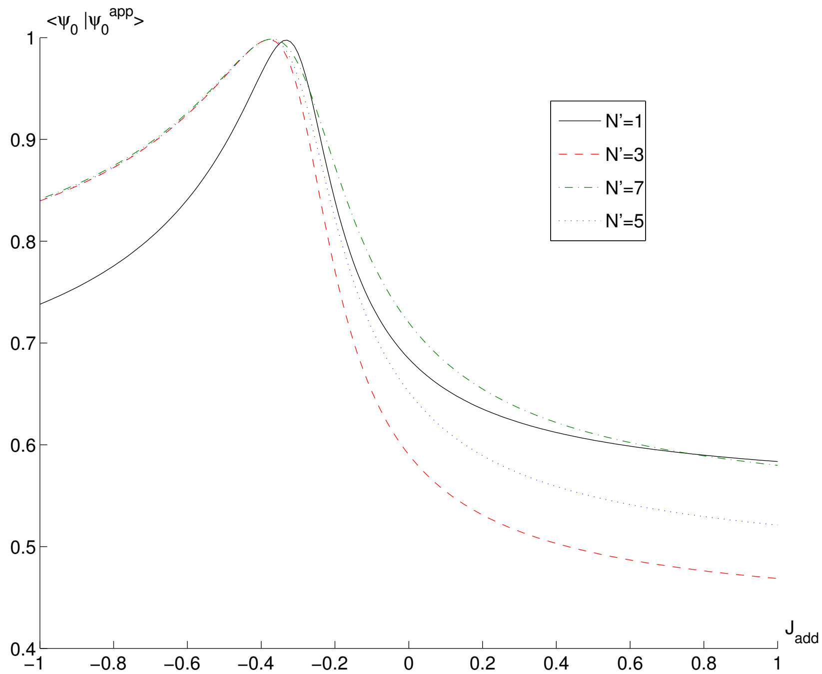

Figure 16: Overlap between actual ground state, and ground state of a Hamiltonian which is applied only to the non-field spins (tensored with spins opposing the field in the field region), but with a modified coupling on the two spins closest to the field. X axis is the additional coupling added to the Majumdar-Ghosh Hamiltonian. Data was taken with h=100, N=16 (open boundaries). Different lines are as follows solid-N'=1, dashed-N'=3, dotted-N'=5, dot dashed-N'=7. Even N' (not shown) are not accurately represented by this model.

IX. LOCAL MAGNETIC FIELD APPLIED TO MAJUMDAR-GHOSH CHAINS WITH PERIODIC BOUNDARY CONDITIONS

Unlike open boundary conditions, periodic boundaries present a case where the unperturbed Hamiltonian has a degenerate ground state. Therefore, the local Hamiltonian for the spins far away from the region subjected to the local field will also always have a degenerate ground state. The complications from this degeneracy add a new series of effects which are not observed in the open-boundary case. These effects are illustrated by Fig. 17 which shows in parts (a) and (b) the closest distance from the singlet subspace for the two furthest spins from the region of the locally applied magnetic field versus polarization on all non-field spins for 3 of 20 and 4 of 20 spins in the field respectively. Parts (c) and (d) show polarization on

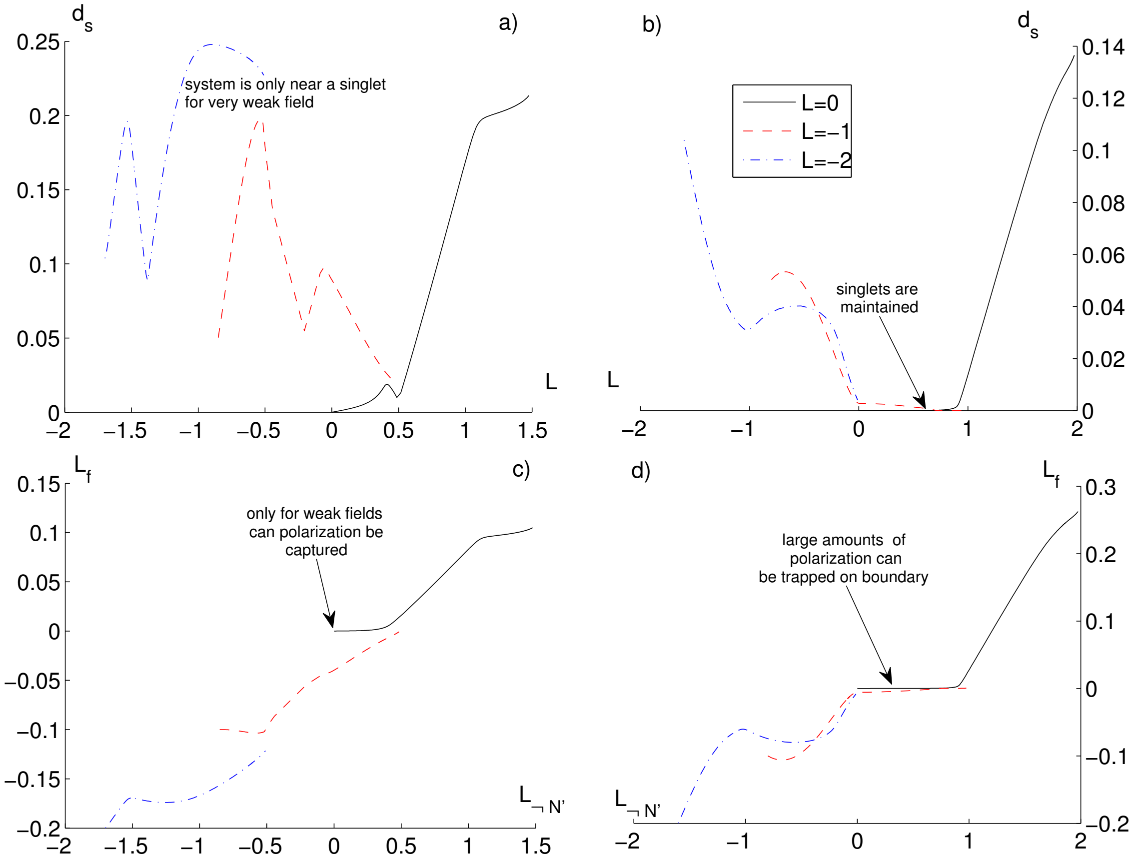

Figure 17: Closest local distance from singlet subspace of 2 furthest spins from the locally applied magnetic field versus polarization on all non-field spins (top row). Polarization on 2 furthest spins versus polarization on all non field spins (bottom row). Field on 3 of 20 spins with periodic boundary conditions (left column). Field on 4 of 20 spins with periodic boundary conditions (right column). On all figures, the solid line is the L=0 sector, dashed lines indicate the L=-1 sector and the dot dashed lines indicate the L=-2 sector, where I call negative L to be in the direction of the field. These plots are all properties relating to the ground states of given sectors.

the two furthest spins from the locally applied field versus total polarization in the non-field region, again for field on 3 of 20 and 4 of 20 spins respectively.

The most immediately obvious difference is that if the local magnetic field is placed on an odd number of spins, neither spin sequestration nor closeness in trace distance to the singlet subspace for any spins are observed, except for the L=0 subspace in weak local fields. Figs. 17(a) and (c) show the trace distance from a singlet in spins far from the applied magnetic field and local angular momentum for spins far from the local magnetic field respectively, both versus total angular momentum in the field free region. For larger fields, the spins far from the region where the external magnetic field is applied do not approach the singlet subspace because of frustration caused by having an odd number of spins in the non-field region. In the case of periodic boundary conditions, the effects of the frustration are stronger than in the case of open boundaries. This is because here a change in the length of the field-to-far-from-field transition region will do nothing to relieve the frustration because of the symmetry between the two field boundaries. Regardless of whether the length of one of these regions is odd or even, the total length of transition regions is always even because it is the length of a single transition region multiplied by two.

A. Effect of local degeneracy on small quenches

Shifting the focus to the case where the external field is placed on an even number of spins, one can consider the effects of now having a locally degenerate ground state, i.e. having a Hamiltonian which has a ground state degeneracy when no field is applied, and therefore is degenerate in a local sense far from the spins with an applied magnetic field. Fist the ground state can be studied by observing Fig. 18, this figure shows in parts (a) and (c) the trace distance from the closest singlet covering and minimum distance from the manifold of singlet coverings respectively for the two furthest spins from the locally applied magnetic field versus field strength, for a field applied to 4 of 20 spins with periodic boundary conditions. Parts (b) and (d) show entanglement maps for a local magnetic field strength of h=1.3J and h=1.6J respectively, again for a field on 4 of 20 spins with periodic boundaries. Fig. 18(c) indicates that the global ground state of the system is always close to the singlet subspace far from the field, however 18(a) suggests that around a field strength of 1.5 the system may undergo a switch between singlet coverings far from the spins to which the field is applied. Figures 18(b,d) confirm this suspicion by showing that indeed before the peak in 18(a) there are an even number of dimers outside of the field region, while after there are an odd number of dimers. This indicates that disturbances from the local field can be felt far from the spins with an applied field, but only for a narrow range of field values.

One can now consider the effect of small quenches at various applied field strengths on spins far from the field spins. The results of such quenches are shown in Fig. 19, parts (a) and (b) show the trace distance to average for the two furthest spins from the locally

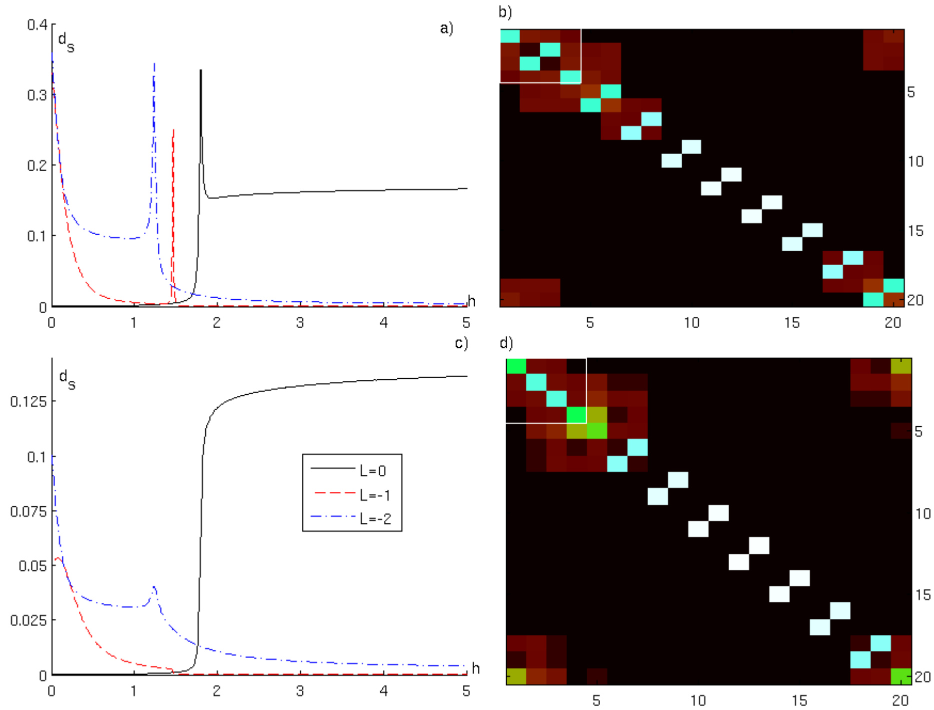

Figure 18: a) Trace distance between the two spins furthest from the field and the nearest singlet covering (see Eq. 35) versus field for 20 spins with periodic boundary conditions and a field placed on 4 of the spins. b) Entanglement map for 16 spins with a field of h=1.3J placed on spins 1-4 (indicated by the white rectangle) with periodic boundary conditions c) Same as (a), but now with distance to the closest state in the degenerate subspace (see Eq. 36) d) Same as (b) but with a field of h=1.6J. On all figures, the solid line is the L=0 sector, dashed lines indicate the L=-1 sector and the dot dashed lines indicate the L=-2 sector, where negative L is in the direction of the field. All plots in this figure are for eigenstates of the Hamiltonian.

applied magnetic field, after a quench which involves a small change in field strength versus the strength of that field for a field on 3 of 20 and 4 of 20 spins respectively with periodic boundary conditions. Parts (c) and (d) show the polarization of the two furthest spins from the locally applied magnetic field versus field, and are included to emphasize the important role played by polarization in this system. One would expect that these disturbances can only be propagated through the still locally degenerate ground state subspace of the no-field Hamiltonian and therefore would only have an effect when the coverings shift. Fig. 19(b) shows that in fact a small quench does disturb the system strongly at the point where the

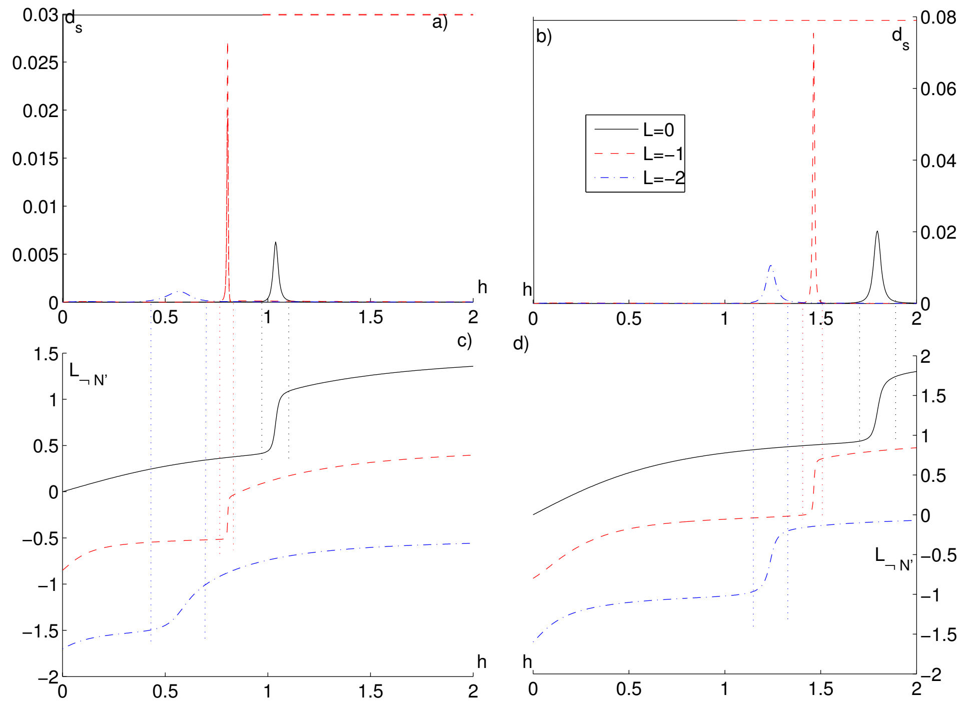

Figure 19: Initial trace distance from average (see Eq. 39) for a subsystem far from the fields after a small field quench $\epsilon = 0.001$ (top row). Polarization on all non-field spins versus field strength (bottom row). 20 spins with field placed on 3 of them and periodic boundary conditions (left column). same with field placed on 4 spins (right column). Dotted vertical lines have been added to emphasize correlation between the two graphs. On all figures, the solid line is the L=0 sector, dashed lines indicate the L=-1 sector and the dot dashed lines indicate the L=-2 sector. Lines at the top are added to show which spin sector the global ground state is in. The top two plots are time averaged quantities from a quench, while the bottom two figures are properties of the ground state of each sector.

coverings switch. The other two peaks in Fig. 19(b) are less relevant because they occur in the ground state of a spin sector, but not in the global ground state of the system. Also none of the quench disturbances which occur far from the spins with an applied field occur in the global ground state in Fig. 19(a), demonstrating another difference caused by even-odd effects. This is to be expected, because the the two degenerate ground states of an odd length Majumdar-Gosh chain lie in different polarization sectors and therefore cannot exhibit level repulsion, at least locally, in the region far from the applied magnetic field.

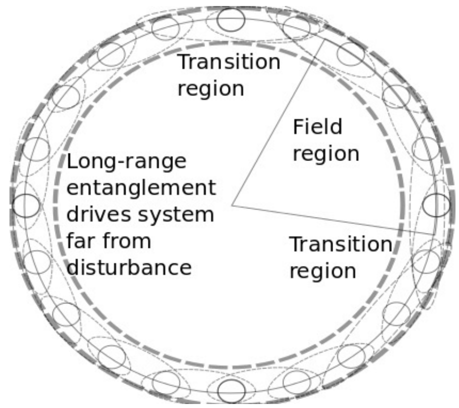

Figure 20: Cartoon of field quench for periodic boundaries.

Note also that Fig. 19 suggests that there is a strong correlation between polarization outside of the subsystem where a magnetic field is applied and quench disturbance to the far spins, in the sense that when the quench has a strong effect, there is a rapid change in polarization in the non-field region. The converse however is not supported by this figure. This demonstrates than polarization plays a strong role in the global behavior of this system.

The same energy arguments used in the static case for behavior of spins far from the spins with an externally-applied magnetic field should be usable as a dynamical argument. A finite local field can only introduce a finite amount of energy into the system. Therefore only states which lie sufficiently close in energy to the ground state can be accessed in any significant way. For a large enough system, all of the low energy states will have to be locally close to the ground state for most of the spins far from the locally-applied magnetic field, therefore locally, far from the field, spins can only be disturbed within the degenerate subspace. Put another way, in gapped systems the effects of a local quench have to be localized, unless there exists a locally degenerate subspace far from the region where the quench is applied. When such a subspace exists it may be able to transport conserved charges, quantum entanglement and dynamical disturbances an unlimited distance away from the disturbance site. A locally degenerate ground state can be thought of as a special symmetry which allows transport of information and charges (but not energy) with no losses throughout the part of a system far from the quench. [22]

Long-range entanglement allows a part of the system which lies entirely in a degenerate subspace to have its evolution driven by local evolution far away, see Fig. 20.

B. Large quenches

Now that it is established that a disturbance will be able to be propagated throughout the entire system from a small quench, one can perform a large quench from h=1.6 to h=1.3 for a local field applied to 4 adjacent spins of 20 total spins with periodic boundary conditions. One can then examine the time statistics of various properties of the system. These statistics are shown in Fig. 21, in this figure part (a) is the trace distance of 4 spins far from the locally applied magnetic field from a singlet state, part (b) is the time statistics of the Loschmidt echo of the entire system, part (c) is the time statistics of the distance from the time averaged state for 4 spins far from the locally applied field, and part (d) is the time statistics of the magnetization of the spins subjected to the field. These statistics will show the ability of the system to equilibrate, even locally for spins far from the spins where the local magnetic field is applied. In the case studied here, the system only equilibrates poorly, even in the global sense, not surprisingly, poor equilibration is also shown in local observables both close to and far from the spins with an applied magnetic field.

The double-peaked pattern of equilibration seen here is typical of small systems, see [5] (see ch. 1 starting on page 8), and is thus consistent with the theory that although the system itself is rather large [23], the actual evolution is only taking place on a few spins in or near the region of externally applied field, the rest of the system is simply being drug along by long range entanglement with these spins. As Fig. 21(c) demonstrates, even though the dynamics is driven by long range entanglement with far away spins, a subsystem of spins is still able to be pushed toward equilibration in the trace distance sense. The fact that there is no local energy difference does not seem to interfere at all with equilibration of these spins. The trace distance from the average is observed quite close to zero at some times, unlike in similar quenches performed at the Majumdar-Ghosh point in [5]. This is because an undisturbed singlet somewhere in the region being observed would yield a large distance from the average at all times as shown in [5] where the quench did not cause a change in singlet coverings. In the case we are observing, where the coverings switch, there are no undisturbed singlets in the region away from the field spins.

Although the equilibration is globally poor in this system, there are no signs that equilibration via long-range entanglement through a locally degenerate subspace is any less effective than direct equilibration of the spins to which the field is applied. The data from

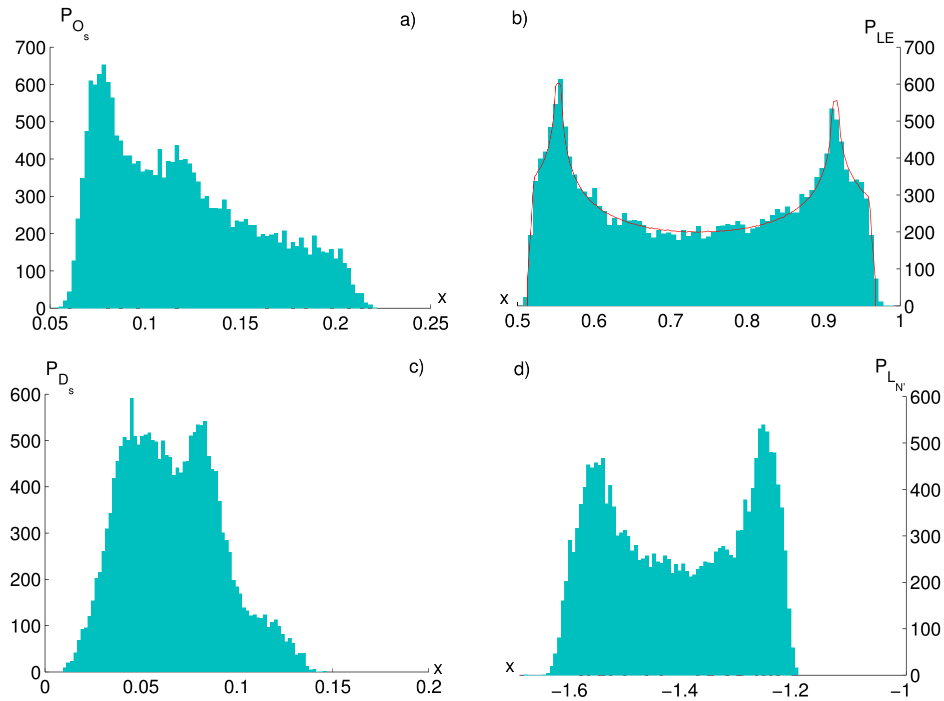

Figure 21: Equilibration statistics for N=20, N'=4 with a quench from $h_{(i)}$=1.6 to $h_{(f)}$ = 1.3. a) Time statistics of the trace distance of 4 spins far from the locally applied magnetic field from a singlet state (Eq. 42). b) Time statistics of the Loschmidt echo (Eq. 40) with an approximation based on few frequencies. c) Time statistics of distance from time averaged state (Eq. 43) for 4 spins far from the locally-applied magnetic field. d) Time statistics of local magnetization (Eq. 41) of the field spins. These plots are all time statistics obtained from evolution.

this quench therefore indicate that the entire system can be equilibrated (at least somewhat) by a quench which only affects a very small region. In fact a system of any size should be able to be brought locally close to equilibrium in this way. Because all states of the far spins locally have the same energy, than they cannot affect the time evolution of the system, therefore the same behavior would be expected for a spin chain of any sufficiently long (even) length.

X. OTHER COUPLING STRENGTHS

One can now ask what would happen if the coupling were changed such that the system was no longer using the Majumdar-Ghosh Hamiltonian, but allowed the next nearest neigh-

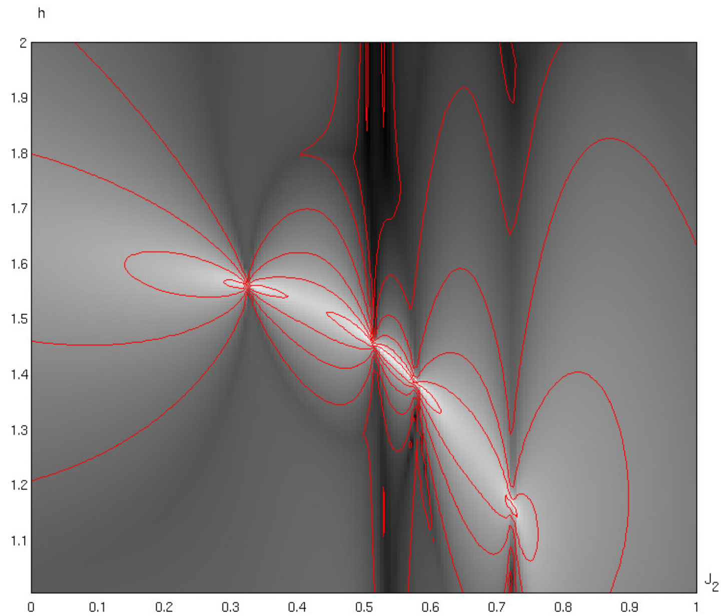

Figure 22: Initial trace distance to average for far spins after a small field quench, larger distances are lighter, smaller distances are darker. Trace distance is plotted on a logarithmic scale, contour lines (red) are included for clarity. Data using 20 spins with periodic boundaries in the L=-1 sector.

bor coupling to take on arbitrary values, see Eq. 46. This study is done with 20 spins and periodic boundary conditions, with a local magnetic field on 4 adjacent spins.

$$H_{J2} = \sum_{j=1}^{N} \vec{S}_j \cdot \vec{S}_{j+1} + J_2 \sum_{j=1}^{N} \vec{S}_j \cdot \vec{S}_{j+2} \tag{46}$$

Small field quenches can be considered on this new Hamiltonian exactly in the same way they can be considered for the Majumdar-Ghosh Hamiltonian, the results appear in Fig. 22 which shows the initial trace distance from average for a small field quench versus coupling and field strength. This data shows that for a wide range of coupling near the Majumdar-Ghosh point, small field quenches can drastically affect spins very far from the spins with an applied magnetic field at specific field strengths. However, when the field strength is eventually different enough, these peaks broaden out and disappear (note logarithmic scale in Fig. 22). The basic behavior seen previously in this paper holds for a wide range of couplings, where the ground state is no longer degenerate.

For an infinite system one would expect that, far spins from the local magnetic field could not be disturbed by a local field quench unless either the system is gapless or there exists a degenerate ground state. For a finite system, this would only be necessarily true if the gap between the ground state and first excited state is sufficiently large compared to the energy introduced by the applied local magnetic field, in which case the field will be unable to introduce enough energy to affect the entire system. In this case the order of magnitude of the energy which the field introduces can be estimated by simply multiplying the field strength by the number of spins it is applied to. Because both of the quantities are of order 1, one would expect that the energy introduced would also be of order 1.

The energy gap in the system which will be used for this calculation can be determined by exact diagonalization. The energy of the gap between the ground state and first excited state of this system are shown in Fig. 23 part (c) which shows the gap energy versus coupling at zero applied field, part (a) shows the initial distance from the average for 4 spins far from the locally applied magnetic field after a large quench (within the $L = -\frac{1}{2}$ sector), part (b) shows the local trace distance from the nearest singlet covering for spins far from the local field in the ground state of the $L = -\frac{1}{2}$ sector versus field strength and coupling, and part (d) is the same as (b), but with trace distance from the nearest state in the ground state manifold. It can be seen from Fig. 23(c) that the gap energy is at most of order 0.1, therefore, one would expect that for the entire range of couplings, the far spins could be disturbed by the local field. The results seen in Fig. 22 are as expected, however if the system size were increased to infinity, one would expect that in the gapped region for $J_2 \gtrsim 0.25$, the peaks in the distance would have to disappear except for exactly at J_2=0.5, or any other point with a degenerate ground state. Twenty spins, however, is still too small a system for changes in the coupling to destroy the ability to dephase far spins with a local field, in other words the system can be considered to have an approximately degenerate (wrt. the energy scale associated with the field) ground state for all values of J_2, the next nearest neighbor coupling.

One can now ask whether the effects seen in Fig. 22 away from the Majumdar-Ghosh point are also caused by some kind of shift in singlet covering. To answer this question, one can compare Fig. 23(b) to Fig. 23(d) and notice that where the peaks in Fig. 22 are located, the trace distance from either covering tends to be relatively large, but the distance from the subspace tends to be relatively small. This indicates that movement within the singlet

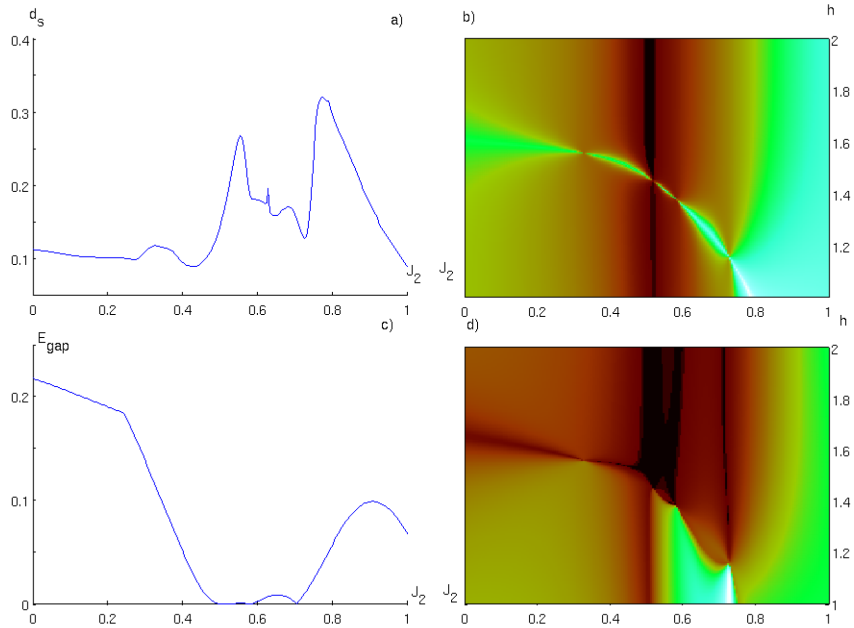

Figure 23: a) Initial distance from average for 4 spins far from the locally applied field for a large quench from h=2 to h=1 for the L=-1 sector. b) distance of far spins from nearest singlet covering (Eq. 35) versus h and J_2, L=-1 sector, color scale same as for entanglement maps, but normalized to largest value. c) gap between ground state energy and first excited state, for different $J_2$and h=0. d) distance from singlet subspace for far spins (Eq. 36) versus h and J_2, L=-1 sector, color scale same as for entanglement maps, but normalized to largest value. All plot except for (a) are static quantities relating to eigenstates.

subspace is the cause of much of the disturbance in the far spins. Also interesting to note is that for a significant portion of the couplings, the spins far from the locally applied magnetic field are closest to the singlet subspace when the small field quenches have the most effect on far spins. It appears that even at many couplings away from the Majumdar-Ghosh point, the model of switching between coverings as a way to spread a disturbance throughout the system is accurate. In fact for many values of J_2, the system appears to move into the singlet subspace for a narrow range of fields only when the covering change occurs. For $J_2 \gtrsim 0.6$ this model seems to break down, but it is still at least relevant for a large range of J_2. Although not directly related to the quench, it is interesting to note that above a certain local magnetic field strength the spins far from the field seem to lie on the singlet superposition manifold for a fairly large range of coupling strengths near Majumdar-Ghosh coupling, as well as a narrow strip between $J_2 = 0.6$ and $J_2 = 0.8$, the reason for this is not known.

The results of a large local magnetic field quench over varying J_2 as shown in Fig.23(a) simply helps to underscore what has already been noted about changing coupling not being an effective way of preventing disturbances from propagating throughout the system at this system size. Not only do the large quenches have a significant effect on far spins from the local magnetic field for all coupling strengths, but the expected trend of decreasing quench effect with increasing gap is not visible in any definitive way, indicating that, not only is the energy scale of the gap (Fig. 23(c)) too small to be the dominating factor in the quench effectiveness, it seems to not even play a very significant role. This result is consistent with the previous energy scale argument, the energy scale associated with the field is always at least an order of magnitude larger than the gap between the first 2 eigenstates.

XI. CONCLUSIONS

In systems with degenerate ground states, quantum entanglement, disturbances, and charges can propagate freely, as long as the quench crosses between pre and post quench ground states which are locally different from each other far away from the region affected by the local quench. This effect is different and independent from gapless excitations, and has been demonstrated to occur in a gapped system. Unlike in gapless systems where excitations carry an arbitrarily small amount of energy far from the quench, these excitations store all energy locally near the quench, and evolution far away is driven solely by long-range entanglement. The local energy far from the region affected by a local quench Hamiltonian is exactly zero in these systems, not arbitrarily small.

To allow a charge to be propagated through a degenerate subspace, the two degenerate ground states must have different local expectation values for said charge far from the region affected by a local quench Hamiltonian. An effectively odd spin chain far from the field is allowed to propagate polarization throughout the far region for example. Again, in such a case, long range entanglement can propagate the charge, but does not propagate any energy far from the field. In cases where two degenerate ground states with different expectation values for a charge far from the region where the quench is applied do not exist, the charge can become locally trapped in part of the system. In the case of the Majumdar-Ghosh

Hamiltonian, the polarization is trapped near the boundary of the local magnetic field region. A locally unique ground state (in a gapped system) means that charges, as well as disturbances, are confined after a local quench. Energy arguments prevent a disturbance from traveling throughout the system and also therefore forbid charges from moving outside of a small area.

In the system studied here, a large local magnetic field causes the spins within the field to become effectively 'fixed', facing in the direction of the field in the ground state. An approximation which does not include these spins directly but includes an effective modulation in coupling between the two spins neighboring the field can faithfully reproduce the ground state when an odd number of spins remain. For the case that an even number of spins are left out of the field region, this simple approximation fails. We believe that the effective transition region between the field and non-field region consists of an odd number of spins, and that this ground state cannot be faithfully reproduced in this way because of odd length frustration effects.

For Majumdar-Ghosh spin chains with periodic boundaries, with a local magnetic field on some even number of spins, there exists a range of fields where a small field quench can propagate a disturbance through the entire system using long range entanglement. This disturbance is propagated locally through the degenerate subspace of the local ground state. In this case, this range of fields is relatively narrow. A quench across this entire range does not only cause equilibration near the field, but also moves the far spins towards equilibration, within the locally degenerate subspace.

Study of systems with different next nearest neighbor coupling indicate that the basic effect which causes disturbances to be propagated to far spins can, at least for small enough systems, be extended away from the Majumdar-Ghosh point. For finite systems, if the gap between the ground state and the first excited state is small enough, the same effect which was described here for degenerate systems can also be applied to systems where the first 2 states are close in energy. In other words, under the right conditions, an approximate degeneracy will work in place of an exact degeneracy. For a system of 20 spins any value of J_2 between 0 and 1 still allows the far spins to be significantly affected by the field. We strongly suspect that for the values of $J_2$where the Hamiltonian is gapped and for which a degenerate ground state does not exist, spins far from a local magnetic field applied to a few spins cannot be affected in the large system limit.

Acknowledgements

This Chapter is based on Propagation of Disturbances in Degenerate Quantum Systems by N. Chancellor and S. Haas [1]. The authors of that paper would like to thank N. Tobias Jacobson for his assistance in editing. We would also like to thank S. Garnerone, B. Normand, and M. Diez for valuable discussions. The numerical computations were carried out on the University of Southern California high performance supercomputer cluster. The work in the original paper was supported by NSF grants: PHY-803304,DMR- 0804914.

Chapter 2 References

[1] N. Chancellor and S. Haas, Phys. Rev. B 84, 035130 (2011)

[2] J. Cardy, arXiv:1012.5116v1 [cond-mat.stat-mech] (2010)

[3] A. Einstein, B. Podolsky, and N. Rosen, Phys. Rev. 47, 777 (1935).

[4] N. T. Jacobson, P. Giorda and P. Zanardi, Phys. Rev. E 82, 056204 (2010)

[5] M. Diez, N. Chancellor, L. Campos Venuti, S. Haas and P. Zanardi, Local Quenches in Frustrated Quantum Spin Chains: Global vs Subsystem Equilibration, arXiv:1007.0041v1 [quant-ph]

[6] L. Campos Venuti and P. Zanardi, Phys. Rev. A 81, 022113 (2010).

[7] L. Campos Venuti and P. Zanardi, Phys. Rev. A 81, 032113 (2010).

[8] Jie Ren and Shiqun Zhu, Phys. Rev. A 81, 014302 (2010)

[9] Benjamin Hsu, Eytan Grosfeld, and Eduardo Fradkin, Phys. Rev. B 80, 235412 (2009)

[10] L. M. Duan, E. Demler, and M. D. Lukin, Phys. Rev. Lett. 91, 090402 (2003).

[11] D.Porras and J.I. Cirac, Laser Physics, Vol. 15, No. 1, 2005, pp. 88–94.

[12] Y. Makhlin, G. Schï¿œn, A. Shnirman, Rev. Mod. Phys. 73, 357 (2001)

[13] L. S. Levitov, T. P. Orlando, J. B. Majer and J. E. Mooij, arXiv:cond-mat/0108266v2 [cond-mat.mes-hall] (2001)

[14] Davide Rossini, Sei Suzuki, Giuseppe Mussardo, Giuseppe E. Santoro, and Alessandro Silva, Phys. Rev. B 82, 144302 (2010).

[15] Rahel Heule, C. Bruder, Daniel Burgarth and Vladimir M. Stojanović, arXiv:1010.5715v1 [quant-ph] (2010)

[16] C K Majumdar 1970 J. Phys. C: Solid State Phys. 3 911

[17] However, one can orthogonalize them, still preserving the symmetry under $a \longleftrightarrow b$, $2l \rightarrow mod_N(2l+1)$, by adding a term $-(a \times \bigotimes_{k=1}^{\frac{N}{2}} \frac{|\uparrow_{2k-1}\downarrow_{2k}\rangle}{\sqrt{2}} + b \times \bigotimes_{k=1}^{\frac{N}{2}} \frac{|\downarrow_{2k-1}\uparrow_{2k}\rangle}{\sqrt{2}})$.

[18] The only case where this is not observed is for the case of periodic boundary conditions with a local field applied to an even number of spins. In this case these spins orient locally like in the frustrated ground state of a Majumdar-Ghosh chain with an odd number of spins.

[19] An example of this would be to consider a superposition of the two singlet coverings. Any

non-adjacent spins will have exactly zero two-point entanglement (see Eq. 45). However, any set of two pairs of adjacent spins will have a finite entanglement between them. To see this, consider the case where one set of two spins is measured to be both in the up direction. If there is an odd number of spins between the two spin pairs, this forces the other pair to be a singlet, regardless of the distance between the pairs.

[20] Showing that this happens consists of demonstrating that the singlet covering is an eigenstate of any field which does not change within a singlet. This can be seen by realizing that the field operator on the first spin of the singlet will give the zero magnetization triplet state $\frac{1}{\sqrt{2}}(|\uparrow\downarrow\rangle + |\downarrow\uparrow\rangle)$, while the operator on the second spin will give the same but with a negative sign. Thus the two will cancel making the singlet covering an eigenstate with a zero eigenvalue.

[21] The closeness to the boundary may also be a factor in the trace distance of the last 2 spins from a singlet, the fact that no entanglement can cross the open boundary may cause spins close to it to assume more localized states, however while this effect could make finite distances smaller, it should not be able to make the trace distance (virtually) zero as it is in many parts of Fig. 11(a).

[22] Note that the excitations which travel through a locally degenerate ground state are not the same as gapless excitations, which locally carry an arbitrarily small amount of energy. The parts of these excitations which exist far from the region affected by the local quench Hamiltonian carry exactly zero energy locally.

[23] One could argue that 20 spins is not such a large system, but it has been shown that the spins far from the evolution are always locally in the degenerate subspace. Adding more far spins and making the system into one which all of the readers would agree would be "large" (for example making the system size 100,000 spins) would not effect the dynamics, and the double peaked pattern would remain.

Chapter 3: Adiabatic Quantum Bus Protocol

This Chapter is based on the paper Using the J1-J2 Quantum Spin Chain as an Adiabatic Quantum Data Bus by N. Chancellor and S. Haas [1].

This chapter investigates numerically a phenomenon which can be used to transport a single qubit down a J1-J2 Heisenberg spin chain using a quantum adiabatic process. The motivation for investigating such processes comes from the idea that this method of transport could potentially be used as a means of sending data to various parts of a quantum computer made of artificial spins, and that this method could take advantage of the easily prepared ground state at the so called Majumdar-Ghosh point. We examine several annealing protocols for this process and find similar results for all of them. The annealing process works well up to a critical frustration threshold. There is also a brief section examining what other models this protocol could be used for, examining its use in the XXZ and XYZ models.

Introduction

The ability to send data from one part of a computer to another accurately and quickly is an essential feature in virtually any design. The use of artificial spin clusters in quantum computing has been of growing interest. There is an implementation which has been demonstrated using superconducting flux qubits[2–6]. This paper demonstrates an effective and scalable way of sending arbitrary qubit states along a spin chain with Heisenberg type coupling using quantum annealing. Assuming one could implement a Hamiltonian which follows this model, for example using the methods proposed in [7] using coupled cavities, this system design could be used for a data bus which transports quantum states to different sections of a quantum computer system. For instance, the protocols discussed in this paper could potentially be used to move states from memory to a system of quantum gates in an implementation of the circuit model.

There has already been significant work done on the subject of quantum data buses using spin chains, [8–11]. However these works differ significantly from the method proposed in this paper in that the encoded qubit is not transmitted through a degenerate ground state manifold, but through excitations of the Hamiltonian.

This paper investigates a method of using qubits as an intermediate bus for the transfer of quantum information. This method can be compared to another method which is that of pulses [12], where a Hamiltonian is applied to a system for a period of time to perform a given operation. In the case of information transfer this operation is usually a swap. Unlike the method of using pulses, this method of using qubits does not require precise timing to insure that the correct operation is performed. The method of using a spin chain Hamiltonian as a data bus also means that one does not need to either be able to address any pair of qubits in the system or perform multiple operations to transfer an arbitrary qubit. The pulse method does have the advantage that every intermediate spin can be used as quantum memory. However this is at the cost of the increased complexity of using dynamic quantum evolution in excited states, and the requirement of precise timing.

The adiabatic quantum bus method also has the advantage that, as in any adiabatic quantum process, only the lowest energy parts of Hamiltonian need to be faithfully realized by the implementation method. For example, a Hamiltonian which actually has an infinite number of excited states on each "spin", but where only the low energy states which act like a spin $\frac{1}{2}$ Heisenberg system, contribute to the ground state would be perfectly acceptable to use as an adiabatic quantum bus without modification. But the higher energy states may cause issues using a method such as pulses. This general feature of adiabatic quantum processes such as the one illustrated in this paper makes them more versatile than their non-adiabatic counterparts.

The effect we will examine exploits the SU(2) symmetry of the Heisenberg Hamiltonian and uses the ground state degeneracy created by this symmetry in a chain with an odd number of spins. It has already been demonstrated [13] (see ch. 2 starting on page 33) that disturbances can be sent an unlimited distance along such chains because of their degenerate ground state. This chapter goes a step further and actually demonstrates how a specific state can be transported across the chain using a quantum annealing protocol. Further investigation will also be provided into application of this method to systems such as the XYZ spin chain which only have a $\mathbb{Z}_2$symmetry.

Setup

The model we consider is the J1-J2 Heisenberg spin chain with open boundaries,

$$H = \sum_{n=1}^{N-1} J_1^n \vec{\sigma}_n \cdot \vec{\sigma}_{n+1} + \sum_{n=1}^{N-2} J_2^n \vec{\sigma}_n \cdot \vec{\sigma}_{n+2}. \tag{47}$$

This model has SU(2) symmetry, which is expressed by the Hamiltonian being block diagonal, such that there are N+1 blocks each with $\binom{N}{k}$ states. Each block represents all of the states with a given number, k, of up spins. If the number of spins in the model is odd, then the additional symmetry under a flip of the spins in the z direction, i.e. $\sigma^z \to -\sigma^z$ implies that all states of the Hamiltonian have a twofold energy degeneracy. In the anti-ferromagnetic case, ($J_1, \ J_2 > 0$) the ground state manifold consists of one state from the k=floor($\frac{N}{2}$) and one from the k=ceil($\frac{N}{2}$) sector. A simple example of this would be taking a system with 5 spins, the ground state would be twofold degenerate and would span the k=2 and k=3 sectors. One can now consider an initial Hamiltonian of the form of Eq. 47 where the couplings are the ones given by

$$J_1^n = \begin{cases} J_1^{n,init} & n < N-1 \\ 0 & n = N-1 \end{cases}, \tag{48}$$

$$J_2^n = \begin{cases} J_2^{n,init} & n < N-2 \\ 0 & n = N-2 \end{cases}. \tag{49}$$

The general condition on $J_1^{n,init}$ and $J_2^{n,init}$ is that the coupling is predominantly anti-ferromagnetic everywhere and that each spin is coupled to the others by at least one non zero J. For simplicity this paper considers only $J_1^{n,init} = 1$ and $J_2^{n,init} = J_2^{init}$. This ground state manifold consists of the tensor product of the (unique) ground state of the chain of length N-1 with the Nth spin in an arbitrary state, a state in this manifold is of the from given by

$$|\Psi^{init}\rangle = |\Psi_0^{N-1}\rangle \times |\psi^{init}\rangle, \tag{50}$$

where $|\Psi_0^{N-1}\rangle$ is the ground state of the spin chain of length N-1 and $|\psi^{init}\rangle$is an arbitrary single spin state. One can now consider the same Hamiltonian, but with $n \to (N-n)+1$.

This Hamiltonian also has the form of Eq. 47, but with couplings

$$J_1^n = \begin{cases} J_1^{n,final} & n > 1 \\ 0 & n = 1 \end{cases}, \tag{51}$$

$$J_2^n = \begin{cases} J_2^{n,final} & n > 2 \\ 0 & n = 2 \end{cases}. \tag{52}$$

The general condition on $J_1^{n,final}$ and $J_2^{n,final}$ is that the coupling is predominantly anti-ferromagnetic everywhere and that each spin is coupled to the others by at least one non-zero J. For simplicity this paper considers only $J_1^{n,final} = 1$ and $J_2^{n,final} = J_2^{final}$. A state in the ground state manifold is now given by

$$|\Psi^{final}\rangle = |\psi^{final}\rangle \times |\Psi_0^{N-1}\rangle, \tag{53}$$

where $|\psi^{final}\rangle$ is an arbitrary single spin state. One can now consider a quantum annealing process with described by

$$\mathrm{H(t;\tau) = A(t;\tau)\ H^{init} + B(t;\tau)\ H^{final}}, \tag{54}$$

where $\mathrm{H^{init}}$ is 47 with the conditions given in 48 and 49 and $\mathrm{H^{final}}$ is 47 with the conditions given in 51 and 52. Also A and B follow the conditions

$$\mathrm{A}(t \leq 0;\tau) = 1, \tag{55}$$

$$\mathrm{B}(t \leq 0;\tau) = 0, \tag{56}$$

$$\mathrm{A}(t \geq \tau;\tau) = 0, \tag{57}$$

$$\mathrm{B}(t \geq \tau;\tau) = 1. \tag{58}$$

For all values of A and B the SU(2) symmetry is preserved. Therefore the Hamiltonian remains block diagonal at all times. The symmetry of the Hamiltonian under $\sigma^z \to -\sigma^z$ is also preserved at all times. This implies that the ground-state degeneracy (as well as the twofold degeneracy of all states) is preserved. The block diagonal structure implies that there will be no exchange of amplitude between spin sectors during the annealing process, while the degeneracy implies that no relative phase can be acquired between the states in

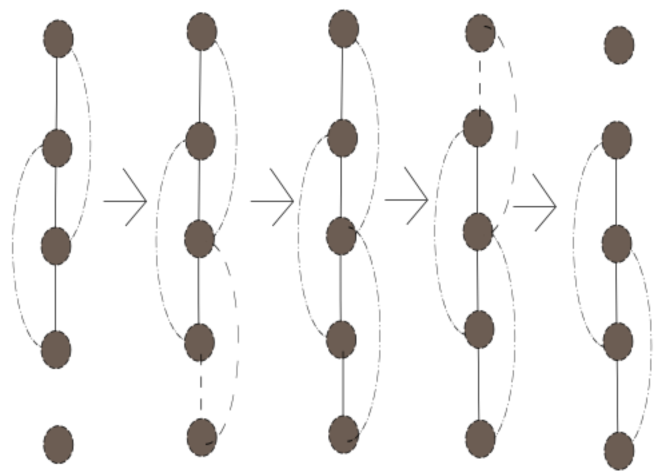

Figure 24: Cartoon representation of a process where a spin is joined to the chain, then the spin on the opposite end is removed. Note that this is only one specific example of many possible processes for transporting a qubit.

the k=floor($\frac{N}{2}$) and the k=ceil($\frac{N}{2}$) sector. From the combination of these two conditions one can see that as long as one anneals slowly enough with H(t;τ) [16] one can start with a state of the form given in Eq. 50 and reach a final state in the form Eq. 53 where $|\psi^{fin}\rangle = \exp(\imath\varphi)|\psi^{init}\rangle$, and φ is an irrelevant phase. One specific example of such an annealing protocol to transport a spin is given in Fig. 24.

Advantages

The use of the J1-J2 Heisenberg chain for transport by quantum annealing has several advantages. First the model with uniform coupling is gapped for $\frac{J_2}{J_1} \gtrsim 0.25$ [14]. This suggests that within the adiabatic evolution process, at least locally, the system should behave as a gapped system in this regime, as long as global effects such as odd length frustration do not cause problems.

It is important to note that even the largest system size considered here is far from the thermodynamic limit. One should note, however, that given the connectivity schemes of adiabatic quantum chips already in existence [6], one may only need to transport a qubit state a few spins to get it to any part of the system.

Further evidence of favorable scaling comes from [13] (see ch. 2 starting on page 33) which demonstrates that disturbances can travel an unlimited distance in the presence of a degenerate ground state, even in a gapped system. Furthermore, [13] suggests that these disturbances can carry entanglement, polarization, and quantum information. The transport by annealing given here is a specific example of how this effect can be taken advantage of.

Another advantage of the use of the J1-J2 Heisenberg Hamiltonian is the existence of the so called Majumdar-Ghosh point [15] ($\frac{J_2}{J_1} = 0.5$). At this point the ground state (with an even number of spins) has the simple form of a matrix product of singlets. Due to this fact the system should be relatively easy to prepare. The system is also gapped at the Majumdar-Ghosh point, making the Majumdar-Ghosh Heisenberg Hamiltonian, an ideal system for transport by quantum annealing and the ideal candidate for building an adiabatic quantum data bus.

Although this paper focuses on the J1-J2 Heisenberg model, it should be noted that this same annealing scheme should work with any pattern of coupling in the intermediate spins (i.e. J1-J2-J3)[17]. One would also expect this scheme to work in models where the SU(2) symmetry is broken but there is a remaining $\mathbb{Z}_2$symmetry such as the XYZ or XY model, again with arbitrary patterns of coupling. Note however that this method will not work in the Ising model, because although there is a $\mathbb{Z}_2$ symmetry, the Hamiltonian lacks terms to exchange qubits between sites because it is diagonal in the computational basis.

XII. PROOF OF PRINCIPLE

None of the arguments so far have given much illumination to the difficulty or ease of annealing within the sector. While we have discussed that transport of a qubit state is possible in principle by annealing, we have not yet shown that the annealing process is fast enough to be practical. For this we turn to numerics. For the purposes of this paper we will consider the annealing time, τ , required to reach a given fixed fidelity, $F(\tau)$, with the true final ground state,

$$F(\tau) = | \left\langle \Psi^{fin} \mid \int_0^\tau dt\, H(t,\tau) \mid \Psi^{init} \right\rangle |. \tag{59}$$

The J1-J2 Heisenberg model is not an analytically solved model, at least for finite values of J_2, so numerical methods must be used in this calculation. One can first consider one

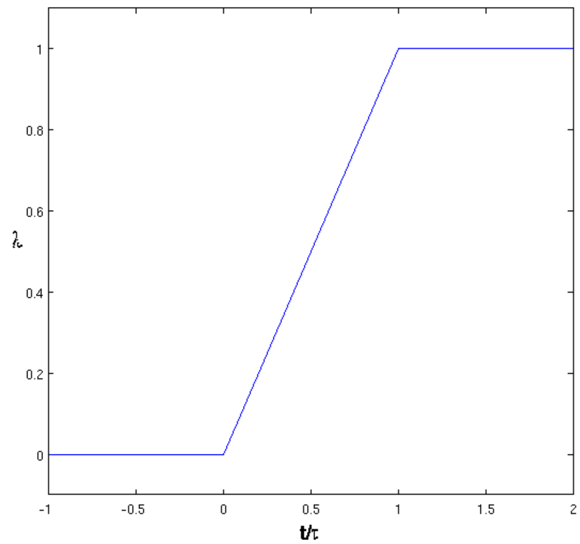

Figure 25: Coupling constant $\lambda(t,\tau)$ from Eq.60 and Eq. 62 versus $\frac{t}{\tau}$.

part of the annealing process, in which a single spin is joined to a even length J1-J2 spin chain, using both J_1 and J_2 couplings which are linearly increased to equal values of those used in the rest of the chain [18],

$$H(t,\tau) = \sum_{n=1}^{N-2} J_1 \vec{\sigma}_n \cdot \vec{\sigma}_{n+1} + \sum_{n=1}^{N-3} J_2 \vec{\sigma}_n \cdot \vec{\sigma}_{n+2} + \lambda(t,\tau)(J_1 \vec{\sigma}_{N-1} \cdot \vec{\sigma}_N + J_2 \vec{\sigma}_{N-2} \cdot \vec{\sigma}_N), \qquad (60)$$

$$\lambda(t,\tau) = \begin{cases} 0 & t \leq 0 \\ \frac{t}{\tau} & 0 < t < \tau \\ 1 & t \geq \tau \end{cases} .$$

As shown in Fig. 26, the annealing time required becomes large and highly sensitive to small variations for larger values of J_2. Also the behavior seems to get worse in this regime as system size is increased, and is poor at the Majumdar-Ghosh point [19].

As a further demonstration of the scaling with annealing time versus J_2, one can plot the annealing time versus system size, as we have done in Fig. 27. This figure shows polynomial or even sub polynomial scaling for small values of J_2, but than shows strongly non-monotonic behavior for stronger coupling. It is important to note however that even the longest chain length considered here is probably far from the infinite system limit, and this data may not

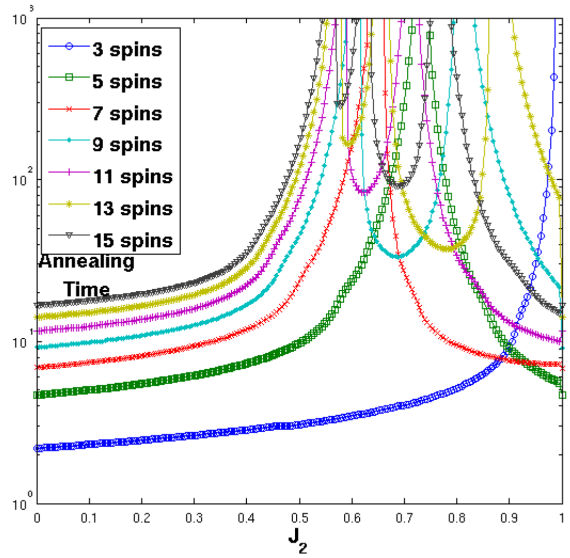

Figure 26: Annealing time required to reach a 90% fidelity with the true ground state within one of the two largest spin sectors of the Hamiltonian vs. J_2, with J_1 set to unity. One can see that for larger values of J_2 the annealing time behaves unpredictably. The annealing time also scales poorly with system size close to the Majumdar-Ghosh point.

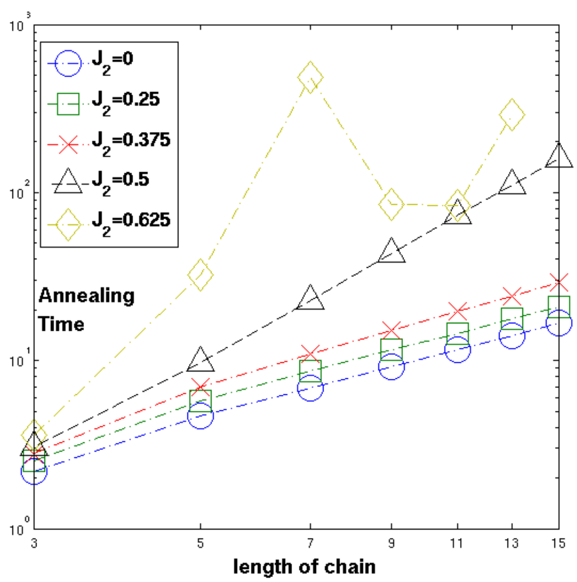

Figure 27: Scaling of annealing time to achieve 90% final ground state fidelity (in units of inverse Hamiltonian energy) versus length of chain on a log-log plot.

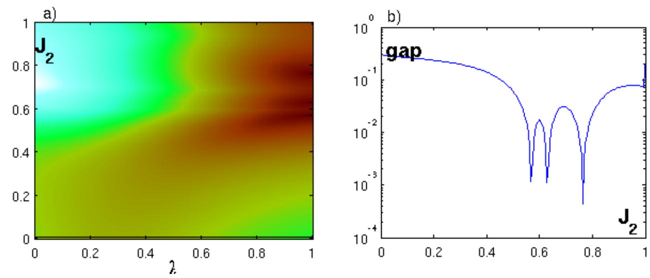

Figure 28: Plots of gap for joining a single spin to an even length J1-J2 Heisenberg spin chain. For density plots lighter colors indicate larger gap. a) gap versus λ in Eq. 60 and J_2 for 15 total spins d) Gap versus J_2 with $\lambda = 1$

be trustworthy for making predictions for scaling as the chain length approaches the infinite system limit.

By examining the gap one can hope to gain insight into the underlying cause of the behavior of annealing time curves. As Figs. 28(a) and (b) show, the behavior of the annealing time curves is reflected by the presence of what appear to be true crossings [20] for the odd length spin chain with uniform coupling. Fig. 28(b) shows the gap for an odd length spin chain and seems to confirm the presence of points with very small gap with uniform coupling for J_2 above 0.5. Figs. 26 and 28 together show that, at least at the length scales considered here, there are good annealing paths for joining a single spin to an even length chain. However, the simplest method of taking advantage of the simple ground-state wavefunction at the Majumdar-Ghosh point is not optimal. Fortunately there are many other possible options to take advantage of the easily prepared ground state and hopefully avoid the regions of small gap found here.

XIII. DYNAMICALLY TUNING J2

One method to avoid regions of small gap while still taking advantage of the Majumdar-Ghosh point would be to start at the Majumdar-Ghosh point and then dynamically reduce the value of J_2 during the annealing process, a simple way of doing this would be to use the Hamiltonian in Eq. 61.

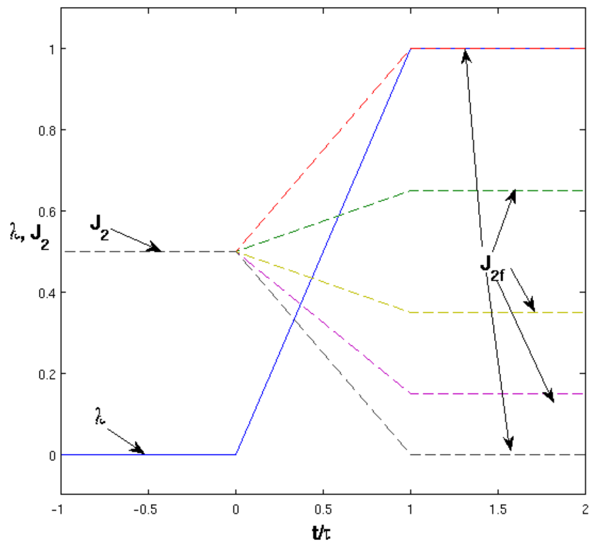

Figure 29: In this annealing protocol not only is a spin coupled to the chain, but $J_2$is also changed dynamically.

$$H(t,\tau) = \sum_{n=1}^{N-2} J_1\vec{\sigma}_n\cdot\vec{\sigma}_{n+1} + \sum_{n=1}^{N-3} J_2(t,\tau)\vec{\sigma}_n\cdot\vec{\sigma}_{n+2} + \lambda(t,\tau)(J_1\vec{\sigma}_{N-1}\cdot\vec{\sigma}_N + J_2(t,\tau)\vec{\sigma}_{N-2}\cdot\vec{\sigma}_N), \quad (61)$$

$$\lambda(t,\tau) = \begin{cases} 0 & t \leq 0 \\ \frac{t}{\tau} & 0 < t < \tau \\ 1 & t \geq \tau \end{cases},$$

$$J_2(t,\tau) = \begin{cases} 0.5 & t \leq 0 \\ 0.5 + \frac{t}{\tau}(J_{2f} - 0.5) & 0 < t < \tau \\ J_{2f} & t \geq \tau \end{cases}.$$

Fig. 30 shows that taking advantage of the easily prepared ground state at the Majumdar-Ghosh point does in fact work, and the curves in this figure are strikingly similar to those in Fig. 26. This similarity is to be expected because Fig. 28 demonstrates that the gap is the smallest where the spin is completely joined. Hence this part of the process should dominate the annealing time.

It is reasonable to argue that because the regions of phase space which are visited are the same in the uncoupling process as coupling, the behavior of the system during the uncoupling

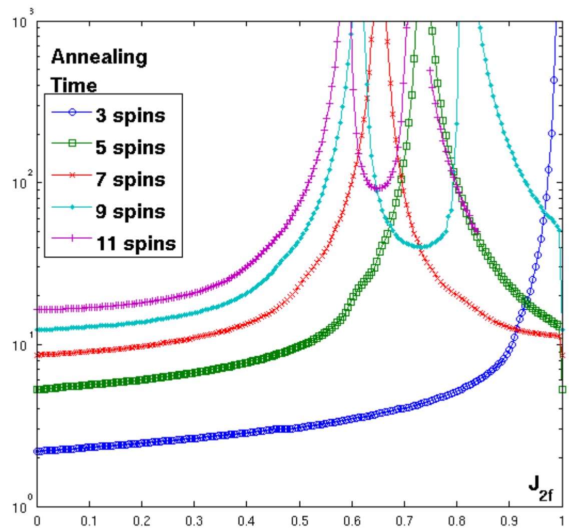

Figure 30: Annealing time required to reach a 90% fidelity with the true ground state within one of the two largest spin sectors of the Hamiltonian with dynamical coupling starting at J_2=0.5 and linearly changing to J_{2f} while also joining a spin to the chain, with J_1 set to unity throughout the process. Notice that this figure is qualitatively and quantitatively very similar to Fig. 26.

process is determined by the gaps shown in Fig. 28, and therefore the annealing times for the uncoupling process should be at least qualitatively similar to those given in Fig. 26. One advantage to the uncoupling process is that unlike the coupling process, the need is not as strong to end in an easily prepared state. The only reason one may have to want to end in the Majumdar-Ghosh point is as an error check. The spins in the chain can be measured after the end of the process to ensure that no error has occurred [21].

Fig. 31 shows the time required to uncouple a spin from the chain, not surprisingly this figure looks very similar to Fig. 26 which is the coupling process. Note that in this system the Hamiltonian is simply Eq. 60 with $\frac{t}{\tau} \rightarrow (1 - \frac{t}{\tau})$.

As expected, except for one curve where a numerical error made some points unable to plot one can see from Fig. 32 that the uncoupling process also requires roughly the same time as the coupling process for dynamically tuned J_2. Note that the Hamiltonian for this process is simply Eq. 61 with $\frac{t}{\tau} \rightarrow (1 - \frac{t}{\tau})$ and $J_{2f} \rightarrow J_{2i}$.

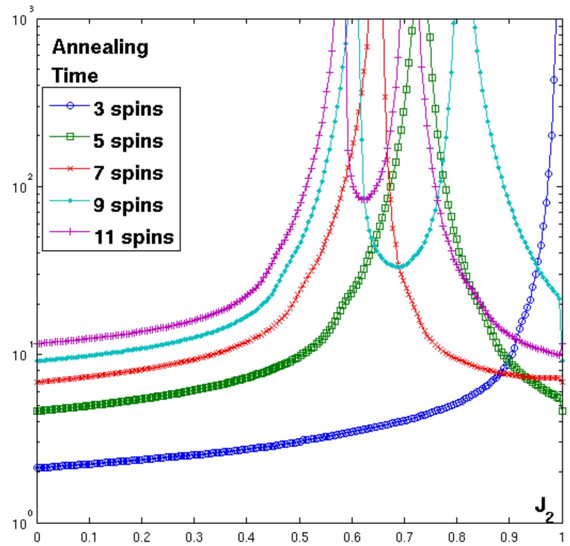

Figure 31: Annealing time required to reach a 90% Fidelity with the true ground state for uncoupling process within one of the two largest spin sectors of the Hamiltonian vs. J_2 with J_1 set to unity. One can see that this figure is very similar to Fig. 26 as one would expect because it is simply the time reversed version of that process.

XIV. SIMULTANEOUS UNCOUPLING AND COUPLING

Because many of the issues encountered with the coupling protocol seem to relate to odd-spin frustration, it may be reasonable to consider simultaneously coupling one qubit to the chain while uncoupling the other. The Hamiltonian in this case is given in Eq. 62.

$$H(t,\tau) = \sum_{n=1}^{N-2} J_1 \vec{\sigma}_n \cdot \vec{\sigma}_{n+1} + \tag{62}$$

$$\sum_{n=1}^{N-3} J_2(t,\tau)\vec{\sigma}_n \cdot \vec{\sigma}_{n+2} + \lambda(t,\tau)((J_1\vec{\sigma}_{N-1}\cdot\vec{\sigma}_N + J_2\vec{\sigma}_{N-2}\cdot\vec{\sigma}_N) - (J_1\vec{\sigma}_1\cdot\vec{\sigma}_2 + J_2\vec{\sigma}_1\cdot\vec{\sigma}_3)),$$

$$\lambda(t,\tau) = \begin{cases} 0 & t \leq 0 \\ \frac{t}{\tau} & 0 < t < \tau \\ 1 & t \geq \tau \end{cases}.$$

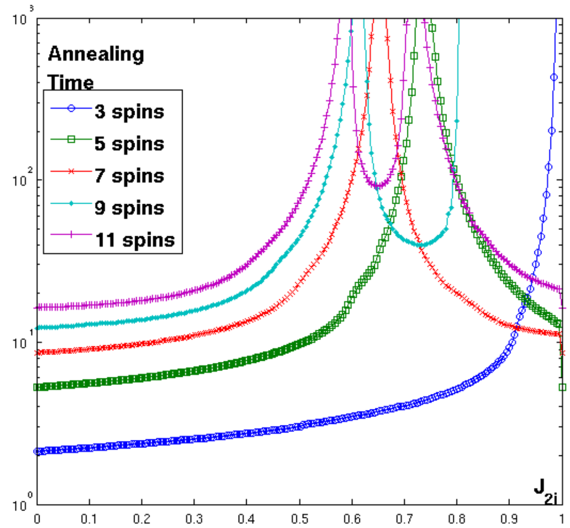

Figure 32: Annealing time required to reach a 90% fidelity with the true ground state for uncoupling process within one of the two largest spin sectors of the Hamiltonian vs. initial J_{2i} with a final J_2 at the Majumdar-Ghosh point with J_1 set to unity. This figure is very similar to Fig. 30 as one would expect, because it is simply the time reversed version of that process.

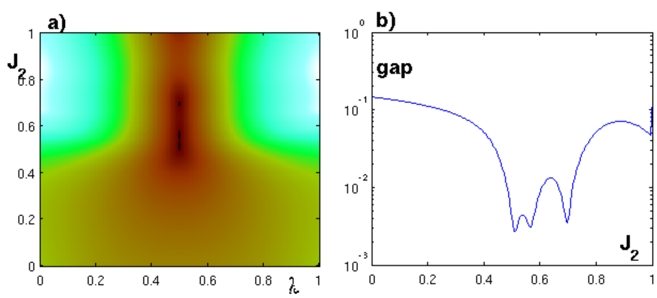

Figure 33: Plots of gap for simultaneously joining a single spin to an even length J1-J2 Heisenberg spin chain and unjoining a spin from the other end. For density plots lighter colors indicate larger gap. a) gap versus λ from Eq. 62 and J2 for 17 total spins b) Gap versus J_2 with $\lambda = 0.5$.

Fig. 33 shows the gaps for various system sizes for the process where the couplings are turned on and off simultaneously. This process does not seem to avoid the area of low gap for $J_2 \gtrsim 0.5$ seen in Fig. 28. However by comparing Fig. 33 d) and Fig. 28 d) one can see that it appears that the process of simultaneous uncoupling and coupling is characterized by avoided crossings rather than true crossings [22].

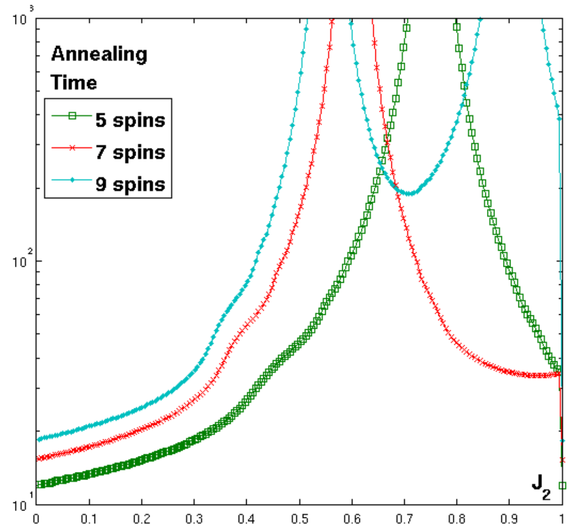

Figure 34: Annealing time required to reach a 90% Fidelity with the true ground state for combined coupling and uncoupling process within one of the two largest spin sectors of the Hamiltonian vs. J_2 with J_1 set to unity.

Fig. 34 shows the time required for annealing processes with for the combined coupling and uncoupling process, the results are consistent with what one would expect from looking at Fig. 33, and confirm that the annealing time also tends to be very long and vary a lot for larger values of J_2.

XV. REQUIREMENTS FOR USE AS AN ADIABATIC QUANTUM BUS

It is now useful to consider a broader class of models that may be used as adiabatic quantum buses, as in general the full SU(2) symmetry of the Heisenberg Hamiltonian is not required.

The requirements for a spin chain (or network) Hamiltonian to be usable as an adiabatic quantum bus are as follow:

1. The ground state must be at least 2 fold degenerate, and the ground state manifold must be able to encode a qubit. In this paper this is achieved by having at least a $\mathbb{Z}_2$symmetry, and an odd number of spins, but there may be other ways.

2. The Hamiltonian (or at least the low energy states) must be predominantly anti-

ferromagnetic in nature. This guarantees that the encoded qubit will be excluded from the larger spin chain (or network) when a single qubit is removed.

3. The Hamiltonian must contain terms which perform exchanges between sites. This excludes models such as the Ising model which, although it has the required symmetry, cannot be used a quantum bus because its Hamiltonian is diagonal in the computational basis

4. One must be able to slowly couple in a spin with an arbitrary state on one end of the chain (network) and also to slowly remove coupling on the other end. More control may improve performance, but is not necessary.

5. Annealing paths in parameter space must not contain true crossings. This is a general requirement for adiabatic quantum computing.

XVI. XXZ AND XYZ MODEL

As previously mentioned, the full SU(2) symmetry of the Heisenberg Hamiltonian is not required. The Hamiltonian must only have a $\mathbb{Z}_2$symmetry to encode and transport one qubit of information. In this section we will briefly examine two other possibilities: the XXZ model, where the SU(2) symmetry is broken, but the block diagonal structure imparted by this symmetry remains, and the XYZ model where only the block diagonal structure of a $\mathbb{Z}_2$ symmetry is present.

As one can see from Fig. 35, the XXZ model can be used as an adiabatic quantum data bus. There is a regime where this system outperforms the XXX Heisenberg model for Z/X between 1 and roughly 2. This is to be expected because adding additional coupling in the z direction may serve to open the gap between the the ground-state manifold and the next excited state. The increasing time as the z coupling is increased further can be explained because the system would behave like an Ising model in the limit of $\frac{Z}{X} \gg 1$.

One can further examine the behavior of an XYZ model as an adiabatic quantum spin bus. For this purpose we consider the quantum bus protocol performed on the following normalized XYZ Hamiltonian

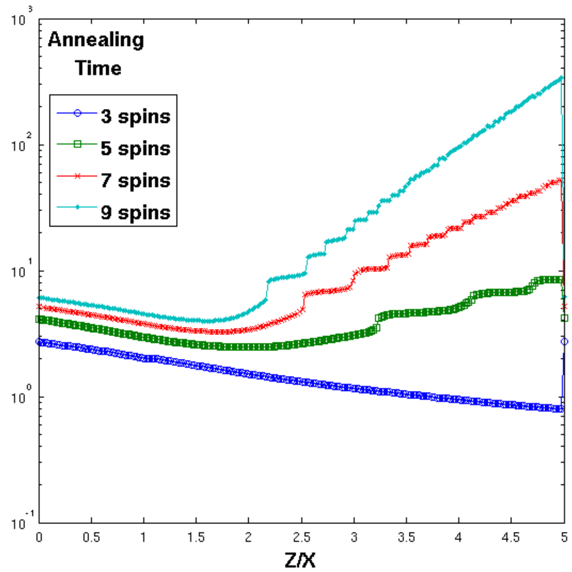

Figure 35: Annealing time to reach 90% fidelity on using the adiabatic quantum bus protocol on an XXZ spin chain versus the ratio of X and Z coupling strengths note that Z/X=0 is an XX model while Z/X=1 is a J1 Heisenberg spin chain. This data was obtained with joining and disconnecting of spins occurring simultaneously.

$$H_{XYZ}(\Delta; N) = C_\Delta \sum_{i=1}^{N-1} \sigma_i^x \sigma_{i+1}^x + (1+\Delta)\sigma_i^y \sigma_{i+1}^y + (1+2\Delta)\sigma_i^z \sigma_{i+1}^z, \tag{63}$$

where the normalization is

$$C_\Delta = \frac{\sqrt{3}}{\sqrt{1+(1+\Delta)^2+(1+2\Delta)^2}}.$$

One can now examine the performance of this Hamiltonian for different values of Δ, noting that $H_{XYZ}(0; N)$ is simply the J1 Heisenberg spin chain of length N.

As Fig. 36 shows, a slight advantage can be gained by using an XYZ model rather than a simple Heisenberg chain. Fig. 36 also seems to suggest that the benefit gained is relatively independent of chain length.

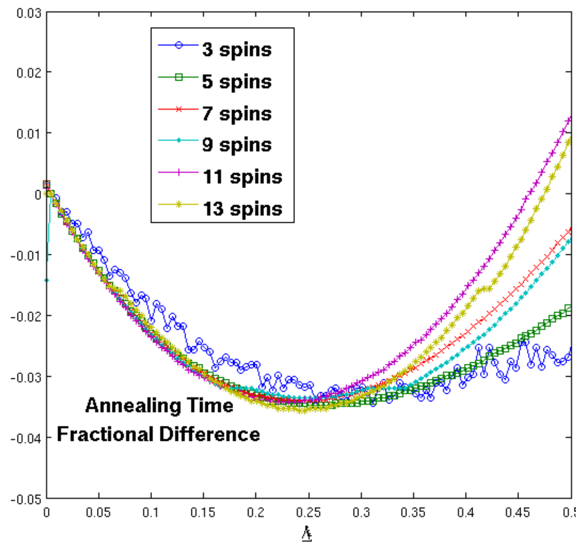

Figure 36: Plot of fractional difference from annealing time for an chain with small Δ (Heisenberg chain). This data is for the adiabatic quantum bus protocol performed on a chain of the form eq. 63 with spins being attached and removed simultaneously.

XVII. OTHER PROTOCOLS

So far we have only investigated a small subset of the possible annealing protocols which meet the criteria given in the introduction. For example the XY spin chain should also have and easily prepared ground state and may be easier to experimentally realize [2]. One could also try to examine the case of dynamically tuning the y and or z direction coupling and starting out at the Majumdar-Ghosh point but using modified coupling in the y and z directions with an XYZ model to avoid low gap regions.

One could also try to change the coupling scheme to avoid the low gap region, by either randomly or systematically modifying the coupling between intermediate spins, if this is done dynamically, one can still take advantage of the Majumdar-Ghosh point. This technique could also be used in conjunction with any of the ideas in the previous paragraph.

This chapter is intended only to provide proof of principle for this method and is by no means an exhaustive search of all possible protocols.

XVIII. CONCLUSIONS

We have demonstrated how a J1-J2 Heisenberg spin chain can be used to transport a qubit state adiabatically. We have also shown that many extensions of this Hamiltonian; such as different coupling schemes or the XY or XYZ model which have only a $\mathbb{Z}_2$ symmetry, will also be able to be used to transport a qubit [23]. We have found that for values of high frustration, transport by quantum annealing does not work very well. We have also demonstrated that this does not prevent us from exploiting the easily prepared ground state at the Majumdar-Ghosh point. We have given some examples of possible annealing protocols in this paper, but have really only investigated a very small section of a vast space of possible protocols for transportation of quantum states by annealing.

Acknowledgements

This Chapter is based on the paper Using the J1-J2 Quantum Spin Chain as an Adiabatic Quantum Data Bus by N. Chancellor and S. Haas [1]. The numerical computations were carried out on the University of Southern California high performance supercomputer cluster. This research in the original paper was partially supported by the ARO MURI grant W911NF-11-1-0268.

Chapter 3 References

[1] N. Chancellor and S. Haas 2012 New J. Phys. 14 095025 (2012).

[2] M. W. Johnson et al. Nature 473, 194-198 (12 May 2011)

[3] R. Harris et al. Physical Review B 81, 134510 (2010)

[4] A. Perdomo et al. Physical Review A 78, 012320 (2008)

[5] S. H. W. van der Ploeg et al. IEEE Trans. App. Supercond. 17, 113 (2006)

[6] R. Harris et al. Phys. Rev. B 82, 024511 (2010)

[7] Z. Chen, Z. Zhou, X. Zhou, X. Zhou, and G. Guo, Phys. Rev. A 81, 022303 (2010)

[8] L. Banchi, T. J. G. Apollaro, A. Cuccoli, R. Vaia, and P. Verrucchi, Phys. Rev. A 82, 052321 (2010)

[9] L Banchi, T J G Apollaro, A Cuccoli, R Vaia, and P Verrucchi, New Journal of Physics 13 (2011) 123006

[10] T. J. G. Apollaro, L. Banchi, A. Cuccoli, R. Vaia, P. Verrucchi, arXiv:1203.5516v1 [quant-ph] 2012

[11] L. Banchi, A. Bayat, Paola Verrucchi, and Sougato Bose, Phys. Rev. Lett. 106, 140501 (2011)

[12] J. Fitzsimmons and J. Twamley, Phys. Rev. Lett. 97, 090502 (2006)

[13] N. Chancellor and S. Haas, Phys. Rev. B 84, 035130 (2011)

[14] Phys. Rev. B 52, 6581 - 6587 (1995)

[15] C K Majumdar, J. Phys. C: Solid State Phys. 3 911 (1970)

[16] Technically one must give the additional condition that there is no true crossing within the spin sectors on the annealing path.

[17] At least this should work for small systems. In the continuum limit many of these systems may become gapless, so that quantum annealing cannot be effectively performed. Also one may be able to construct certain pathological cases with paths which pass through true crossings.

[18] Note that this Hamiltonian (and all other annealing Hamiltonians in this paper) can be rewritten in the form of 54. However it is much more compact not to write the unchanging parts of the Hamiltonian twice.

[19] At least for fixed coupling, the case of dynamically changing coupling will be considered later.

[20] Strictly speaking nothing in this paper has demonstrated them to be true crossings, they could just be close avoided crossings, it does not matter for the purposes of this chapter.

[21] For example if two spins which should be in a singlet together ended up being measured to be facing in the same direction than the annealing process would have failed.

[22] This statement is based on the fact that the gap does not have a cusp when plotted on a log scale. Strictly speaking this just shows that there is not a true crossing at the line where the two couplings are equal.

[23] Assuming there is not a true crossing along the annealing path, the coupling must also be (at least predominately) anti-ferromagnetic so that the excess spin does not become trapped in the larger spin chain.

Chapter 4: Holonomic Quantum Computation by Transport and Application with Superconducting Flux Qubits

This chapter is based on [1]. In this chapter we examine the use of an adiabatic quantum data transfer protocol to build a universal quantum computer. Single qubit gates are realized by using a bus protocol to transfer qubits of information down a spin chain with a unitary twist. This twist arises from altered couplings on the chain corresponding to unitary rotations performed on one region of the chain. We show how a controlled NOT gate can be realized by using a control qubit with Ising type coupling. The method discussed here can be extended to non-adiabatic quantum bus protocols. We also examine the potential of realizing such a quantum computer by using superconducting flux qubits.

Introduction

It has recently been demonstrated how an open-ended antiferromagnetic Heisenberg spin chain can be used as an adiabatic quantum data bus [2]. This data bus takes advantage of antiferromagnetic couplings to transfer qubits of information adiabatically. First a single qubit, encoded in a single spin is joined to an even length Heisenberg spin chain slowly enough such that the adiabatic theorem applies. Then a single spin on the other end of the chain is separated, again slowly enough for the adiabatic theorem to apply. As long as the interactions between the spins on the chain are predominately antiferromagnetic, the qubit will be successfully transferred from one end of the chain to the other. This protocol is illustrated in Fig. 37. Antiferromagnetic spin clusters have been studied for there potential usefulness in quantum computing in other contexts, for example in Refs. [3, 4].

This paper demonstrates how by applying particular unitary operations to spin chains for single qubit gates, and by using a specific spin network for a CNOT gate, one can achieve

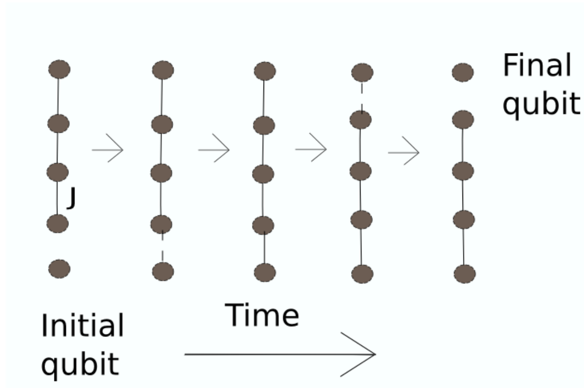

Figure 37: Cartoon of an adiabatic quantum bus protocol for the Heisenberg spin chain [2]. A spin with the encoded qubit is connected to one end of an even length antiferromagnetic chain. Afterwards, the spin on the opposite end is removed adiabatically. As long as the chain interactions are predominately antiferromagnetic and the adiabatic theorem is satisfied the qubit will be transferred.

universal holonomic quantum computation. This method uses open-loop holonomies, meaning that the Hamiltonian is not necessarily returned to the same state after the adiabatic process. The methods used here can also be extended to non-adiabatic implementations of geometrical quantum computing.

Holonomic quantum computation (HQC) was conceived and shown to be universal by Zanardi and Rasetti [5] and was formulated in terms of a non-abelian Berry phase. HQC is considered to be an appealing method for achieving fault tolerant quantum computing because of its geometrical nature and because it can be implemented adiabatically, and therefore has all of the advantages of adiabatic quantum computation [6]. Although many implementations of holonomic and geometric quantum computation are adiabatic, there are examples which are not [7, 8].

Other proposed architectures for holonomic quantum computation use a variety of architectures, including superconducting systems with Josephson junctions [9]. Further examples propose using quantum dots [8, 10]. Single molecule magnets have been another system of interest [8]. A recent proposal has also been made for using Holonomies which involve attaching and removing a spin from a spin 1 chain[11]. This architecture, although it looks superficially very similar to ours, performs computations locally, at the site of the spin rather than by transport as our's does. Ref. [11] also proposes an implementation on ultracold polar molecules. Another interesting proposal involves using a quantum wire with a twisted cluster state Hamiltonian[12]. This proposal is similar to ours, but implements the twist in a fundamentally different way.

Most other approaches to HQC involve building a system, and explicitly calculating the holonomies caused by various manipulations of the system. In our proposal we start with a process which has a trivial Berry phase[27]. Real space twists are then performed on the spin chain used in this process. Unlike most examples of HQC, all results can be derived without explicitly considering the curvature of the underlying manifold of states, all single qubit gates result from the same underlying Hamiltonian with basis rotations applied to it.

The mathematical differences of this approach from others affords us the advantage that the spectrum of the underlying Hamiltonian is the same for all twists, meaning that, by construction, all single qubit gates can be implemented in a way which requires the same annealing time to reach a given accuracy. This architecture has the advantage that the only operation it ever requires to be adiabatically performed is the joining or removal of a spin from a chain or cluster. The nature of the twists used here also means that a non-adiabatic transport protocol could be used instead, and universal computation would still be achieved.

This chapter also outlines an implementation of the necessary components of this design using superconducting flux qubits. Superconducting flux qubits are a popular architecture for implementing scalable adiabatic quantum computing [2–6], and therefore are a natural choice for designing a scalable holonomic quantum computer. An additional advantage of the use of superconducting flux qubits is that the designs tend to have spatially extended qubits and a high degree of connectivity[17]. The large spatial extent of the qubits means that a design could be implemented in which a qubit would only need to be transferred across a small number of spins to be moved from one location in a computer to any other arbitrary location. For this reason it is only necessary that the transport protocol be efficient for short chains, as has already been demonstrated in [2], rather than in the thermodynamic limit.

There has been recent experimental work involving quantum annealing to degenerate ground state manifolds using currently available superconducting flux qubit hardware[18]. In this paper it was demonstrated experimentally that signatures of quantum behaviors can be observed in the final state within a degenerate ground state manifold. This provides an indication that a ground state manifold can be produced accurately enough on current hardware that quantum effects dominate over classical effects and design inaccuracies. Although the architecture proposed here cannot be implemented on the hardware used in [18], this experiment does provide proof of principle for the use of degenerate manifolds in superconducting flux qubit systems.

While it is not the main focus of this chapter, we would also like to point out that there are other potential methods of implementing this architecture. One example of such an implementation would be to use a coupled cavities scheme similar to the one explored in [19]. For such an implementation long spin chains may be required, and as a result properties in the thermodynamic limit may be important. For such an implementation, the architecture given in this paper could easily be generalized to a J1-J2 spin chain with $\frac{J_2}{J_1} \gtrsim 0.25$ which is know to be gaped in the thermodynamic limit[20]. In this case, another option would be to implement the architecture non-adiabatically using the methods described in [8–11].

XIX. SINGLE Q-BIT GATES

A. The Twisted Spin Chain

Consider initially an antiferromagnetic Heisenberg spin chain. It has been shown that such a chain can act as a quantum data bus, both adiabatically[2] and by using the dynamics of its excitations [8–11]. The initial Hamiltonian is given by

$$\mathrm{H} = \sum_{i=1}^{N-1} \vec{\sigma}_i \cdot \vec{\sigma}_{i+1} = \sum_{i=1}^{N-1} (\sigma_i^x \sigma_{i+1}^x + \sigma_i^y \sigma_{i+1}^y + \sigma_i^z \sigma_{i+1}^z). \tag{64}$$

Now imagine that one inserts a twist into the spin chain by applying a local unitary transformation of the form $x, y, z \rightarrow x', y', z'$ on $N' = N - L$ spins, where x', y', z' are all mutually orthogonal to each other. This yields a new Hamiltonian of the form

$$\mathrm{H}_{\mathrm{twist}} = \sum_{i=1}^{L-1} \vec{\sigma}_i \cdot \vec{\sigma}_{i+1} + \vec{\sigma}_L \cdot \vec{\sigma}'_{L+1} + \sum_{j=L+1}^{N-1} \vec{\sigma}'_j \cdot \vec{\sigma}'_{j+1}. \tag{65}$$

Such a twist does not effect the spectrum of the Hamiltonian, and therefore the dynamics of the adiabatic quantum bus protocol, or other quantum bus protocols which may make use of the unitary dynamics of the Hamiltonian. It is important to note, however, that after transfer across the chain, the spin will be rotated into the x', y', z' basis. As we will

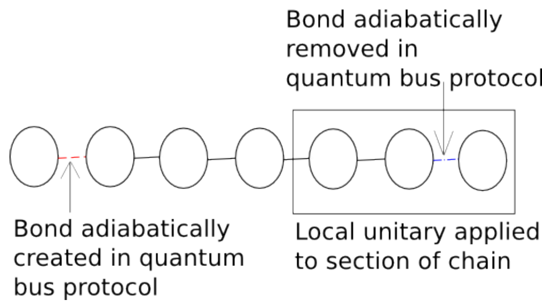

Figure 38: Illustration of a single unitary gate implemented by adiabatic transport on a twisted chain.

demonstrate later, transfer through this twisted spin chain can perform any desired unitary rotation on the qubit being transferred, and thus can be used to implement any single qubit gate, see Fig. 38.

One should note that while in this example we consider a simple Heisenberg spin chain, gates can be implemented in this way on an XYZ spin chain or a J1-J2 spin chain, or other sufficiently complex quantum spin Hamiltonians [28]. Figuring out which twist to use to perform a given gate can be done easily and will be illustrated in the next section.

B. Example: Implementing a Hadamard Gate

The local twist to implement the Hadamard gate is $\sigma^x \to \sigma^z$, $\sigma^y \to -\sigma^y$and $\sigma^z \to \sigma^x$. This twist can be calculated without difficulty, for details see Sec. XXIV A.

One can therefore conclude that the Hadamard gate can be implemented by performing the quantum bus protocol on the Hamiltonian

$$\mathrm{H}_{\mathrm{Hadamard}} = \sum_{i=1}^{N'-1} \vec{\sigma_i} \cdot \vec{\sigma}_{i+1} + \sigma^x_{N'}\sigma^z_{N'+1} + \tag{66}$$

$$\sigma^x_{N'}\sigma^z_{N'+1} - \sigma^y_{N'}\sigma^y_{N'+1} + \sum_{j=N'+1}^{N-1} \vec{\sigma_j} \cdot \vec{\sigma}_{j+1}$$

C. Other Single Qubit Gates

One can perform similar twists to implement any given single qubit gate. The calculation to find x', y', z' in Eq. 65 for other gates can be performed in the same way as the one in the

Gate Name	Matrix	$\sigma^{x'}$	$\sigma^{y'}$	$\sigma^{z'}$
Hadamard	$\frac{1}{\sqrt{2}}\begin{pmatrix} 1 & 1 \\ 1 & -1 \end{pmatrix}$	σ^z	$-\sigma^y$	σ^x
$\frac{\pi}{8}$	$\begin{pmatrix} 1 & 0 \\ 0 & \exp(\imath\frac{\pi}{4}) \end{pmatrix}$	$\frac{1}{2}(\sigma^x + \sigma^y)$	$\frac{1}{2}(\sigma^y - \sigma^x)$	σ^z
phase	$\begin{pmatrix} 1 & 0 \\ 0 & \imath \end{pmatrix}$	$-\sigma^y$	σ^x	σ^z
NOT[a]	$\begin{pmatrix} 0 & 1 \\ 1 & 0 \end{pmatrix}$	σ^x	$-\sigma^y$	$-\sigma^z$

[a]This gate is needed for the construction of the CNOT

Table IV: Twists for implementing various single qubit gates

previous section for the Hadamard. Table IV shows how to implement single qubit gates. These gates are sufficient to perform an arbitrary unitary operation on a single spin. It is shown in [25] that any unitary rotation can be approximated to arbitrary precision with the gates given in table IV. We have already shown how to build an adiabatic quantum bus to move qubit states to arbitrary locations in the system. Next we discuss that a CNOT gate can be implemented under this architecture. Then we have demonstrated a universal quantum computer.

XX. IMPLEMENTATION OF THE CONTROLLED NOT GATE

A. CNOT design

Let us now turn our attention to the implementation of a controlled NOT (CNOT) using an adiabatic quantum bus protocol. In Fig. 39a) we show a design for such a gate. The time dependent Hamiltonian for this gate is

$$
\begin{aligned}
\mathrm{H}_{CNOT}(t;h,t_{fin}) = \lambda(t;t_{fin})\vec{\sigma}_{in}\cdot(\vec{\sigma}_1+\vec{\sigma}_2+\vec{\sigma}_3+\vec{\sigma}_4) \\
+\vec{\sigma}_a\cdot(\vec{\sigma}_1+\vec{\sigma}_2+\vec{\sigma}_3+\vec{\sigma}_4)+h((\sigma_1^z-\sigma_2^z)(1-\sigma_c^z)+(\sigma_3^z-\sigma_4^z)(1+\sigma_c^z)) \\
+(1-\lambda(t;t_{fin}))(\vec{\sigma}'_{out}\cdot(\vec{\sigma}_1+\vec{\sigma}_2))+\vec{\sigma}_{out}(\vec{\sigma}_3+\vec{\sigma}_4), \quad (67)
\end{aligned}
$$

$$
\lambda(t;t_{fin}) = \begin{cases} 0 & t<0 \\ \frac{t}{t_{fin}} & 0\le t\le t_{fin} \\ 1 & t>t_{fin} \end{cases}.
$$

Here “in” refers to the spin which is the input spin, where the target qubit is initially encoded; “out” refers to the spin to which the target qubit is transferred to, “c” refers to the control qubit, “a” to an ancilla to make the number of intermediate spins odd. The other 4 spins are assigned numbers 1-4. $\vec{\sigma}'_{out}$ refers to a NOT twist being performed on these Pauli matrices, see Tab. IV. This gate operates by having 2 channels through which a qubit of information can pass. One channel, consisting of spins 3 and 4, allows the information to pass through the gate unaltered, while another channel, consisting of spins 1 and 2 performs a twist on the qubit as it travels though the gate. The control spin c controls though which channel the information travels. The control spin is connected with Ising type coupling to spins 1-4 in such a way that when the control spin is up the external field on spins 1 and 2 cancels with the effect of the Ising bond with spin c because $(\frac{1}{2}- < \sigma_c^z >) = 0$, and the information can easily pass though these spins. On the other hand $(\frac{1}{2}+ < \sigma_c^z >) = 1$. So spins 3 and 4 both have an effective magnetic field of 2h. For sufficiently large h these spins are frozen in the direction of the field and will therefore not be able to transport any information. As we show in Fig. 39b) the net effect is that information all travels though spins 1 and 2, and therefore a NOT twist is performed. In the case where the spin c is in the down direction, information will instead be allowed to travel though spins 3 and 4 and blocked on spins 1 and 2. Therefore in that case the gate acts trivially on the qubit.

Any state of the control spin c can be expressed as $|\psi_c\rangle = a|\uparrow\rangle + b|\downarrow\rangle$ where a and b are complex numbers. With an arbitrary input state $|\psi_{in}\rangle = \alpha|\uparrow\rangle + \beta|\downarrow\rangle$ we have before the gate $|\psi_{init}\rangle = |\psi_{in}\rangle\otimes|\psi_c\rangle = \alpha a|\uparrow\uparrow\rangle + \alpha b|\uparrow\downarrow\rangle + \beta a|\downarrow\uparrow\rangle + \beta b|\downarrow\downarrow\rangle$. After the gate is performed, the final state becomes $|\psi_{fin}\rangle = \alpha a|\downarrow\uparrow\rangle + \alpha b|\uparrow\downarrow\rangle + \beta a|\uparrow\uparrow\rangle + \beta b|\downarrow\downarrow\rangle$. From these general states we see that

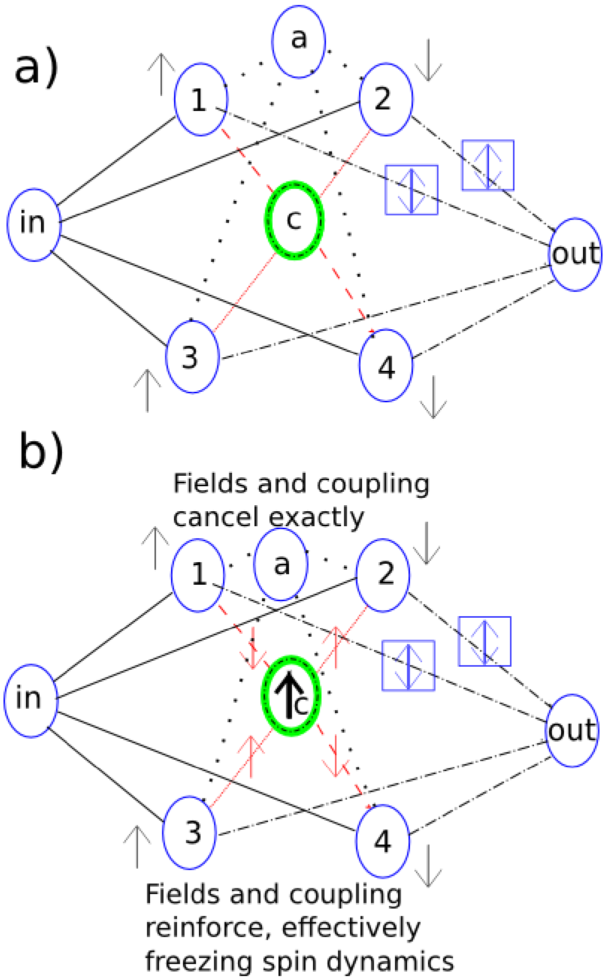

Figure 39: a) Design of a CNOT gate which uses the adiabatic data bus protocol. Note that one could replace the NOT operation with any other single qubit unitary. b) CNOT system with control central spin up, executes a NOT twist on target spin under quantum bus protocol. See Tab. V for the meaning of various symbols. Labels are based on Eq.67.

$$|\psi_{fin}\rangle = \begin{pmatrix} 1 & 0 & 0 & 0 \\ 0 & 1 & 0 & 0 \\ 0 & 0 & 0 & 1 \\ 0 & 0 & 1 & 0 \end{pmatrix} |\psi_{init}\rangle, \tag{68}$$

which is the definition of a controlled NOT gate [25].

Symbol	Meaning
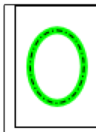	spin $\frac{1}{2}$ control spin
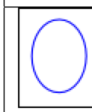	spin $\frac{1}{2}$ working spin
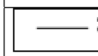	initial AF Heisenberg bond (weak)
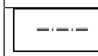	final AF Heisenberg bond (weak)
	fixed AF Heisenberg bond (weak)
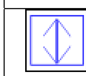	twist to perform NOT operation
	fixed F Ising bond (strong)
	fixed AF Ising bond (strong)
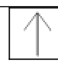	fixed "up" magnetic field (strong)
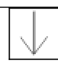	fixed "down" magnetic field (strong)

Table V: Legend of symbols used in Figs. 39.

B. Performance of Controlled NOT Gate

We need to test how this design for a CNOT gate performs because we cannot rely on previous work to show that the qubit is actually transferred accurately. The two free parameters in Eq. 67 are the strength of the Ising bonds and the fields which we denote by h, and the time for the protocol to be performed, t_{fin}.

We now examine whether this Hamiltonian actually implements a CNOT gate effectively for reasonable values of h and t_{fin}. To test this we need to answer 2 questions. Firstly, is the system close enough to the adiabatic limit for reasonable values of t_{fin}? Secondly, is the desired effect of shutting off one possible path for the information achieved for reasonable values of h? To answer these questions, we examine the overlap of the final output state (final state of the "out" qubit in Fig. 39) with the expected output state from a controlled NOT gate (Fig.40). Note that because the case where a NOT gate is performed, and the case where the gate acts trivially are related by a simple unitary transformation on the Hamiltonian, acceptable performance in one of these cases implies acceptable performance

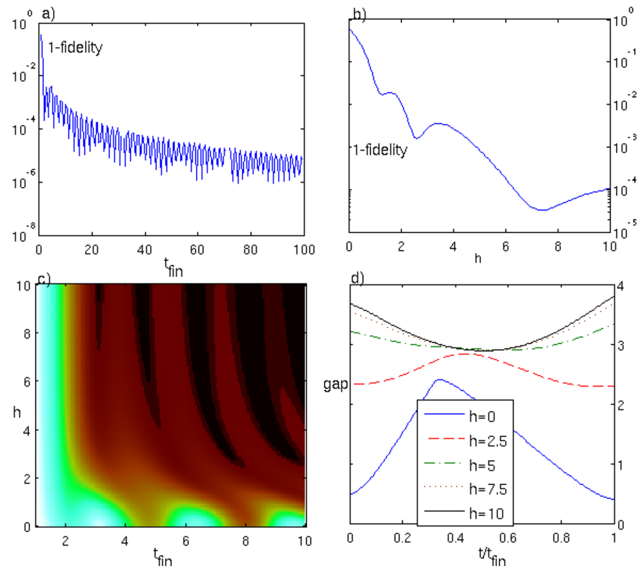

Figure 40: Measures of performance of the CNOT gate a) 1-fidelity of the output spin versus t_{fin} for h=10 b) 1-fidelity of the output spin versus h for t_{fin}=10 c) output fidelity for initial up spin with a NOT performed versus h and t_{fin} light is larger (more positive), dark is smaller (more negative) d) gap versus $\frac{t}{t_{fin}}$ for various values of h.

in the other. Averaging over different initial states is therefore unnecessary as it would yield the exact same result as any particular choice of control and input states.

Fig. 40 demonstrates the effectiveness of this gate. Fig. 40 a) shows that for a moderate field and Ising bond strength the gate can be made to perform well as long as the annealing time is sufficient. This figure also shows that the gate can continually be made more effective by running it longer without having to raise h. The oscillations in the fidelity are related to the time scale of small excitations produced during the annealing process. In many applications one may have enough control over t_{fin}that the annealing time can be chosen in a way that the process lies near one of the local minima of error shown in Fig. 40 a).

Fig. 40 b) shows the effect of h on fidelity for an annealing time of 10 (in units of inverse Heisenberg couplings). In this figure one can see that increasing h is ineffective at improving performance above a certain value. This indicates that at this point the field is already effectively completely blocking one path that the information transport can take. Fig. 40 c) shows the combined effects of h and t_{fin}on the output polarization. It is consistent with the conclusions we have reached from a) and b). Finally, Fig. 40 d) shows that the system gap remains quite large throughout the process. It also demonstrates that beyond a certain value of h the gap does not increase significantly with changing h, which is consistent with the picture of one path being completely closed to information transfer. It is interesting to note that increasing h increases the gap throughout the process.

XXI. IMPLEMENTATION USING SUPERCONDUCTING FLUX QUBITS

To build an implementation of this holonomic architecture based on superconducting flux qubits one needs to design circuits that implement Heisenberg spins and the appropriate gate couplings between spins. Fortunately significant work has already been done, for example in Refs. [2–6], towards the design of couplers for superconducting flux qubits. However since the previously discussed schemes were based on Ising spin systems, we still need to establish a method for designing circuits which emulate Heisenberg spins. It is interesting to point out that this computational architecture works with the limited connectivity of the designs proposed in Refs. [2–6]. Specifically the CNOT gate we have proposed fits in a single 2x4 chimera lattice cell like the one used in Ref. [17].

A. Flux Qubit Motivation:

It has been shown in [14] that a qubit which behaves like an Ising spin can be constructed from a Hamiltonian of the form

$$\mathrm{H}_{Ising} = \sum_{n=1}^{2}(\frac{Q_n}{2C_n} + U_n\frac{\phi_n - \phi_n^x}{2}) - U_q\cos(\alpha_1\phi_1)\cos(\alpha_2\phi_2), \tag{69}$$

where the applied fluxes ϕ_n^x act as effective magnetic fields, altering the shape of a potential well for the system in a way that mimics a spin constrained to move in a plane. The constants α simply act to scale the effect of the flux. To construct a Heisenberg qubit one needs to add a third direction, leading to a Hamiltonian of the form

$$\mathrm{H}_{Heis.} = \sum_{n=1}^{3}(\frac{Q_n}{2C_n} + U_n\frac{\phi_n - \phi_n^x}{2}) \tag{70}$$

$$-U_q\cos(\alpha_1\phi_1)\cos(\alpha_2\phi_2)\cos(\alpha_3\phi_3).$$

Such a Hamiltonian would allow the shape of the potential well to be changed along 3 directions and would therefore mimic a Heisenberg spin rather than an Ising spin. Previously proposed designs also only couple qubits along one direction. If a new type of coupler were added to the currently implemented circuits which couple the spins in the y direction in addition the z direction, then an XY model could be implemented. To implement an XYZ Heisenberg model, one needs to both design qubits which are not constrained to lie in a plane and build 3 types of couplers, one for each direction in space.

XXII. FLUX QUBIT DESIGN:

First consider a CCJJ (Compound-Compound Josephson Junction) circuit as defined in [14].

The effective Hamiltonian of this circuit is given by [14]

$$\mathrm{H} = \sum_n \left(\frac{Q_n}{2C_n} + U_n \frac{\phi_n - \phi_n^x}{2}\right) - U_q \beta_{eff} \cos(\phi_q - \phi_q^0), \tag{71}$$

where $n \in \{q, cjj, l, r\}$. Note that there are more indeces than in [14] because we do not have the condition that $\phi_L = \phi_L^x$ or $\phi_R = \phi_R^x$. The first two terms of the Hamiltonian in Eq.71 are not important for what we are trying to demonstrate here [14]. The definition of all of these terms can be found in Eq. B4b-f in [14], and in Sec. XXIV B of this paper.

Let us make the simplifying assumption that all of the critical currents are equal for all junctions. In practice there is variability in junction fabrication, but this error can be compensated by building a CCCJJ device (see Fig. 41). Let us also assume that our circuit is designed in such a way that we can inductively couple the left and right loop to each other very strongly such that $\phi_y \equiv \phi_L = \phi_R$ and $\phi_y^x \equiv \phi_L^x = \phi_R^x$. These assumptions cause the equations to simplify greatly (see Sec. XXIV B), yielding

$$\beta_{eff} = \beta_+ \cos\left(\frac{\phi_{ccjj}}{2}\right), \tag{72}$$

$$\beta_+ \equiv 2\beta_L = 2\beta_R,$$

$$\beta_{L(R)} = \frac{4\pi L_q I_c}{\Phi_0} \cos\left(\frac{\phi_y}{2}\right). \tag{73}$$

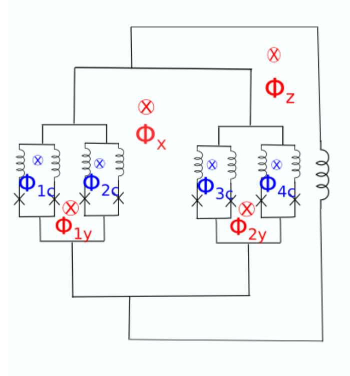

Figure 41: One can build a CCCJJ by replacing every Josephson Junction with a pair of parallel junctions in the CCJJ. By controlling the flux in any of the smallest loops (Φ_{nc}) one can effectively change the critical current of the junction pair and compensate for manufacturing errors. A similar example with a CJJ and a CCJJ can be found in [14].

This leads to an effective Hamiltonian of the form

$$\mathrm{H} = \sum_n \left(\frac{Q_n}{2C_n} + U_n \frac{\phi_n - \phi_n^x}{2}\right) - U_q \beta_+ \cos\left(\frac{\phi_{ccjj}}{2}\right)\cos(\phi_q) \tag{74}$$

When we substitute in $\beta_+$from Eq. 73, this Hamiltonian becomes

$$\mathrm{H} = \sum_n \left(\frac{Q_n}{2C_n} + U_n \frac{\phi_n - \phi_n^x}{2}\right) \tag{75}$$

$$-U_q \frac{8\pi L_q I_c}{\Phi_0} \cos\left(\frac{\phi_y}{2}\right)\cos\left(\frac{\phi_{ccjj}}{2}\right)\cos(\phi_q),$$

which is of the form given in Eq. 70. The corresponding circuit is shown in Fig. 42.

XXIII. CONCLUSIONS

We have demonstrated an architecture for a universal quantum computer using Heisenberg spin chains and clusters. This architecture has the advantage that it can be implemented adiabatically and therefore has all of the advantages of adiabatic quantum computing. It has already been demonstrated in [2] that the single qubit gates and data bus used in this computer can be implemented with high fidelity for reasonable annealing time. We further demonstrate that a controlled NOT gate can be implemented at high fidelity with a reasonably short annealing time and reasonable Hamiltonian parameters.

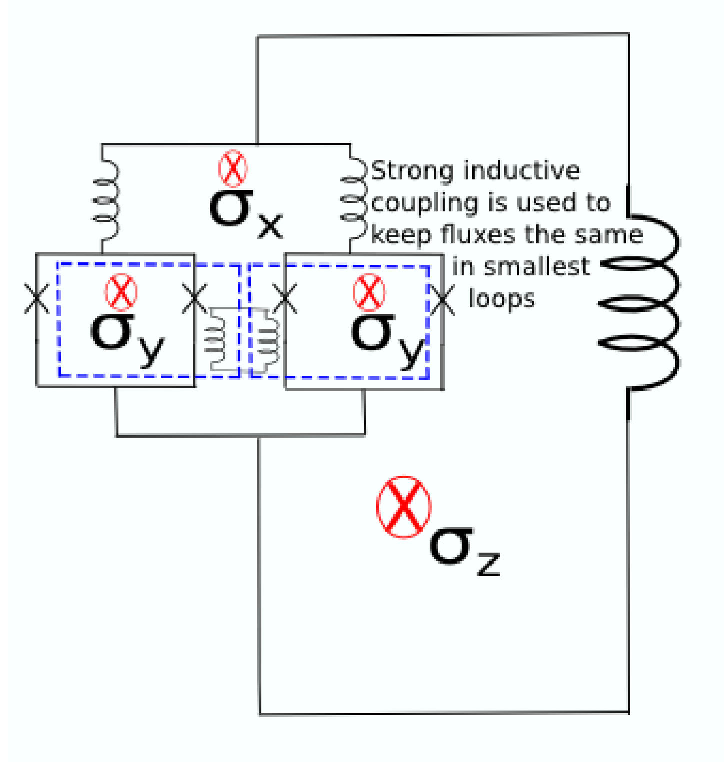

Figure 42: Design using strong inductive coupling between small loops, where fluxes mimic various magnetic fields applied to a spin. Note that this design assumes that all Josephson junctions are identical.

In addition to suggesting an architecture, we also propose a design to physically realize this architecture. We suggest a method for building superconducting flux qubit systems which model the low energy degrees of freedom of a Heisenberg model. Because the architecture we propose can be implemented adiabatically, only the low energy degrees of freedom need to be reproduced. We choose a superconducting flux qubit implementation because of the experimental success of these systems in performing non-universal adiabatic quantum computing with an Ising spin glass model. Furthermore it has been shown that these Ising spin glass models can be realized accurately enough that the degeneracy of the ground state manifolds is not broken. The universal Heisenberg spin based computer would represent a significant improvement over the current non-universal Ising systems because it would allow these computers to implement important algorithms which the Ising spin glass system has not been able to, such as Shors algorithm for factoring large numbers [2–6].

Acknowledgments

The authors would like to thank P. Zanardi, I. Marvian, S. Boixo, D. A. Lidar, L. C. Venuti, and S. Takehashi for helpful conversations. Some numerical calculations were performed on the USC high performance computing cluster. This research is partially supported by the ARO MURI grant W911NF-11-1-0268.

XXIV. APPENDIX

A. Calculation of twist for Hadamard gate

Showing how to implement any given single spin gate using this method is straightforward. Take for example the Hadamard gate $\mathcal{H}$,

$$\mathcal{H}|\psi\rangle = \frac{1}{\sqrt{2}}\begin{pmatrix} 1 & 1 \\ 1 & -1 \end{pmatrix}|\psi\rangle. \tag{76}$$

We now consider the action of $\mathcal{H}$ on the eigenvectors of the Pauli spin matrices, first for σ^x:

$$x_+ = \frac{1}{\sqrt{2}}\begin{pmatrix} 1 \\ 1 \end{pmatrix} \to x'_+ = \mathcal{H}x_+ = \begin{pmatrix} 1 \\ 0 \end{pmatrix} = z_+$$

$$x_- = \frac{1}{\sqrt{2}}\begin{pmatrix} 1 \\ -1 \end{pmatrix} \to x'_- = \mathcal{H}x_- = \begin{pmatrix} 0 \\ 1 \end{pmatrix} = z_-$$

Similarly for σ^z:

$$z_+ = \begin{pmatrix} 1 \\ 0 \end{pmatrix} \to z'_+ = \mathcal{H}z_+ = \frac{1}{\sqrt{2}}\begin{pmatrix} 1 \\ 1 \end{pmatrix} = x_+$$

$$z_- = \begin{pmatrix} 0 \\ 1 \end{pmatrix} \to z'_- = \mathcal{H}z_- = \frac{1}{\sqrt{2}}\begin{pmatrix} 1 \\ -1 \end{pmatrix} = x_-$$

And for σ^y:

$$y_+ = \frac{1}{\sqrt{2}}\begin{pmatrix} 1 \\ \imath \end{pmatrix} \to y'_+ = \mathcal{H}y_+$$

$$= \frac{1}{2}\begin{pmatrix} 1+\imath \\ \imath - 1 \end{pmatrix} = \frac{\imath + 1}{\sqrt{2}}\begin{pmatrix} 1 \\ -\imath \end{pmatrix} = y_- \exp(\imath\phi)$$

$$y_- = \frac{1}{\sqrt{2}}\begin{pmatrix} 1 \\ -\imath \end{pmatrix} \to y'_- = \mathcal{H} y_-$$

$$= \frac{1}{2}\begin{pmatrix} 1+\imath \\ \imath - 1 \end{pmatrix} = \frac{\imath - 1}{\sqrt{2}}\begin{pmatrix} 1 \\ \imath \end{pmatrix} = y_+ \exp(-\imath\phi)$$

In this case the phase factor ($\phi = \frac{\pi}{4}$) is irrelevant because of the overall U(1) symmetry.

B. Detailed discussion of simplifying assumptions for superconducting flux qubits

The last term U_q in Eq. 71 is a constant which is not relevant for this discussion. However the other constants in this term are relevant and are defined as follow (Eq. B4b-f in [14])

$$\beta_{eff} = \beta_+ \cos(\frac{\gamma}{2})\sqrt{1 + (\frac{\beta_-}{\beta_+}\tan(\frac{\gamma}{2}))^2}, \tag{77}$$

$$\phi_q^0 = \frac{\phi_L^0 + \phi_R^0}{2} + \gamma_0, \tag{78}$$

$$\gamma \equiv \phi_{ccjj} - (\phi_L^0 - \phi_R^0), \tag{79}$$

$$\gamma_0 \equiv -\arctan(\frac{\beta_-}{\beta_+}\tan(\frac{\gamma}{2})), \tag{80}$$

$$\beta_\pm \equiv \beta_L \pm \beta_R. \tag{81}$$

Here we need the additional definitions:

$$\beta_{L(R)} = \beta_{L(R),+}\cos(\frac{\phi_{L(R)}}{2})\sqrt{1 + (\frac{\beta_{L(R),-}}{\beta_{L(R),+}}\tan(\frac{\phi_{L(R)}}{2}))^2}, \tag{82}$$

$$\phi_{L(R)}^0 = \arctan(\frac{\beta_{L(R),-}}{\beta_{L(R),+}}\tan(\frac{\phi_{L(R)}}{2})), \tag{83}$$

$$\beta_{L(R),\pm} = \frac{2\pi L_q(I_{1(3)} \pm I_{2(4)})}{\Phi_0}. \tag{84}$$

Let us make the simplifying assumption that all of the critical currents are equal, $I_1 = I_2 = I_3 = I_4$. In practice there is variability in junction fabrication, but this error can be compensated by building a CCCJJ device (see Fig. 41). This assumption causes the equations to simplify greatly because $\beta_{L(R),-} \rightarrow 0$, which has the consequence that $\phi^0_{L(R)} \rightarrow 0$ and $\gamma \rightarrow \phi_{ccjj}$. We can further assume that in our design that $\phi_L = \phi_R$, this additional assumption causes $\beta_- = 0$ and $\gamma_0 \rightarrow 0$, which in turn causes $\phi^0_q \rightarrow 0$. After this simplification we now have

$$\beta_{eff} = \beta_+ \cos(\frac{\phi_{ccjj}}{2}), \tag{85}$$

$$\beta_{L(R)} = \frac{4\pi L_q I_c}{\Phi_0} \cos(\frac{\phi_{L(R)}}{2}). \tag{86}$$

Chapter 4 References

[1] N. Chancellor and S. Haas, Phys. Rev. A 87, 042321 (2013).

[2] N. Chancellor and S. Haas 2012 New J. Phys. 14 095025 (2012).

[3] F. Meier, J. Levy, D. Loss, Phys. Rev. B 68, 134417 (2003).

[4] S. C. Benjamin and S. Bose, Phys. Rev. Lett. 90, 247901 (2003).

[5] P. Zanardi and M. Rasetti, Phys. Lett. A264 (1999) 94-99

[6] J. Pachos and P. Zanardi, Int. J. Mod. Phys. B15 (2001) 1257-1286

[7] G. F. Xu, J. Zhang, D. M. Tong, Erik Sjoqvist, L. C. Kwek, Physical Review Letters 109, 170501 (2012)

[8] Vahid Azimi Mousolou, Carlo M. Canali, Erik Sjï¿œqvist arXiv:1209.3645 (2012)

[9] L. Faoro, J. Siewert, and R. Fazio Phys. Rev. Lett. 90, 028301 (2003)

[10] P. Solinas, P. Zanardi, N. Zanghi, F. Rossi, arXiv:quant-ph 0301090v1 (2003)

[11] J. M. Renes, A. Miyake, G. K. Brennen, S. D. Bartlett arXiv:1103.5076 (2011)

[12] D. Bacon, S. T. Flammia, G. M. Crosswhite, arXiv:1207.2769 (2012)

[13] M. W. Johnson et al. Nature 473, 194-198 (12 May 2011)

[14] R. Harris et al. Physical Review B 81, 134510 (2010)

[15] A. Perdomo et al. Physical Review A 78, 012320 (2008)

[16] S. H. W. van der Ploeg et al. IEEE Trans. App. Supercond. 17, 113 (2006)

[17] R. Harris et al. Phys. Rev. B 82, 024511 (2010)

[18] S. Boixo, T. Albash, F. M. Spedalieri, N. Chancellor, D. A. Lidar arXiv:1212.1739 (2012)

[19] Z. Chen, Z. Zhou, X. Zhou, X. Zhou, and G. Guo, Phys. Rev. A 81, 022303 (2010)

[20] R. Chitra, S. Pati, H. R. Krishnamurthy, D. Sen, Diptiman, S. Ramasesha Phys. Rev. B 52, 6581 - 6587 (1995)

[21] L. Banchi, T. J. G. Apollaro, A. Cuccoli, R. Vaia, and P. Verrucchi, Phys. Rev. A 82, 052321 (2010)

[22] L Banchi, T J G Apollaro, A Cuccoli, R Vaia, and P Verrucchi, New Journal of Physics 13 (2011) 123006

[23] T. J. G. Apollaro, L. Banchi, A. Cuccoli, R. Vaia, P. Verrucchi, arXiv:1203.5516v1 [quant-ph]

2012

[24] L. Banchi, A. Bayat, Paola Verrucchi, and Sougato Bose, Phys. Rev. Lett. 106, 140501 (2011)

[25] Nielsen, Michael A. & Chuang, Isaac L. (2000), Quantum Computation and Quantum Information, Cambridge University Press

[26] N. Chancellor and S. Haas, Phys. Rev. B 84, 035130 (2011)

[27] Here I mean trivial if the adiabatic bus protocol were performed twice, once to transport the spin to another site and once to return it to its original location.

[28] This argument breaks down in general if one considers cases where there is not coupling in all three spin directions, for example in an XY model.

Summary

In this thesis I put forward a design for a universal holonomic quantum computer based on an adiabatic transport protocol using Heisenberg spin chains and clusters. This work is based on four published papers, each of which provide a different piece of motivation and background for the main topic of this thesis.

In chapter 1 I discussed the equilibration of finite spin chains subject to local quenches, which provides important background on the types of systems examined in later chapters. This section also provides a flavor of the interesting physics of finite spin clusters, of which this thesis only provides a small glimpse.

In chapter 2 I showed a specific example of a type of phenomenology in spin chains which can propagate disturbances an unlimited distance even in a gapped system by taking advantage of a ground state degeneracy. The effects shown here provide an underlying physical explanation of the effects exposited in the for the adiabatic implementation of the proposed architecture.

In chapter 3 I demonstrated specifically how an adiabatic transport protocol can be implemented which takes advantage of the effects observed in the previous chapter. This transport protocol is important for the holonomic quantum computing architecture discussed in the next chapter.

In chapter 4 I established an architecture for holonomic quantum computing based on transport though twisted Heisenberg chains. This architecture can be implemented either adiabatically using the methods proposed in the previous chapter or non-adiabatically. This chapter also outlined how the adiabatic implementation of this architecture may be constructed from superconducting flux qubits.

This thesis not only shows a viable design for a universal quantum computer and proposes how it might be built, it also provides context of the ideas relating to the design and background for where these ideas came from.